ENGINEERING SMALL EXTRACELLULAR VESICLE-DERIVED VEHICLES CARRYING OPTIMIZED MICRORNA FOR CARDIAC REPAIR AFTER MYOCARDIAL INFARCTION

A Dissertation
Presented to
The Academic Faculty

by

Sruti Bheri

In Partial Fulfillment
of the Requirements for the Degree
Doctor of Philosophy in the
Wallace H. Coulter Department of Biomedical Engineering

Georgia Institute of Technology & Emory University
May 2023

ENGINEERING SMALL EXTRACELLULAR VESICLE-DERIVED VEHICLES CARRYING OPTIMIZED MICRORNA FOR CARDIAC REPAIR AFTER MYOCARDIAL INFARCTION

Approved by:

Dr. Michael E. Davis, Advisor
School of Biomedical Engineering
Georgia Institute of Technology & Emory University

Dr. Julie A. Champion
School of Chemical and Biomolecular Engineering
Georgia Institute of Technology

Dr. Manu O. Platt
School of Biomedical Engineering
Georgia Institute of Technology

Dr. Hee Cheol Cho
Department of Surgery
Johns Hopkins University

Dr. Vahid Serpooshan
School of Biomedical Engineering
Georgia Institute of Technology & Emory University

Date Approved: December 6th, 2022

This dissertation is dedicated to my Mum, my Dad and all my grandparents, upon whose shoulders I stand today. Thank you for your eternal love and support.

ACKNOWLEDGEMENTS

This work and this thesis would not have been possible without the support of an army who believed in, encouraged, and guided me throughout. I'd first like to thank my advisor, Dr. Michael Davis, who's always been a supportive figure. Mike gave me the freedom and flexibility to design my own thesis project, was as excited as me when I told him about it and was always available to bounce ideas off, when I needed it. He gave me the scope to define and execute my PhD on my own terms, which, although tough at times, helped me gain the confidence to explore my research interests fully and taught me the importance of seeking help when I reached a roadblock. I'd also like to thank my thesis committee, Dr. Manu Platt, Dr. Vahid Serpooshan, Dr. Julie Champion and Dr. Hee Cheol Cho. They have helped to identify gaps in my research, provided critical and insightful feedback during research updates and made me appreciate the greater scope of my work.

I would also like to thank my prior teachers, mentors and advisors. My undergraduate advisor, Dr. Ross Ethier embodied the technical prowess I hoped to gain during graduate school and was my advocate throughout. My mentors, Dr. Julia Raykin and Dr. Eric Snider first introduced me to the field of biomedical research, patiently taught me my initial lab skills and endured my mistakes as I learned! Dr Pai showed me how far a passion for teaching can take one and remained an advocate as I transitioned from an undergraduate to graduate researcher. I also want to thank my mentor, Marisa Casola, who showed me how to translate my graduate school knowledge into applicable, real-world skills. Finally, I want to give a special thanks to my Year 3 (J1) teacher from Wales, Mr. Rogers, who emphasized

finding out the ‘why’ behind everything, and always remained my cheerleader ever since - I’ll cherish all your handwritten letters of encouragement.

On the day to day, I wouldn’t have been able to get through my experiments with a (semi) sane mind if it wasn’t for my lab group. From my early days, Aline, David, Don, Matt and Ben showed me the importance of lab camaraderie and always looked out for me as I found the ropes. Farnaz became like an older sister in lab, took me under her wing and always encouraged my ideas. Since then, the “EV crew”: Hyun-Ji and Jess, made the PhD research a pleasure – from sharing my enthusiasm for new projects to brainstorming solutions to being emotional support systems to being overall great friends both inside and outside of lab. The younger students, Preety, Olga, Kenneth, Kimmai, Jay and Felipe, gave me the chance to guide, mentor and support and taught me the value of teamwork. Olga and Kenneth have kept lab a fun and positive place, always been down for tea-times and have been genuine supporters for me. Finally, I need to give a special acknowledgement to my first Davis lab bench-mate, Milton. When joining the lab, I wished for a lab manager who was compassionate – but I got so much more. Milton has truly been my advocate. He’s always looked out for me, helping with last-minute orders, finding contacts on campus when I needed reagents or resources, grabbing food when experiments ran long and even providing guidance with non-lab or car-related matters. But beyond even this, his perseverance, unwavering effort, and dedication to my research were pivotal for the success of my project, especially the *in vivo* aim. Together, the Davis lab group have been more my family than colleagues and this acknowledgement doesn’t begin to substantiate the impact they all have had in my graduate career.

I also want to thank my friends from graduate school and beyond. To Vickie, who has been my friend since Secondary school in the UK, thank you for the constant check-ins, and cross-Atlantic trips to explore America together. Surabhi and Sushmita, you both have always been ready to chat, be involved in my graduate journey and provide encouragement, all the way from India. To my friends from undergrad, Bhavani, Meena, Zinka, Melody, Lian and Esther, thanks for the catch ups, visits and video calls to help me take my mind off research frustrations. My roommates, Ayesha and Eashani, you both made coming home each evening a pleasure and were always ready to explore Atlanta together. To my graduate friends, especially those from Asha, you made Atlanta feel like home and gave me constant reasons to do more beyond my PhD research with hikes, board games, potlucks and more. Shyam, Manisha, Suganya and Sanjay, thanks for being the absolute best friends I could have. From the regular library stints to the long car chats to the 'must see' checklists to the long nights of laughter, you all truly made my final graduate years a joy.

Finally, I want to thank my family. Nachiket, we grew through the graduate career together; from being my best friend to being my husband, you've remained a companion and confidante through it all. Thanks for all the late-night discussions, virtual company while preparing for graduate school deadlines and the many trips to take our minds off our work. Sharing our PhD journeys together has truly been a pleasure, and I cannot imagine completing this journey without you by my side.

Ramesh mama and Dipali aunty, you've always made your place feel like home for every break and have been there to help with navigating life in the US. Attha and Jagan mama, you've always cared for my well-being and success dearly, right from the first US-visa application in Chennai, you've kept up with my research and stayed involved. Karthik,

Varun and Anika, you've been little siblings to me, sometimes listening to my 'sage' advice, but always being there to have fun together.

Mum and Dad, you are both the reason I got into the field of science and chose to pursue my PhD. You are not only my role models but my biggest support system, providing a constant place of warmth, comfort, and encouragement. Right from being on video call whenever I tried home recipes, to creating Python scripts to speed up my data analysis, to listening to my tirades (at any hour of the day or night) when I felt stuck, you both have been pivotal to the progress of my graduate career. Mumma, you have always understood me like no other, accepted me for exactly who I am and kept my wellbeing and joy above all else. Dad, you have shown me the power of curiosity and pursuing my interests relentlessly, given me the strength to tackle life-challenges, and always dropped everything to be there for me when I needed help. You both are my constant sources of inspiration and I owe the success of this PhD to you both.

I cannot end this without acknowledging my dearest grandparents, Nani, Vizag Thatha, Amamma and Kakinada Thatha. It's your fight for and value for education that our whole family and I build upon today. You have only ever seen the best in me, always believed in me and showered me with never-ending love. It's my honor to be your grandchild, thank you.

TABLE OF CONTENTS

LIST OF TABLES

LIST OF FIGURES

LIST OF SYMBOLS AND ABBREVIATIONS

MI	Myocardial infarction
sEV	Small extracellular vesicle
ELV	sEV-like vehicle
miR	microRNA
CPC	C-kit+ progenitor cell
MSC	Mesenchymal stem cell
SUV	Small unilamellar vesicle
LV	Left ventricle (or left ventricular)
IR	Ischemia-reperfusion
CEC	Cardiac endothelial cell
CF	Cardiac fibroblast (or RCF: Rat CF)
IL-x	Interleukin-x (e.g., IL-6: interleukin-6)
TNF	Tumor necrosis factor
CC/CXC/CX3C	Chemotactic chemokine subfamilies
MHC	Major histocompatibility complex (also, Myosin heavy chain)
DAMP	Damage-associated molecular patterns
RV	Right ventricle (or right ventricular)
BM	Bone marrow
PC	Phosphatidylcholine
PE	Phosphatidylethanolamine
PS	Phosphatidylserine
SM	sphingomyelin

CHOL	Cholesterol
CM	Ceramide
CDC	Cardiosphere-derived cell
MECP2	Methyl CpG binding protein 2
PTEN	Phosphatase and tensin homolog
CD-	Cluster of differentiation
HSP-70	Heat shock protein-70
PAPP-A	Pregnancy associated plasma protein-A
TFH	Thin film hydration
FBS	Fetal bovine serum
hFGF-β	Human fibroblast growth factor-β
EGM	Endothelial growth medium
EBM	Endothelial bare medium
VEGF	Vascular endothelial growth factor
IGF	Insulin-like growth factor
EGF	Epidermal growth factor
GA	Gentamicin/Amphoterin
LDH	Lactate-dehydrogenase
DLS	Dynamic light scattering
NTA	Nanoparticle tracking analysis
LAD	Left anterior descending artery
TTC	1-2-3 triphenyl tetrazolium chloride
WGA	Wheat germ agglutinin
DiR	DiIC18(7);1,1′-dioctadecyl-3,3,3′,3′-tetramethylindotricarbocyanine iodide

SMA	Smooth muscle actin
MHC	Myosin heavy chain (also, Major histocompatibility complex)
ROS	Reactive oxygen species
PSLAX	Parasternal long axis
SAX	Short axis
PLS	Partial least square
EdU	5-ethynyl-2’-deoxyuridine
FITC	Fluorescein isothiocyanate
TRITC	Tetramethylrhodamine
RMSE	Root-mean-square error

SUMMARY

Myocardial infarction (MI) is one of the leading causes of morbidity and mortality worldwide. One promising therapy involves delivering small extracellular vesicles (sEVs). These sEVs are 30-150 nm vesicles containing protein and/or nuclear cargo. Despite their reparative potential, sEV therapies have several issues due to their cellular origin, including variable sEV yield and uncontrolled and low-density cargo encapsulation. Synthetic sEV-mimics have been developed which allow optimized cargo loading but these have high toxicity, compromised membranes and poor uptake. Therefore, there is a need for cell-free vehicles with sEV-like membrane and uptake, which allow delivery of customized cargo.

To address these needs, the aim of this study was (1) to develop an sEV-like vehicle (ELV) with select microRNA (miR) cargo for cardiac repair and (2) to understand the role of the sEV membrane on vesicle uptake and ELV functionality. We hypothesized that ELVs comprised of an sEV membrane and loaded with miR cargo will improve cardiac tissue repair after MI compared to sEVs alone and that membrane composition will affect ELV functionality. We successfully engineered ELVs using two different approaches. The ELVs were loaded with miR-126, an endothelial marker, and when administered to cardiac endothelial cells, improved angiogenesis compared to sEV treatment. We then injected miR-126+ELVs into a rat model of ischemia-reperfusion wherein the ELVs reduced infarct size, fibrosis and hypertrophy and increased angiogenic parameters. We then assessed the relationship between sEV membrane composition and uptake mechanism finding that sEV origin affects both composition and uptake. We tested this by engineering miR-126+ELVs from two cell types and found differences in their angiogenic and proliferative capacity.

Taken together, this study demonstrates the value of engineering vehicles with sEV membranes and their potential to deliver selective cargo for cardiac repair after MI.

CHAPTER 1. INTRODUCTION

1.1 Motivation

Myocardial infarction (MI) is one of the leading causes of morbidity and mortality worldwide with an estimated 805,000 events annually in the United States alone[1]. Cell-based therapies for MI have been under investigation, including those using cardiac c-kit+ progenitor cells (CPCs) and mesenchymal stem cells (MSCs)[2–4]. More recently, paracrine signaling, specifically through small extracellular vesicle (sEV) release has been attributed for the reparative effects of cell therapies[4–7]. sEVs are 30-150 nm vesicles released by cells and they contain protein and/or nuclear cargo. However, current sEV therapies have several issues due to their stem cell origin: variability in sEV yield; uncontrolled and low concentration cargo encapsulation; dependence on cell survival and cell retention *in vivo*[8–10]. To overcome these limitations, synthetic nanoparticles such as small unilamellar vesicles (SUVs) have been developed. Although this cell-free approach allows for selective and high concentration cargo loading, mimics have high toxicity, compromised membranes and poor cellular uptake[11,12]. Thus, there is a need for a cell-free vehicle which has sEV-like membrane and uptake properties and still allows for SUV-like custom cargo loading.

The overall goal of this dissertation was to engineer the optimal nanovesicular structure to deliver selective cargo to induce cardiac repair after MI. In this study our objective was twofold (1) to develop an sEV-like vehicle (ELV) with select microRNA (miR) cargo for cardiac repair and (2) to understand the role of the sEV membrane on vesicle uptake and ELV functionality. Our central hypothesis was that ELVs comprised of an sEV membrane and loaded with miR cargo will improve cardiac tissue repair after MI compared to sEVs

alone and that membrane composition will affect ELV functionality. The rationale for this work is that it will help us design customized nano-scale cardiac therapies for MI and allow us to understand the effect of vesicle composition, and tailored cargo on relevant cardiac cell responses. We tested these objectives by accomplishing three specific aims.

1.2 Specific Aims

Aim 1: To assess the properties and functionality of ELVs engineered from CPC-derived sEVs.

We hypothesized that ELVs with membrane composition and properties similar to that of CPC sEVs and with customized cargo will result in increased pro-reparative cardiac cell functionality *in vitro*. We first engineered and characterized ELVs with a modified thin film hydration (TFH) method to look at ELV shape, concentration profile, polydispersity index and uptake compared to sEVs. We then loaded miR-126 into the ELVs, confirmed miR encapsulation and assessed functional responses of ELVs when delivered to endothelial cells through cytotoxicity and angiogenesis assays. Further, to reduce batch-to-batch variability with ELV synthesis, we also engineered electroporation-based miR-126+ELVs. We again characterized these ELVs, assessed uptake by endothelial cells and measured functional response with an angiogenesis assay.

Aim 2: To assess whether ELV delivery to a failing left ventricular (LV) myocardium improves cardiac function after MI.

We hypothesized that ELVs preserving the sEV membrane while controlling the encapsulated cargo will allow for a more targeted and reparative response from an ischemic

LV myocardium then sEVs alone. To assess this, we administered two doses of ELVs and sEVs intramyocardially into a rat LV ischemia-reperfusion (IR) model. Infarct size was quantified 24 hours after injection. We also looked at global and regional cardiac function at Day-7, -14 and -28. At four weeks post-injection, histological analysis was performed to look at fibrosis, hypertrophy, and angiogenesis. Controls were animals which received only IR with saline (no treatment) and sham IR surgery.

Aim 3: To study the effect of parent cell type on vesicle uptake and functionality.

The working hypothesis is that parent cell type alters vesicle membrane composition and in turn alters ELV functionality. First, sEVs were isolated from CPCs, MSCs, cardiac endothelial cells (CECs) and cardiac fibroblasts (CFs) under normoxic and hypoxic conditions. The sEV lipid and protein profiles were quantified with mass-spectrometry. Uptake mechanism of sEVs by CECs and CFs was assessed through an uptake inhibition study. Next, the relationship between the sEV parent cell type, uptake mechanism and receipt cell was established through computational modeling. Further, to understand the parent cell role on ELV function, miR-126+ELVs were synthesized from MSC and CPC sEVs, characterized, and differences in their function quantified when treated to CECs with angiogenesis and proliferation assays.

CHAPTER 2. BACKGROUND

2.1 Myocardial infarction (MI)

MI is one of the leading causes of morbidity and mortality worldwide with an estimated 805,000 events occurring annually in the United States alone[1]. MI is the onset of cardiac ischemia following coronary artery occlusion. After an MI event, the cardiac tissue can be subdivided into three regions: the central infarcted zone (non-functional tissue); a penumbra surrounding the infarct known as the border zone (mild ischemia, partially functional) and the healthy cardiac tissue beyond the border zone (fully functional)[13]. Most interventions target the border zone, where there is larger scope of tissue revival than in the central infarcted zone.

2.1.1 Pathophysiology

From a pathological standpoint, MI is defined as death of cardiomyocytes caused by an ischemic onslaught[13]. Predominantly, the coronary artery occlusion that results in MI is from atherosclerotic disease and thrombotic occlusion of an epicardial artery[14]. In some instances, plaque can dislodge and obstruct or rupture the vessels and, in rare cases, non-atherosclerotic MI's can occur wherein the coronary vessels are severely narrowed. These include coronary embolism from endocarditis, coronary artery dissection, arteritis, or prosthetic valve thrombosis[15]. The size of the resulting infarct depends on the size of the ischemic area at risk, the duration of the artery occlusion and the extent of microvascular disfunction and collateral capillary blood flow[16]. Once the ischemia has occurred, the infarct progression is sequential, first starting in the subendocardial layers in the area at

risk of infarct, then progressing to the subepicardial layers, and then to the border zone of the area at risk, depending on the duration of the coronary artery occlusion[17,18]. Despite this progression of the infarction, 30-50% of the area at risk remains salvageable by reperfusion after 4-6 hours of MI onset[19]. Up to 12 hours after the occlusion, myocardial intervention by reperfusion of the tissue can still reduce the final infarct size[20]. Despite reperfusion salvaging some of the myocardium, the reperfusion process also induces further injury which can be irreversible, thereby leading to greater increase in infarct size and microvascular dysfunction.

2.1.2 Cellular level alternations

At a cellular level, the ischemia leads to local tissue hypoxia which, in the span of hours, results in cardiomyocyte apoptosis and necrosis[21,22]. This is compounded by reperfusion injury wherein the rapid reperfusion of the ischemic tissue induces further cardiomyocyte death and microvascular damage[23]. This cardiomyocyte necrosis releases danger signals which activate an inflammatory response and leukocyte infiltration[15]. This rapid inflammation and immune cell infiltration is known as the "inflammatory phase" and aims to clear out necrosed cells and damaged extracellular matrix. During this phase, several pro-inflammatory cytokines (IL-1, TNF, IL-6, and IL-18) and chemokines (CC, CXC and CX3C) are released to recruit mononuclear cells, neutrophils, and more leukocytes[24–27]. The inflammatory response is followed by a "reparative phase" wherein the excess inflammation is resolved and there is proliferation of myofibroblasts and the initial onset of scar formation[28,29]. The initial inflammatory response also activates resident endothelial cells which are implicated with local neovascularization during the reparative phase[30]. Beyond this, as cardiomyocytes have limited regenerative capacity, myocardial

repair after MI is primarily through the myofibroblast-activated extracellular matrix deposition (primarily collagen) resulting in scar formation[31,32]. This helps to recover some of the structural integrity of the infarcted myocardium but as the scar lacks contractile capacity, excessive deposition becomes maladaptive to ventricular function[33]. Therefore, over time, despite all the inflammatory and fibrotic cellular alterations and attempts at repair, the ischemia often leads to irreversible myocardial damage, unfavorable cardiac remodeling, and eventually cardiac failure.

2.1.3 Clinical interventions and therapies

To enable cardiac recovery after MI, rapid medical intervention is crucial as this allows the recovery of the partially injured cardiomyocytes and microvasculature in the border zone, thereby reducing the overall size of the infarct. Current treatments for MI include timely reperfusion and revascularization to salvage the functional myocardium. This includes pharmacological therapies, such as beta-blockers, ACE inhibitors, calcium channel blockers and antithrombotic therapies to lower the blood pressure and reduce the myocardial oxygen demand. This is at times combined with mechanical interventions, such as angioplasty and stenting to structurally re-open occlusions and maintain an open lumen[34]. If these preliminary interventions are insufficient, and especially in later-stage cases, more invasive procedures might be used, such as surgical intervention with coronary bypass or in end-stage cases, implantation of LV assistive devices to compensate for a failing LV[35,36]. Despite these stage-based therapies, the onset of each MI increases the likeliness of future events, thereby progressively diminishing the functional contractile myocardium.

2.2 Cellular Therapies

2.2.1 Cells in the myocardium

2.2.1.1 Cardiomyocytes

Cardiomyocytes comprise a major portion of the myocardium accounting for 20-35% of all the cells present[37]. They comprise the primary machinery for myocardial contraction through calcium signalling and provide the structure and integrity for the heart. However, after the onslaught of MI, cardiomyocytes have very poor proliferative capacity with only limited generation of new cardiomyocytes once they reach the adult phenotype[38]. This limits their scope after injury and makes the myocardium vulnerable to longer term dysfunction.

2.2.1.2 Cardiac endothelial cells (CECs)

CECs comprise the second largest portion of the myocardium, representing 60% of non-myocyte cells in the adult heart[39]. They serve several purposes in the myocardium including aiding with cardiac development, aiding with cardiomyocyte organization and survival, vascular homeostasis as well as healing, angiogenesis, and regeneration after ischemic assault[40]. After the MI, rapid neovascularization from junctures of ruptured endothelial vessels improves the perfusion in the myocardial border zone and aids in recovery of some of the cardiomyocyte populations[41].

2.2.1.3 Cardiac fibroblasts (CFs)

CFs reside in the myocardium and aid with hemostasis and maintenance of the cardiac extracellular matrix. After the onset of MI, these CFs convert into a myofibroblast phenotype, with higher proliferative capacity to rapidly lay down extracellular matrix, especially collagen, and initiate the scar formation process[42]. They also release inflammatory factors which recruit neutrophils to the infarct site[42,43]. Beyond this, studies have shown that myofibroblasts can phagocytose apoptotic cells to help clear up the local environment after MI[44]. However, the regulation of CF-based scar deposition is poor, therefore after fibrotic scar initiation, excessive scar tissue deposition can occur, thereby impairing the myocardial repair.

2.2.1.4 Immune cells

Immune cells include neutrophils, monocytes, and macrophages. At the onset of MI, DAMP signals rapidly recruit neutrophils and monocytes to the infarcted site[45]. At the same time, cardiac-resident mast cells release inflammatory mediators into circulation to activate the innate immune system[45]. In addition, resident macrophages release chemo-attractants to home the neutrophils and aid with removal of necrotic cells[46]. With time, these are overtaken by monocyte-derived macrophages and help support scar resolution and neovascularization[47]. As the recovery progresses, macrophages can convert from a pro-inflammatory M1 phenotype to an anti-inflammatory M2 phenotype[48]. In concert, all these immune cells aid in the initial response to the injury and the downstream repair.

2.2.2 Cardiac-relevant stem and progenitor cells

2.2.2.1 C-kit+ progenitor cells (CPCs)

CPCs are defined by their membrane expression of c-kit or CD117 and are typically isolated from right atrial appendage biopsies through magnetic bead sorting [49–51]. CPCs are present in a very small percentage in the atrial appendage of the myocardium and are thought to be potent for cardiac repair[49]. Although they are cardiac-derived, the notion that CPCs differentiate into cardiomyocytes has been hotly contested in the field and multiple studies have since shown that endogenous CPCs are not cardiomyocyte progenitors[52,53]. However, it's found that injection of CPCs, specifically those isolated from younger patients, into the myocardium is pro-reparative[54,55]. In fact, Simpson *et al*. noted that neonatal patient (<1 month old) atrial appendages have a comparatively higher number of CPCs[56].

Although not comprising a major percentage of myocardial cells, CPCs can be proliferated *in vitro* and their therapeutic benefit through direct implantation and through their release of cardioprotective paracrine signalling is well established by our laboratory and others[57–59]. Agarwal *et al*. explored the age-dependency of CPCs by comparing neonate CPCs, infant CPCs (1 month – 1 year old) and child CPCs (1 to 5 years old) in a model of right ventricular (RV) heart failure[58]. They found that neonate CPCs improved RV ejection fraction, tricuspid annular plane systolic excursion and decreased wall thickness, unlike the infant or child cells. Another study by Trac *et al*., investigated the aggregation of CPCs into spheres and found that the 3D CPCs significantly improved RV function compared to 2D culture[59].

An important avenue through which CPCs mediate their therapeutic benefit is paracrine signalling, specifically through sEV release. Gray *et al*. investigated the role of hypoxia on rat CPC-derived sEVs and found that these sEVs enhance tube formation of CECs and are

anti-fibrotic when administered to CFs[60]. Agarwal *et al*. also investigated the role of hypoxic conditioning on CPCs sEVs derived from neonate and older children[9]. This study found that neonate CPC sEV therapeutic potential was independent of oxygen conditioning, whereas CPC sEVs from older children improved cardiac function only under hypoxic culture. Taken together, these studies highlight the scope of CPC-based therapies, a field that is growing and is highly explored by our group.

2.2.2.2 Bone marrow (BM)-derived mesenchymal stem cells (MSCs)

BM-MSCs, originally discovered in 1970 by Friedstein[61], are a subset of bone-marrow derived stem cells that have the scope to differentiate into osteoblasts, adipocytes and chondroblasts[62]. MSCs contain low expression of major histocompatibility complex (MHC) class I and completely lack MHC class II thereby being efficient at minimizing immune response upon implantation[63]. Prior studies have shown that MSCs can regulate inflammatory response by activating anti-inflammatory innate and adaptive immunity[64,65]. Further, the administration of MSCs to the injured myocardium reduced the number of proinflammatory monocytes and encouraged M2 polarization of macrophages[65,66]. In addition to their anti-inflammatory ability, MSCs are also known to be antifibrotic and aid with angiogenesis[67]. This makes them an attractive source for cell therapies, including after MI.

2.2.3 Current scope of cellular therapies

Cellular therapies for cardiac diseases have been promising, with potential to induce cardiac repair and recovery when administered to the tissue site[68]. Specifically, CPCs and MSCs have been shown to be pro-reparative when delivered after MI[4]. Although the extent

of improvement in cardiac function after cell therapy varies with the cell types administered, it is established that cellular therapies are safe for LV function. CPCs encapsulated in synthetic and extracellular matrix patches are known to increase angiogenesis and reduce fibrosis[69,70]. Similarly, Yoon *et al.* first observed that injecting MSCs in a mouse MI model significantly reduced the infarct size[71]. Recently, the exact benefits of CPCs and MSCs for cardiac repair have been further explored both individually and in combination, with clinical trials underway[3,72,73].

2.2.4 Limitations of cellular therapies

Despite the potency of cellular therapies and several pre-clinical and clinical trials underway, the evidence for the direct benefit of cell therapy in MI is unclear[74]. Several studies have since hypothesized that the benefit of cell therapy for myocardial repair can be attributed to paracrine signaling, specifically through sEV release[75,76]. A study by Ibrahim *et al.*, explored this with cardiosphere derived cells (CDCs) in an acute MI model[77]. They found that observed improvements in LVEF after cell treatment were attenuated when the cells were initially dosed with an sEV-inhibitor (GW4896). This clearly underscores that sEV release from cells in crucial and likely their primary avenue for cell therapy mediated cardiac repair.

2.3 Small extracellular vesicles

2.3.1 Types of vesicles

Small EVs (historically referenced as exosomes), sEVs are <30-150 nm vesicles containing protein and nuclear cargo and are secreted by nearly all cell types. These vesicles form in

the cytoplasm from the inward budding of endosomes. They were initially discovered in sheep reticulocytes in 1985 and were labeled as nothing more than carriers for waste export.[78] After several decades of sEV-related research, they have now been accepted as major players in paracrine signaling and potential biomarkers for several diseases.[79] sEVs traffic mRNA, miR, DNA and proteins between cells. As cell-free components, these vesicles are often enriched in cargo compared to their parent cells, making sEV-based therapies a potential alternative to cell therapies for various diseases.

Medium/large EVs (historically termed as microvesicles), microvesicles are slightly larger in size ranging from approximately 100 - 1000 nm. They were originally thought to be 'dust material' derived from platelets and their universal role in cellular interaction was only uncovered recently. These vesicles form from the outward budding of the cell's plasma membrane.[80] Like sEV, they also play a role in cell-cell communication with the transport of mRNA, miRNA, DNA, and proteins between cells.[81] The precise differences between sEV and microvesicle mediated transport is still unclear but being larger in size, microvesicles have been shown to successfully carry plasmid DNA[82]. Despite this, microvesicles remain poorly explored as a therapeutic for tissue repair and regeneration.

Medium/large EVs produced during cellular apoptosis (historically called apoptotic vesicles) can range from ~50 nm to 10 µm depending on their parent cell type and are produced during cellular apoptosis. They are formed by indiscriminate blebbing of a cell's membrane during apoptosis.[83] Consequently, their cargo usually consists of remnants of the parent cell such as cytoplasm, organelles, and nuclear contents. As the frequency of cell apoptosis is higher in disease conditions, these vesicles could play an important role in regulating local disease microenvironments. For example, apoptotic vesicles from mature

endothelial cells induced differentiation in endothelial progenitor cells.[84] However, the detailed role of apoptotic vesicles and their cargo in tissue homeostasis and repair remains unclear.

2.3.2 sEV composition, biogenesis and uptake

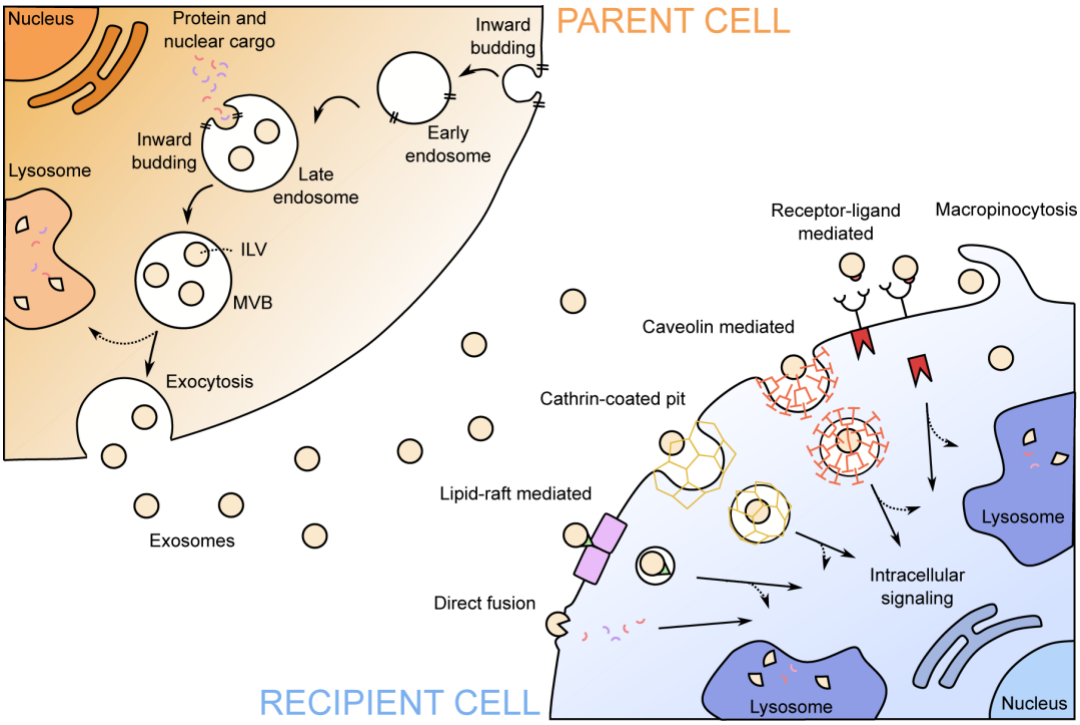

Figure 1. sEV biogenesis and uptake. Biogenesis of sEV in parent cell (orange) and endocytosis of sEV by recipient cell (blue), with different uptake mechanisms shown. Image adapted from Bheri *et al*. (2020).

sEVs are released by cells during paracrine signaling. sEVs are composed of an amphiphilic bilayer vesicle membrane consisting of phospholipids (e.g., phosphatidylcholine (PC) phosphatidylethanolamine (PE), phosphatidylserine (PS)), sphingomyelins (SM), cholesterol (CHOL), ceramides (CM), as well as transmembrane

proteins (e.g., tetraspanins CD9, CD63, CD81). This complex membrane composition is often credited for efficient sEV uptake by cells with minimal clearance[85]. Further, the aqueous interior cavity of sEVs contains protein/nuclear cargo (e.g., mRNA, miR, proteins) which is often enriched from the parent cell, making sEVs potent therapeutics. sEVs are formed in the cell cytosol through the inward budding of the plasma membrane to form the early endosome, transition of the early endosome into the late endosome, another inward budding of the late endosome to form sEVs, and finally fusion of the late endosome with the plasma membrane to release sEVs (Figure 1). Once the sEVs reach the recipient cell, uptake of sEVs can occur through several mechanisms. Endocytosis methods include direct fusion of sEVs with the recipient cell plasma membrane, lipid-raft/caveolin mediated uptake, clathrin-coated-pit/dynamin mediated uptake, receptor-ligand mediated uptake or through macropinocytosis. After endocytosis, sEVs can be trafficked into the cytoplasm or nucleus for functional responses or fuse with the lysosome for degradation. Although sEV biogenesis is well understood, the determining factors relating sEV composition to sEV uptake mechanism are still unclear.

2.3.3 sEV therapies for cardiac repair

Despite the promise of cell-based therapies, more recent studies have attributed the implanted cell-based recovery to paracrine signaling, especially to sEV release[4–7,86,87]. Indeed, sEVs carry therapeutic cargo that can be as effective as parent cells in encouraging cardiac tissue repair[88,89]. This suggests that sEV therapy could be a suitable strategy for myocardial repair[7,90–92]. Recently, emerging evidence has suggested that a primary role of sEVs in CVD is through shuttling proteins and noncoding RNAs, specifically miRs, between cells. In detail, sEVs activate signaling pathways by transferring functional

proteins and/or miRs, substantially contributing to the beneficial effects of stem cell therapies for diseases such as cardiac hypertrophy[93,94] and MI[95,96] among others. CPCs[9,88], CDCs[89,97], and MSCs[98,99] are the most studied sources of sEVs implicated in cardiac repair by cellular therapy. The cargo of these sEVs has been shown to increase cardioprotective and regenerative signals.[100]

One such reparative cargo molecule carried by CPC-sEVs was miR-210, which was shown to enhance endothelial migration and capillary density *in vitro*.[60] In addition, the same study implicated CPC sEV miR-17 delivery to cardiac tissue to reduce fibrotic scar tissue formation in an MI animal model. Another study using CPC sphere-derived sEVs suggested sEV-mediated miR delivery could effectively increase angiogenesis and ablate fibrosis *in vitro*, especially through miR-320a and miR-423-5p.[88] Moreover, CDC- or CPC-sEVs had cardioprotective effects (inhibition of apoptosis and stimulation of angiogenesis) via miR-132 delivery to the injured heart.[101]

Other studies have shown that preconditioning MSCs further improved the treatment of cardiac diseases. Under hypoxic conditions, MSCs produced miR-22 enriched sEVs, which targeted apoptotic methyl CpG binding protein 2 (MECP2) and resulted in a reduction of the ischemic myocardium.[102] In addition, GATA-4 overexpressing MSCs released miR-19a enriched sEVs, which targeted phosphatase and tensin homolog (PTEN) in cardiomyocytes.[103] The downregulation of MECP2 and PTEN levels was directly correlated to anti-apoptosis of cardiomyocytes. Therefore, there are significant benefits to using MSC sEVs for the treatment of various cardiac diseases. Likewise, functional proteins on the sEV surface have a significant role in cardiovascular diseases. One study showed the cardioprotective role of rat plasma sEVs in cardiomyocytes through heat shock

protein 70 (HSP70) mediated TLR4 signaling.[104] Specifically, HSP70 activated TLR4 on cardiomyocytes, leading to the activation of ERK/p38MAPK and subsequent HSP27 phosphorylation in the cells. In another study, pregnancy-associated plasma protein-A (PAPP-A) expressed on CPC sEV surfaces was shown to reduce cardiomyocyte apoptosis by enhancing IGF-1 proteolytic cleavage and subsequent IGF-1 receptor activation.[7]

These studies show that, in the cardiac field, stem cell-derived sEVs are a primary vehicle for pro-reparative miR and protein transfer. This underscores the importance of such stem-cell based nanovesicles and their cargo for cardiac repair and regeneration.

2.3.4 Limitations of sEV therapies

Despite their crucial role in paracrine signaling for cardiac regeneration and repair, stem/progenitor cell-derived sEVs have several limitations hindering their success as a therapeutic. One major drawback involves a supply and demand discrepancy. Cell-derived sEVs have variable, low yield which makes it challenging to meet demand for *in vivo* applications.[8] Further, although several techniques exist for isolating sEVs from cells, efficient and reproducible sEV isolation is often inconsistent or costly.[105] Additionally, current sEV therapies are dependent on cell-based sEV release[101,106,107]. As sEVs are isolated from the conditioned media of parent cells, there is limited control over their composition and cargo encapsulation varies based on the physiologic state of the parent cell.[108] . Thus, there is a variability in sEV yield, its physiochemical properties, and the loaded cargo[8,109]. Moreover, specific parameters such as CPC-donor age and hypoxia impact sEV release, alter the cargo and in turn affect cardiac function[9,60]. Besides this, these

sEV therapies also depend upon *in vivo* cell survival, retention, and functionality[10]. Moreover, sEVs also contain various types of cargo, of which pro-reparative miRs compose only a small fraction[110]. Therefore, even if certain nucleic acids are known to be favorable for cardiac repair, the potency of each sEV is limited, requiring higher dosing of vesicles to meet demand. Such higher doses pose their own risks including accumulation in the lungs and potential asphyxiation.[111] Moreover, when delivering sEV therapies, the targeting of the vesicles is likely dependent on membrane proteins over which there is limited control too. Finally, to be clinically relevant, it is important that sEV therapies avoid lysosomal degradation and minimize unfavorable immune responses.[112]

Due to the multitude of challenges present in developing translational sEV therapies, there is value in studying methods to engineer sEVs specifically for cardiac repair. When designing vesicles, it is important to tailor the cargo to increase potency, home the sEVs to the cardiac site and minimize unfavorable vesicle loss.

2.4 Synthetic vesicle mimics

2.4.1 Types of mimics

Significant research has focused on developing completely synthetic nanovesicles using phospholipids to emulate the function of EVs.[113–115] Still, these vesicles lack the varied and diverse lipid/protein membrane of sEVs. They cannot match sEVs and modified sEVs in terms of vesicle stability, tissue targeting, and immune evasion. Despite these challenges, these nanovesicles are easier to scale up as they do not depend on cellular sEV production

and can be designed to have controlled cargo release under specific physiological conditions. In addition, although challenging, their membranes can be specifically designed to reflect some of the functionally important components of sEV membranes.

Several types of synthetic nanovesicles have been designed depending on the cargo to be carried. The first of these are liposomes, which mimic the lipid bilayer of cells and EVs, and consist primarily of PC and PE.[116,117] Liposomes can range from nano to micro scales and can contain several lamellar membranes.[118] The smallest of these liposomes, SUVs, are the closest match to sEVs. A modification of liposomes are niosomes, named as such because their bilayer contains a non-ionic surfactant typically composed of CHOL derivatives.[119,120] Their non-ionic surface increases their biocompatibility and lowers their toxicity. Another modification involves adding ethanol to the membrane. Two examples include ethosomes, which are composed of phospholipids with water and ethanol, and transfersomes, which are composed of PC, surfactants, and ethanol.[121,122] In these vesicles, the presence of ethanol helps solubilize the loaded cargo making the cargo easier to embed. Further, the presence of the surfactant makes the structure of transfersomes ultra-flexible, so they can easily be delivered through spaces much smaller than their own size.[123]

Another group of synthetic nanovesicles are NPs coated with membranes. Lipospheres consists of a lipid vesicle with a solid lipid core which remains solid at room and body temperature.[124] They have better higher stability and easier preparation methods compared to traditional liposomes.[125] However, as they contain a lipid core and have an amphiphilic membrane, they are poor carriers of hydrophilic cargo. Some other membrane coated NPs capitalize on cell membranes to coat synthetic particles. Specifically, stem cell membranes are known to activate reparative and regenerative intracellular pathways in recipient cells,

therefore, using their membranes as coats can be a clever way to mask the foreign NPs.[126] In Table 1**.** we summarize these synthetic nanovesicles and discuss their benefits and drawbacks for use as cargo-laden nanocarriers.

In the cardiac field, several groups have studied synthetic nanoparticles as therapeutic carriers for MI. For example, liposomes loaded with erythropoietin and CD15s were delivered to rabbit MI models.[127] These synthetic vesicles reduced infarct size, improved LV function and induced favorable cardiac remodeling through pro-angiogenic and anti-fibrotic signaling. Liu *et al.* investigated the role of ligustrazine loaded ethosome patches in cardiac repair after acute MI.[128] The ethosome-based drug delivery prolonged drug concentrations to the blood compared to controls and reduced MI in a long-term ischemia model. In another study, Tang *et al.* developed synthetic nanoparticles cloaked in CDC membranes as therapeutics for MI.[129] The delivery of these particles to a mouse model of MI helped preserve the viable myocardium and also reduced T-cell infiltration. These studies highlight the potential of such synthetic nanovesicles as carriers for cargo. Although they cannot completely recapitulate the benefits of sEVs, they remain a promising avenue for cardiac repair.

Table 1. Types of synthetic nanovesicles. Outline of key synthetic nanovesicles and their benefits and drawbacks compared to naturally derived sEVs.

Type	Description	Benefits	Drawbacks	Literature
Liposomes	Bilayer vesicle of synthetic amphiphilic lipids	• Similar structure and scale • Robust methods for synthesis • Therapies in pre-clinical & clinical trials • Enhanced stability *in vivo*	• More Immunogenic than sEVs • Poorly recapitulates complex sEVs membrane – important for trafficking • Unmodified liposomes have quick degradation *in vivo*	116,130–132
Niosomes	Vesicles with non-ionic surfactant bilayer	• High biocompatibility • Low toxicity due to non-ionic membrane	• Poor stability • Potential to aggregate • Cargo leakage • Temperature based size alteration	119,120,133
Ethosomes	Vesicles with ethanol and water combined with the phospholipid bilayer	• High penetration • Easy size modulation • Useful for transdermal therapies	• Requires high amounts of alcohol	121,134
Transfersomes	Vesicles with ethanol and surfactants combined with a phospholipid bilayer	• Ultra-flexible vesicles • Useful for transdermal therapies	• High levels of surfactant can damage cell membranes • Poor chemical stability • Impure phospholipid membrane	122,123
Lipospheres	Vesicles with a solid lipid core which encapsulate hydrophobic cargo	• High stability • Low-cost synthesis	• Not suitable for hydrophilic protein/nucleic acid cargo • Inconsistent cargo release	124,125,135
Membrane coated NPs	Nanoparticles encased in cell membrane	• Immuno-compatibility • Tissue homing • Prolonged retention and circulation *in vivo*	• Potentially larger particle size because of extra membrane • Off-target effects with systemic delivery unknown	129,136–138

2.4.2 Therapeutic potential and limitations of mimics

To address the limitations of parent cell dependence and cargo inconsistencies with sEVs, sEV mimics have been developed including exogenously modified sEVs and nanoparticles such as SUVs[139]. Exogenously modified sEVs focus on modifying the cargo by adding therapeutic agents into the vesicle via active or passive encapsulation[109,140–143]. Although some functional molecules have been delivered using these methods, they have high immunogenicity, high toxicity and compromised vesicle membranes[141,143,144]. SUVs on the sEV-scale have been more promising, composed of either synthetic or chemically derived natural lipids. These vesicles are biocompatible, have the potential to carry tailored cargo and can be engineered for cell-specific targeting[11]. However, SUV membranes usually consist of only a couple of lipid types unlike sEVs which have complex, multi-molecule-based membranes[145,146]. This often leads to SUVs having low solubility and stability, limited encapsulation, and rapid clearance from tissues[11,85,115,145–147]. Thus, despite their cargo customizability, SUVs fall short of matching the *in vivo* cardiac reparative potential of sEVs.

CHAPTER 3. TO ASSESS THE PROPERTIES AND FUNCTIONALITY OF ELVS ENGINEERED FROM CPC-DERIVED SEVS

3.1 Introduction

MI is one of the leading causes of morbidity and mortality worldwide with an estimated 0.8 million events occurring annually in the United States alone [148]. MI involves the onset of cardiac ischemia following coronary artery occlusion. At a cellular level, ischemia leads to hypoxia which initiates an inflammatory response and activates neovascularization and fibroblast-activated scar formation [15,22,30]. Despite these attempts at local tissue repair, ischemia leads to irreversible myocardial damage, unfavorable cardiac remodeling and eventually results in end-stage cardiac failure. To enable cardiac recovery after MI, rapid medical intervention is crucial. Treatments include prompt reperfusion and revascularization through pharmacological agents, antithrombotic therapies, or mechanical interventions such as angioplasty and stenting [34]. Beyond these traditional approaches, cell-based therapies have shown promise, with scope to induce cardiac repair and recovery when delivered to the injured site [68,149]. Specifically, CPCs have been implicated as pro-reparative agents for cardiac recovery with phase II clinical trials completed (NCT02501811) [3,150,151]

More recently, the benefits of cell-based myocardial therapies have been attributed to paracrine signaling, specifically through sEV release [7,152]. sEVs are 30-180nm vesicles carrying nucleic acid cargo, such as RNA and miR, enveloped in an amphiphilic lipid and

protein bilayer [153]. Their cargo is often enriched in specific RNA compared to the parent cell and sEVs can be similar to or even more effective than parent cells in inducing cardiac repair [77,89]. However, current sEV therapies depend on parent cell-based sEV release, which can vary with the cellular microenvironment and the state of the cell [88,107]. Consequently, there is variability in sEV yield, physiochemical properties, and the loaded cargo [8]. Moreover, specific parameters such as CPC-donor age, CPC aggregation, and hypoxia impact sEV release, alter the cargo, and in turn affect cardiac function [9,60,88]. The CPC-based sEV therapies also depend on *in vivo* cell survival, retention, and functionality. Finally, even if sEVs are successfully delivered and retained in the injured myocardium, the fraction of total sEV cargo that is cardio-protective is low, thereby minimizing the potency sEVs [154]. Therefore, despite observed benefits of sEVs for cardiac repair, there remains a need for reliable sEV-based therapies with optimized, high concentration cargo to ensure potent and lasting reparative effects after MI.

To address the parent cell dependency and cargo variabilities of sEV therapeutics, synthetic mimics have been designed. These can be grossly divided into exogenously modified sEVs and synthetic nanoparticles such as SUVs. Exogenously modified sEVs focus on modifying the cargo by adding therapeutic agents into the vesicle via active or passive encapsulation [140–142]. Although some functional molecules have been delivered using these methods, they have high immunogenicity and compromised vesicle membranes [143,144]. SUVs on the sEV-scale have been more promising, composed of either synthetic or chemically derived natural lipids. These vesicles are biocompatible, have the potential to carry tailored cargo and can be engineered for cell-specific targeting [155]. However, SUV membranes usually consist of only a couple of lipid types unlike sEVs which have

complex, multi-molecule-based membranes [145,146]. This often leads to SUVs having low solubility and stability, and rapid clearance from tissues [115,146,147]. Thus, despite their cargo customizability, SUVs fall short of matching the *in vivo* cardiac reparative potential of sEVs.

Here, we aimed to engineer an sEV-like vesicle (ELV) by combining the benefits of sEV membranes with the cargo loading capacity of synthetic mimics. Previous methods to exogenously modify vesicles have included sonication, extrusion, freeze-thaw cycling, and forming cell-membrane derived vesicles [139]. However, these processes have shown variable successes with cargo loading and can induce cytotoxicity [141,143]. Further, some methods involving a temporary rupture and resealing of the membrane can compromise membrane integrity and increase vesicle aggregation [109]. Here we utilize two methods for ELV synthesis. First, we used a well-established for synthetic nanoparticle design from artificial lipids is TFH[156–158]. This method involves the formation of a lipid film followed by rehydration with an aqueous solvent to form vesicles. Although this is primarily limited to synthetic nanoparticles, this allows for high level inherent cargo depletion prior to cargo loading efficiency and even allows for membrane lipid modifications unlike most exogenously modified sEV methods [159]. Next, to allow more efficient ELV synthesis for scalability and minimize batch-to-batch variability, we also investigated a modified electroporation method of cargo loading.

The objective of this work was to develop scalable and potent vesicle therapies for cardiac repair, specifically through loading of miRNA. More specifically, we aimed to (1) synthesize ELVs from CPC-sEV membranes and (2) allow for customized miRNA cargo loading into ELVs. Our findings show that CPC-sEV derived ELVs can successfully be

formed on the sEV scale with miR-126 cargo encapsulated. Further we show ELVs can be internalized and have pro-angiogenic potential compared to sEVs when administered to CECs. This study provides the groundwork for developing ELV-based therapies for highly potent and tunable RNA delivery after the onset of MI.

3.2 Materials and Methods

3.2.1 Isolation and culture of human CPCs

Human CPCs were isolated from the right atrial appendage tissue of neonatal pediatric patients, through CD-177 magnetic bead sorting as described previously[58]. Neonate patients were classified as patients <1week old at the time of appendage removal during surgical intervention for a congenital heart defect. CPCs were cultured in Ham's F-12 medium (Corning Cellgro®, Corning, NY) with 10% fetal bovine serum (FBS), 1% penicillin-streptomycin, 1% L-glutamine and 0.04% human fibroblast growth factor-β (hFGF-β).

3.2.2 Culture of rat CECs

Rat CECs were cultured in endothelial growth medium (EGM-2 Endothelial Cell Growth Medium-2 BulletKit™, Lonza, Bend, OR) supplemented with 1% penicillin-streptomyocin and 2% FBS, 0.4% hFGF-β, 0.1% vascular endothelial growth factor (VEGF), 0.1% long arginine 3 insulin-like growth factor (R3-IGF- 1), 0.1% ascorbic acid,

0.1% human epidermal growth factor (hEGF), 0.1% Gentamicin/Amphotericin-B (GA-1000), 0.1% heparin, and 0.04% hydrocortisone as per manufacturer's protocol.

3.2.3 Isolation and characterization of sEVs

2D cultures of CPCs (~100 × 10^6 cells) between passages 9-13 were grown to 90% confluency. When confluent, CPCs were transferred to FBS-depleted media and their conditioned media was collected after 24 hours. sEVs were isolated from conditioned media using differential ultracentrifugation (Optima XPN-100, Beckman Coulter, Indianapolis, IN). The CPC conditioned media was sequentially depleted of cells at 1000 RPM for 5 minutes (Centrifuge 5810 R, Eppendorf, Hamburg, Germany) and cell debris at 15,000 RPM for 20 minutes (SW32Ti, Beckman Coulter) after which sEVs were pelleted at 31,000 RPM for 114 minutes (SW41Ti, Beckman Coulter) [160]. sEV pellets were collected and resuspended in PBS as required and stored in -80°C until further use. sEV shape was assessed with transmission electron microscopy (JEOL JEM-1400, Peabody, MA), particle size and concentration determined through nanoparticle tracking analysis (NTA) (NanoSight NS-300 with NTA 3.4 software, Malvern Panalytical, Malvern, UK) and polydispersity index through Dynamic Light Scattering (DLS) (DynaPro Plate Reader III, Wyatt, Santa Barbara, CA).

3.2.4 Formation of sEV lipid bilayer

ELVs were synthesized from sEVs using a variation of the TFH method, a commonly used process for synthetic vesicle formation. Specifically, the TFH method was modified to allow lipid film creation directly from sEVs instead of from synthetic lipids, as is required for traditional TFH. For this, inherent sEV cargo was removed using repeated sonication and flash freeze-thaw cycling. Samples were sonicated at #3 with probe sonicator (Sonic Dismembrator Model 100, Thermo Fisher Scientific, Waltham, MA) for 30 seconds (in sets of 10 seconds) followed by rapid freezing in liquid nitrogen. Samples were then rapidly reheated in a water bath (80°C), and this sonication-freeze-thaw cycle was repeated 5 times. Samples were then transferred to 10 mL single neck round bottom flasks (14/20 joint, Corning) along with 1 mL chloroform to confirm initial sample evaporation during TFH. The rotary evaporator (Rotovapor R-100, BUCHI, New Castle, DE) was set up with the heating bath at 50°C (Heating Bath B-100, BUCHI) and fresh dry ice and acetone in the condenser. The flask was secured to rotary evaporator and initial chloroform was evaporated at 332 mbar vacuum followed by aqueous sEV buffer evaporation at 42 mbar vacuum. Sample was submerged into the heating bath for complete aqueous solvent evaporation, as required, and left to dry for 10-15 minutes. Once thoroughly dried, 1-2 mL chloroform was again added to flask and left to rotate at #5 for 30 minutes to allow the sEV membrane to dissolve. After 30 minutes, rotary evaporation was repeated until all chloroform was evaporated, and a uniform lipid film formed in the flask. Samples were then desiccated over night at room temperature to remove any trace solvents.

3.2.5 Synthesis of miR-loaded ELVs with TFH

Desiccated sEV samples (from 2.4.) were treated with 1 µg/mL RNase A (Thermo Fisher Scientific) and incubated with rotation at room temperature for 30 minutes to deplete inherent sEV RNA cargo. Sample was then dried by rotary evaporation in 50°C water bath and 42 mbar vacuum to remove aqueous buffer. 1 mL chloroform was again added and incubated at room temperature for 30 minutes followed by evaporation (332 mbar) to dissolve lipids and reform a lipid film. Samples were then incubated with 40 units/20 µL ribonuclease inhibitor (RNaseOUT, Invitrogen, Carlsbad, CA) and 1 mM DTT (Invitrogen) for 1 hour at 37°C followed by evaporation to inhibit further RNase A activity. Again, 1 mL chloroform was added and evaporated after a 10-minute incubation to reform lipid film. Samples were run through inert gas and desiccated over night to stabilize and remove trace chemicals. Desiccated samples were loaded with miR-126-5p at 200 µg/mL, vortexed for 10 seconds and incubated at 4°C overnight, with shaking, to allow lipid film to rehydrate and ELVs to self-assemble in aqueous medium [154]. Following this, PBS was added to samples to dilute excess glycerol from RNaseOUT to ≤3% and provide ELV stability. Samples were passed under inert gas and centrifuged at 1000 RPM for 5 minutes to deplete larger particles (Centrifuge 5810 R, Eppendorf). To remove unencapsulated miRNA and concentrate the samples, samples were ultracentrifuged at 31,000 RPM for 114 minutes (SW41Ti, Beckman Coulter) and resuspended in PBS as needed.

3.2.6 Synthesis of miR-loaded ELVs with electroporation

After isolation of sEVs from CPC culture, the inherent sEV cargo was removed with repeated sonication cycles. Based on an initial study to optimize the inherent cargo

depletion used for TFH (Figure 9A), the sEVs were treated with 100 µg/mL RNAse-A (Thermo Fisher Scientific). Samples were then sonicated at #3 with probe sonicator (Sonic Dismembrator Model 100) for 3 minutes in repeated pulses of 15 seconds sonication and 15 seconds in an icy bath (to avoid sample overheating). 8 such 3-minute cycles were repeated for each sample after which samples were incubated at 37°C under rotation for 30 minutes. RNAseOUT ribonuclease inhibitor (Invitrogen) was then added at 40 units/ 20 µL along with 1 mM DTT and the 8 sonication cycles of 3 minutes each were repeated. Samples were then incubated at 37°C for 1 hour under rotation and then storage at -80°C to allow stabilization. Samples were then loaded into 0.1 cm transfection cuvettes (Biorad, Hercules, CA) along with 100 pmol miR-126, 33 uL Gene Pulser® electroporation buffer (Biorad) to a maximum volume of 100 µL. Samples were electroporated on a Gene Pulser Xcell with a square wave at 750 V, with 8 pulses. Samples were immediately mixed with 100 µL cold serum-free media and collected from cuvette. Samples were the incubated at 37°C for 30 minutes under rotation followed by overnight incubation at 4°C. The next day, samples were sequentially centrifuged (Centrifuge 5810 R, Eppendorf) at 1000 RPM for 5 minutes, ultracentrifuged (Optima XPN-100, Beckman Coulter) at 15,000 RPM for 25 minutes and then at 31,000 RPM for 1 hour 54 minutes to deplete debris, unencapsulated miR and isolate ELVs. ELVs were then stored at -80°C until further use.

3.2.7 RNA isolation and ELV cargo quantification

RNA was isolated from 1.00×10^6 particles of ELVs or sEVs using the miRNeasy Micro Kit (Qiagen, Germantown, MD) as per manufacturer's protocol. Total isolated RNA

concentration was quantified (NanoDrop One, Thermo Fisher Scientific) and miR-126 encapsulation in ELV and sEV groups was detected through standard curve Real Time quantitative polymerase chain reaction (RT-qPCR) on a StepOnePlus system (Applied Biosystems, Foster City, CA). Data were represented as miR-126 RNA mass.

3.2.8 ELV internalization

ELV internalization by CECs was observed by confocal laser scanning microscopy and quantified through flow cytometry. Briefly, CECs cultured until 90% confluency were seeded at 0.20×10^6 cells/mL in 40 µL/well onto 6-channel cell culture slides (IBIDI sticky Slide VI 0.4, Fitchburg, WI) pre-coated with 0.1% gelatin. Slides were incubated for 3-4 hours until CECs adhered after which channels were filled until 180µL to avoid channel drying and incubated at 37°C overnight. CECs were then quiesced in endothelial bare media (FBS and growth factor free) with 1% penicillin-streptomycin for 12 hours. After 12 hours, CECs were treated with sEVs or miR-126+ELVs stained with membrane dye calcein (Thermo Fisher Scientific) at 5.00×10^8 particles per 1.00×10^6 cells and incubated at 37°C for 2-3 hours. Next CECs in channels were fixed with 4% paraformaldehyde and stored at 4°C. Prior to imaging, CEC were stained with LysoBrite NIR (AAT Bioquest, Sunnyvale, CA) and DAPI (Thermo Fisher Scientific) and incubated at 37°C for 30 minutes to visualize vesicle trafficking to the lysosome. Slides were imaged with confocal laser scanning microscope (Olympus FV1000, Center Valley, PA).

For quantification, CECs were cultured until 90% confluency and then seeded at 0.05×10^6 cells/well into 24 well plates pre-coated with 0.1% gelatin. After incubation for

attachment, CECs were then quiesced overnight in endothelial bare media (FBS and growth factor free) with 1% penicillin-streptomycin. CECs were treated with calcein-stained sEVs or miR-126+ELVs at 5.00×10^8 particles per 1.00×10^6 cells and incubated at 37°C for 2-3 hours. CECs were then washed to remove free vesicles, collected, and resuspended in flow buffer (2% FBS in PBS). Internalization of sEVs and ELVs was quantified through flow cytometry (Cytek Aurora, Fremont, CA) for $\lambda_{Ex}/\lambda_{Em}$ = 495/515 nm. Negative control was CECs treated with calcein-stained ELVs or sEVs and incubated at 4°C to inhibit uptake.

3.2.9 Live-dead/Cytotoxicity Assay

For qualitative assessment, CECs were cultured until 90% confluency and were then seeded at 50,000 cells/well into a 96 well plate and incubated overnight for attachment. CECs were then quiesced in endothelial bare media (FBS and growth factor free) overnight with 1% penicillin-streptomycin. CECs were then treated with 5.00×10^8 sEVs or miR-126+ ELVs per 1.00×10^6 cells and incubated for 48 hours. CECs were then stained with 0.003 mM calcein-AM (live dye, Invitrogen) and 0.004 mM ethidium-homodimer-1 (dead dye, Thermo Fisher Scientific) for 30 minutes in full media followed by 3 washes with PBS. CECs were then imaged using a fluorescent microscope (Olympus IX71) such that each well had 1 image corresponding to one technical replicate (with biological replicates used for data analysis). Cells without sEV/ELV treatment were used as controls.

For quantitative assessment, CECs were again seeded into 96 wells and treated in the same manner with incubation for 48 hours. After 48 hours, 3 wells of untreated cells were killed

with 0.1% Triton-X, as a negative control, by incubating at 37°C for 15-30 minutes. After this, the cell lysate was collected from all samples and spun down at 1000 RPM for 5 minutes (Centrifuge 5810 R, Eppendorf) to deplete any detached cells. The conditioned media was then used to run the lactate dehydrogenase (LDH) assay (LDH Cytotoxicity Assay Kit, Cayman Chemical, Ann Arbor, MI), as per manufacturer's protocol. 0.1% Triton-X treated cells were used as negative control and cells without sEV/ELV treatment were used as positive controls.

3.2.10 Tube formation assay

CECs were cultured until 90% confluency. CECs were then quiesced in endothelial bare media (FBS and growth factor free) with 1% penicillin-streptomycin. Quiesced CECs were seeded at 10,000 cells/well onto µ-slide Angiogenesis slide (IBIDI) pre-coated with 10 µL/well Matrigel (Matrigel® Matrix, Corning) as per manufacturer's protocol. CECs were then treated overnight at 5.00×10^8 sEVs or miR-126+ ELVs per 1.00×10^6 cells. CECs were then stained with calcein-AM (Thermo Fisher Scientific) and imaged using a fluorescent microscope (Olympus IX71) such that each image captured one complete well, representing one technical replicate of a sample group. ImageJ software was used to quantify different tube length parameters (Fiji, National Institutes of Health, Bethesda, MD) [161]. The Angiogenesis Analyzer plug-in for ImageJ, specifically created to analyze the vascular organization of endothelial cells, was used to quantify images (three technical replicates per group)[162]. Output parameters of number of tubules, total tube length and total segment length were calculated, with lengths measured in pixels. Negative and positive

controls consisted of quiesced CECs with no treatment, and EGM-grown CECs with no treatment, respectively.

3.2.11 Statistical Analysis

All statistical analysis was performed using GraphPad PRISM 8 software (GraphPad, San Diego, CA) with specific testing details outlined in figure captions.

3.3 Results

3.3.1 sEVs successfully isolated and characterized from 2D CPC cultures.

Human CPCs were grown in 2D cultures until 90% confluency and sEVs were isolated from CPC conditioned media through differential ultracentrifugation (Figure 2A). sEV shape and presence of the bilayer membrane were detected through transmission electron microscopy (Figure 2B). Further, sEV size was within the expected range (147.4 ± 59.2 nm) and sEVs were isolated at approximately $8.87 \times 10^{10} \pm 8.42 \times 10^{9}$ particles/mL (Figure 2C).

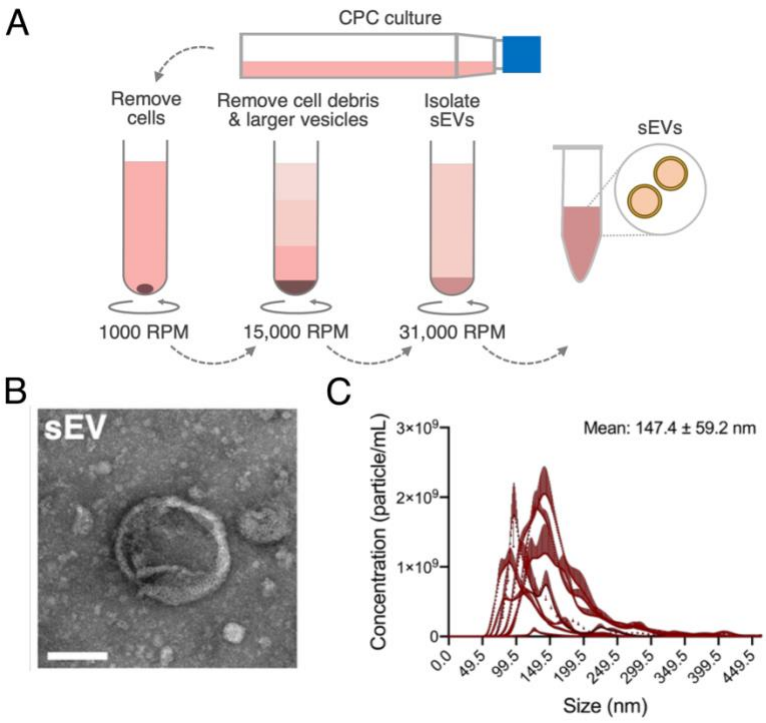

Figure 2. CPC-derived sEV isolation and characterization. (A) Workflow of sEV isolation from 2D cultures of CPCs with differential ultracentrifugation to sequentially remove cells, cell debris and larger vesicles. (B) Transmission-electron microscopy image of isolated CPC-sEV. Scale bar=100 nm. (C) Concentration-size profile of isolated sEVs with NTA. n=11.

3.3.2 ELVs on a sEV scale successfully synthesized with TFH with selective miR loading.

A modified version of the TFH method, used for synthetic vesicle formation, was chosen to synthesize ELVs from sEVs (Figure 3A). Briefly, initial sEV cargo removal was attempted through a combination of sonication and repeated freeze-thaw cycling. Following this, rotary evaporation was used to form a uniform lipid layer to which chosen miRNA, suspended in aqueous buffer, was added to initiate self-assembly of ELVs. ELV shape, similar to that of sEVs, was detected through transmission electron microscopy to show successful formation of vesicles (Figure 3B). The size profiles of ELVs were similar to that of sEVs (169.8 ± 93.4 nm vs. 147.4 ± 59.2 nm for sEVs) with no significant

difference observed (Figure 3C and D). Further, ELV concentration was similar to that of sEVs at $3.49 \times 10^{10} \pm 3.14 \times 10^{9}$ particles/mL, although there was greater batch-to-batch variation observed (Figure 3C and D). This variability is likely due to sample loss during the multi-step ELV synthesis. The polydispersity index of ELVs was 0.20 ± 0.055, suggesting a uni-modal population, and that of sEVs was 0.33 ± 0.006 with no statistical difference between the two groups (Figure 3E). Overall, ELV external structure matched that of the sEVs.

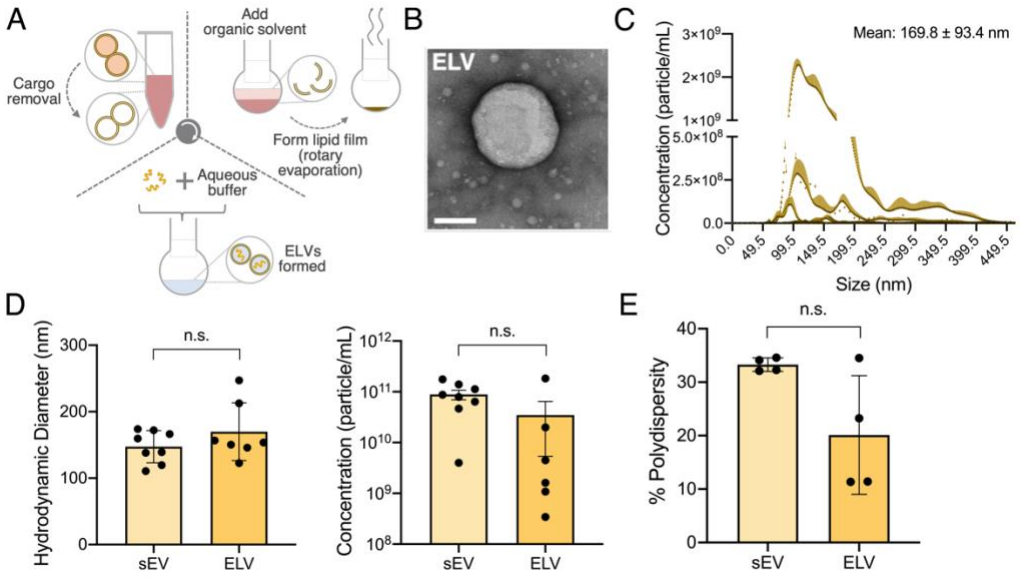

Figure 3. Synthesis and characterization of sEV-derived ELVs using a modified TFH method. (A) Workflow of ELV synthesis from CPC-sEVs by depleting sEV cargo, forming a lipid film and rehydrating with customized miR. (B) Transmission-electron microscopy image of an engineered ELV. Scale bar=100 nm. (C) Concentration-size profile of an ELV with NTA. n=10. (D) Comparison of ELV and sEV size and concentration. (E) Comparison of percentage poly-dispersity of ELVs and sEVs. n=4-8. Mean±SEM. Significance was tested with two-way, Student's paired *t* test. n.s.=not significant.

To demonstrate cargo loading ability, miR-126-5p was loaded into the ELVs. miR-126 was specifically chosen as it has low abundance in CPC-sEVs but is implicated in

cardioprotective endothelial function, so its presence would indicate successful active loading [163]. After ELV synthesis, post-processing was performed to stabilize the ELVs, deplete larger particles and unencapsulated miRNA (Figure 4A). miR-126 cargo was encapsulated in ELVs with an average of 34.9 pg RNA per 1.00×10^6 particles, a large increase compared to sEVs (miR-126 not detected), highlighting the scope of this modified TFH method for selective and tailored cargo enrichment (Figure 4B).

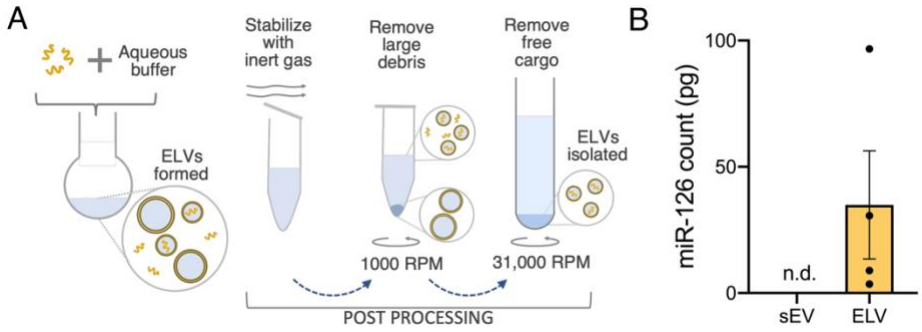

Figure 4. miR-126 was encapsulated into ELVs with the modified TFH. (A) Workflow of ELV post-processing to stabilize ELVs, remove larger debris and cargo-free vesicles, remove free un-encapsulated miRNA cargo and isolate miRNA+ELVs. (B) Quantification of endothelial specific miR-126 loading into ELVs as compared to presence in sEVs as counts per 1.00×10^6 particles. n=4. Mean±SEM. n.d.=not detected.

3.3.3 miR-126+ ELVs are taken up by CECs and do not impair CEC viability

miR-126+ ELV uptake by CECs was confirmed qualitatively with confocal laser scanning microscopy (Figure 5A). Calcein+ ELVs are taken up by the CECs, similar to sEVs, without primary trafficking into the lysosome for degradation. Quantitative analysis of ELV and sEV uptake through flow cytometry shows ELVs were taken up to a similar extent to that of sEVs, with no statistical difference between ELV and sEV internalization (Figure

5B). Further, treatment of CECs with ELVs or sEVs did not affect CEC viability after 48 hours incubation, indicating miR-126+ ELVs are not cytotoxic (Figure 6).

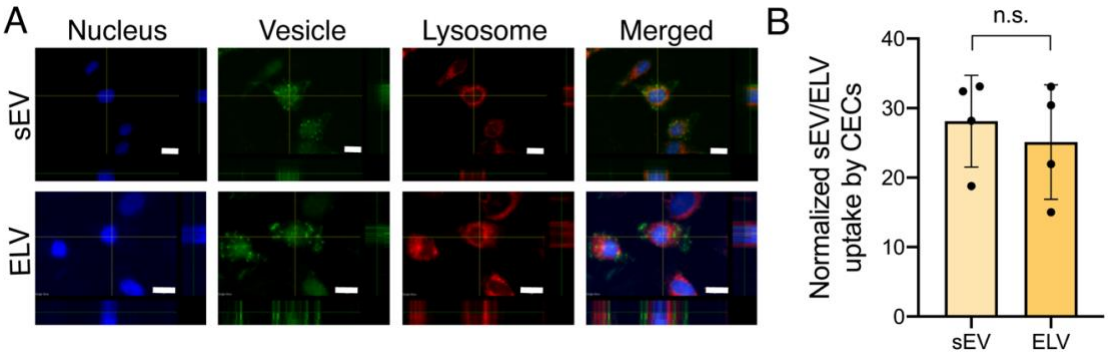

Figure 5. miR-126+ ELVs are successfully taken up by CECs. (A) Representative images of calcein stained ELV and sEV (green) uptake by 2D CEC cultures labelled for nuclei (blue) and lysosome (red). Images were obtained by confocal laser scanning microscopy from central focal plane with orthogonal images on right and bottom. Scale bar=10 µm. (B) Quantification of uptake of calcein+ ELVs and sEVs by CECs through flow cytometry. Data normalized to negative control. n=4. Mean±SEM. Significance was tested with two-way Student's paired *t* test. n.s.=not significant.

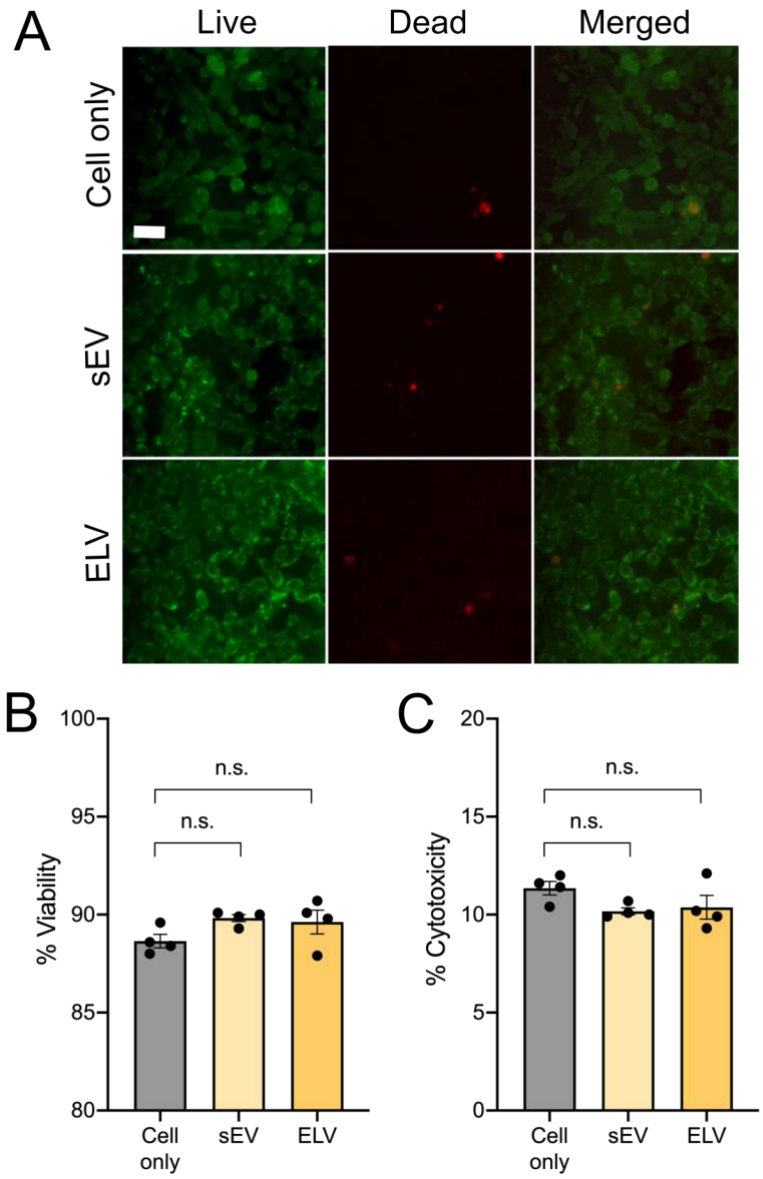

Figure 6. miR-126+ ELVs are not cytotoxic when administered to CECs. (A) Cell viability images of CECs after 48 hours incubation with miR-126+ ELVs or sEVs as measured by fluorescence microscopy. Green (live): calcein-AM and red (dead): ethidium homodimer-1. (B) Viability and (C) Cytotoxicity of CECs from panel (A) as measured with the LDH assay. Data shows no significant difference in viability or cytotoxicity both qualitatively and quantitatively after administration of ELVs or sEVs. Data normalized to negative control (0.1% Triton-X treated CECs). n=4. Mean ± SEM. Significance was tested with one-way ANOVA. Scale bar = 25 μm.

3.3.4 miR-126+ ELVs induce tube formation in CECs

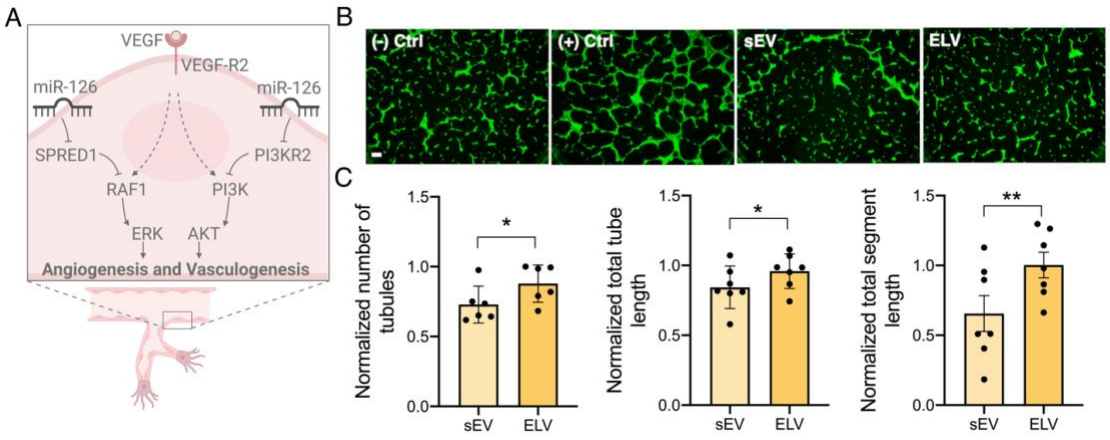

Figure 7. miR-126+ ELVs induce pro-angiogenic response in CECs. (A) Schematic of miR-126 mechanism of action for angiogenesis. VEGF: vascular endothelial growth factor; RAF1: rapidly accelerated fibrosarcoma proto-oncogene; ERK: extracellular signal regulated kinase; AKT: protein kinase B; PI3K: Phosphoinositide 3-Kinase. (B) CECs (green) treated with miR-126+ ELVs or sEVs incubated on Matrigel form tubes after overnight incubation. CECs treated with calcein-AM. Scale bar=200µm. (C) Quantification of angiogenic parameters (ImageJ software) shows increase in number of tubules, total tube length and segment length for CECs treated with miR-126+ ELVs compared to sEVs. Data normalized to negative control. n=6-7. Mean±SEM. Significance was tested with two-way Student's paired *t* test. *p≤0.05, **p≤0.01.

Next, to validate the functional effect of miR-126+ ELVs, angiogenic potential was assessed through the endothelial tube formation assay. miR-126 is implicated in angiogenesis through the ERK and AKT pathways by targeting SPRED1 and PI3KR2 (Figure 7A). The addition of both sEVs and ELVs induced the formation of tubes by CECs on Matrigel® Matrix (Figure 7B). However, treatment with ELVs increased the formation of tubules, tube length and segment length compared to sEVs (Figure 7C). This underscores the functional benefit and scope of customized cargo loading into vesicles.

3.3.5 CPC-derived ELVs synthesized with electroporation

Having established the synthesis and functionality of ELVs with selective cargo loading, we sought to address the batch-to-batch variability inherently present with the TFH method

of ELV synthesis. Further, for larger scale manufacture, an optimized process to improve time efficiency would also be beneficial. Hence, we explored electroporation as an alternative ELV synthesis method. Unlike the chemical approach of TFH, this method uses small voltage pulses to create temporary openings in the vesicle membrane (because of the formation of an potential gradient) which reseal when the voltage is removed (Figure 8A). During these membrane openings, miR of choice, present in the buffer, can get encapsulated into the vesicle down a diffusion gradient. We used this method to synthesize CPC derived ELVs are first confirmed their shape was similar to CPC sEVs (Figure 8B). Comparing the concentration profiles assessed through NTA, both sEVs and ELVs had similar profiles (Figure 8C). The electroporated ELV sizes were slightly higher than that of sEVs but still within the EV range of 30-150 nm (Figure 8D). Further, the ELV concentration was significantly less than that of sEVs, but the batch-to-batch variation was dramatically reduced with much smaller deviation ($1.30 \times 10^{10} \pm 7.73 \times 10^{9}$) between batches. Further, these vesicles were still on the 10^{10} scale which provided sufficient particles for downstream assessment. Finally, we determined the percentage polydispersity of these ELVs, which were similar to that of sEVs suggesting a similar modality in the samples.

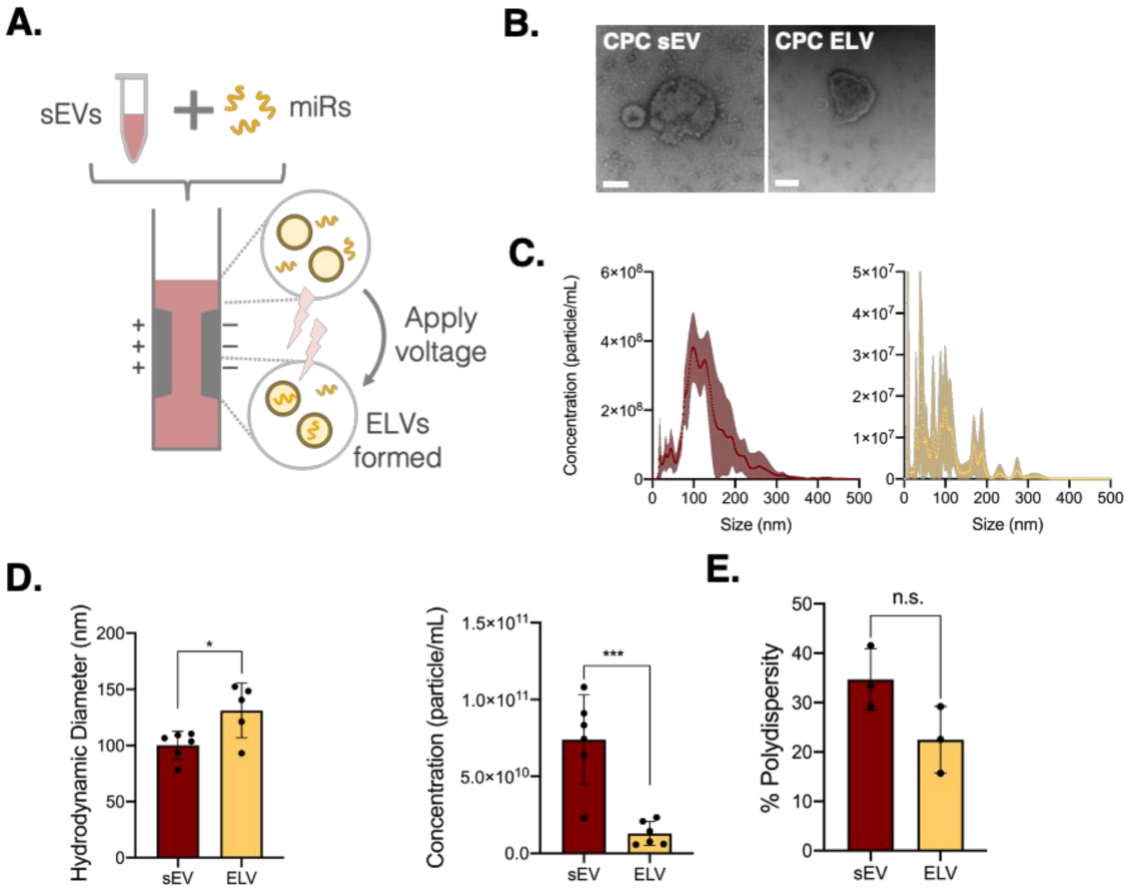

Figure 8. Synthesis and characterization of ELVs using an electroporation method. (A) workflow of ELV synthesis from CPC-sEVs by sonication-based cargo removal and electroporation-based miR-126 loading. (B) Transmission electron microscopy images of CPC sEV and electroporation-based CPC ELV. Scale bar = 100 nm. (C) Concentration-size profiles of CPC-sEVs and electroporated ELVs measured with NTA. (D) Comparison of ELV and sEV size and concentration. (E) Comparison of percentage polydispersity index of ELVs and sEVs. Mean±SEM. Signficance was tested with two-way Student's paired *t* test. n.s. = not significant. *P<0.05, ***P<0.001.

3.3.6 Electroporation of ELVs allows for cargo tunability

Having addressed the batch-to-batch variability by electroporating the ELVs, we next aimed to improve upon on cargo tunability with TFH. Given that the ELVs form by self-assembly, tuning the amount of cargo loaded was challenging. For scaling up the studies and usage of ELVs, we explored potential tunability of miR loading with electroporation.

First, we chose to optimize inherent RNA cargo depletion to provide a more uniform baseline of vesicle to synthesize the ELVs. For this we tried 4 different sonication and RNAse A treatments and observed that Method D (maroon plot) resulted in the maximum depletion, so we proceeded with that (Figure 9A). We then explored the effect of voltage pulsing on miR-126 loading into ELVs and found that greater pulsing (up to 8 pulses) allows for a significantly higher total miR-per-vesicle than the sEV group (Figure 9B). Further, the batch-to-batch variation in miR-loading was much less than with TFH, which addressed our initial concern. Therefore, moving forward we used Method D for cargo removal and 8 pulses during electroporate to load the cargo. We also confirmed that uptake of the electroporated ELVs by 2D cultures of CECs using flow cytometry and found that there is no significant difference in percentage uptake between sEVs and ELVs (Figure 9C).

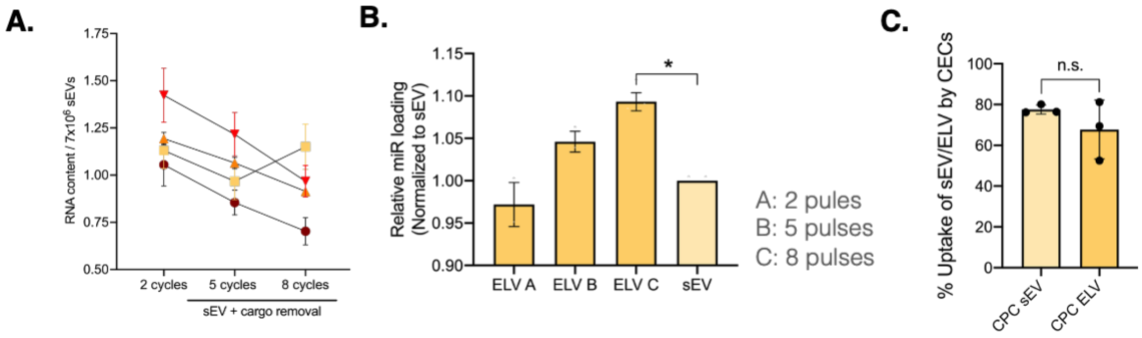

Figure 9. sEV cargo depletion, ELV cargo tunability and uptake. (A) Sonication-based cargo depletion from sEVs using different cycle lengths (2, 5 and 8 cycles) wherein 1 cycle is 3 minutes of 15 second on-off sonication pulses. (B) Tunability of miR-126 loading into ELVs by modulating the number of electroporation pulses in a square-wave electroporating setup. (C) Uptake of calcein+ sEVs and electroporated ELVs by 2D culture of CECs. Significance was tested with one-way ANOVA with Tukey post-hoc and two-way Student's paired *t* test. n.s. = not significant. *P<0.05.

3.3.7 Electroporated miR-126+ ELVs induce tube formation in CECs.

Finally, to confirm that the electroporated ELVs with miR-126 improve functional outcomes compared to sEVs (as did the TFH ELVs) assessed the effect of administering the electroporated ELVs to 2D cultures of CECs. Similar to with TFH ELVs, we administered the ELV or sEV treatment and incubated the CECs overnight on Matrigel to assess tube formation. All groups induced the formation of tubes after overnight incubation (Figure 10A). Upon quantification of tube formation parameters, we found that electroporated ELVs significantly increase total tube length and total segment length of the CECs compared to sEVs (Figure 10B). Given this functional improvement with ELVs, we moved forward with electroporated ELVs for all downstream studies.

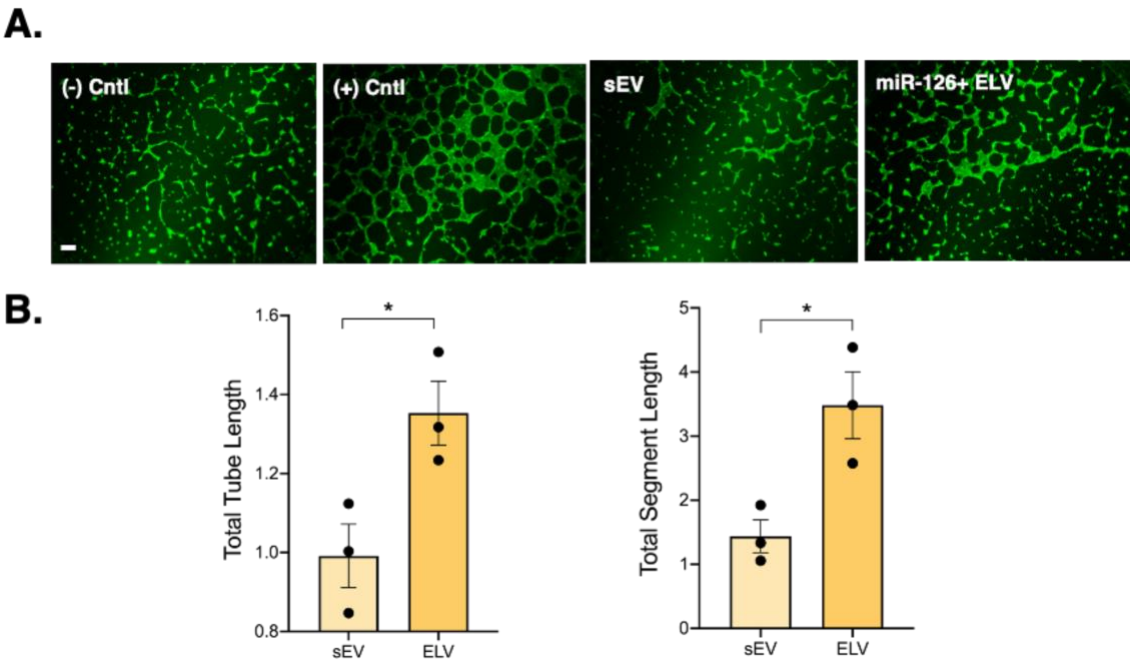

Figure 10. Electroporated miR-126+ ELVs induce pro-angiogenic response in CECs. (A) Calcein-AM+ CECs (green) treated with electroporated miR-126+ ELVs or sEVs incubated on Matrigel form tubes after overnight incubation. (B) Quantification of angiogenic parameters of total tube length and total segment length show increase in ELVs compared to sEVs. Data normalized to negative control. Mean±SEM. Significance was tested with two-way Student's pair *t* test. *P<0.05. Scale bar = 200 µm.

3.4 Discussion

CPC-sEVs are important mediators of cell-cell communication and specifically contain cardioprotective RNA and miRNA cargo crucial for cell-based cardiac repair after MI. Despite their therapeutic benefits, sEV cargo content is often variable, with limited external control of cargo composition. Synthetic mimics such as SUVs allow for such cargo modulation but suffer other challenges such as low stability and rapid clearance when administered, possibly attributed to their simpler membrane composition. In this study, we show the successful synthesis of CPC-sEV derived ELVs with select miRNA using TFH to combine the benefits of the sEV membrane with that of the SUV's custom cargo loading. Further, the results show the ability of such selective miR-loaded ELVs to be internalized by CECs and their functional scope to initiate pro-angiogenic effects *in vitro*. Next, having established the value of CPC-ELVs for functional improvements, we address the batch-to-batch variations in ELV synthesis and miR cargo loading by using another method of ELV synthesis, electroporation. We again confirm the characterization, uptake, and functionality of these electroporation ELVs. This updated method allows for reduced batch-to-batch variation in sample production and miR loading, thereby improving scalability. Taken together, these findings underscore the potential of ELVs to be potent and tunable alternatives to sEVs for cardiac therapies, and the value of further exploration in this field.

Different methods to exogenously modify sEV cargo have been studied, such as sonication, saponification, extrusion, and parent-cell transfection. However, these largely focus on slight cargo modifications, suffer inconsistent loading and typically do not clear inherent sEV cargo first, making it difficult to develop reliable and consistent miRNA-loaded sEV cardiac therapeutics. TFH is a well-established process for the synthesis of SUVs and other

synthetic vesicle mimics that utilizes the creation of a lipid-film. To address some of the limitations of purely artificial SUVs, hybrids of SUVs and sEVs have been created utilizing TFH and extrusion with sEVs. Specifically, hybrids designed from CPC-sEVs increased activity of AKT, a downstream target of miR-126 [164]. In this study, we take this idea of hybrids one step further, by utilizing a completely sEV-based membrane to form our sEV-scale ELVs (Figure 3A). With our modified TFH approach we allow for ELV creation from sEVs instead of pure lipids and aim to minimize the presence of inherent sEV cargo, to improve cargo consistency. Given the high encapsulation efficiency of TFH and the ability to modify TFH to develop sEV membrane-derived vesicles, the scope of TFH as a tool for exogenously modified sEVs is present. Thus, TFH can now be utilized to design other exogenously modified vesicles, as a counterpart to currently established methods such as sonication, saponification etc. Beyond this, the modified TFH method established here also allows for versatility in synthesis by allowing ELV engineering from any parent cell type-derived sEVs beyond CPC-sEVs. However, given the batch-to-batch variability of TFH and the ELV self-assembly process during rehydration in an aqueous buffer, larger starting samples may be required for large scale ELV production.

To address the batch-to-batch inconsistency in ELV synthesis and miR loading present with TFH, after validating the benefit of ELVs, we explored synthesizing ELVs with alternative methods. We again integrated this with our sonication-based cargo depletion method to deplete inherent cargo first and allow for less variability in vesicle cargo prior to loading our cargo of choice. Of the different liposome/vesicle loading methods developed recently, electroporation is considered beneficial for small non-coding RNA which yields sufficient loading efficiency and uses minimal toxic additives[87,139,165].

However, electroporation has previously been shown to aggregate siRNA and partially encapsulate RNA into the membrane instead of cytosol, thereby not having as much potency when exposed to RNAse enzymes[166]. This concern was mitigated by increasing the concentration of vesicles used for miR-loading, which was suggested to reduce aggregation, and using higher initial miR concentrations to incentivize diffusion into vesicles[166]. Further, samples were post-processed with RNAse enzymes before ultracentrifugation, to deplete partially encapsulated miRs before downstream characterization. Another concern with electroporation of small vesicles is that their smaller diameters provide more structural stability and therefore, higher voltages and more pulses are required to induce temporary permeabilization[167]. This can damage the membrane and induce aggregation of nucleic acids, particularly when loading multiple cargoes[165,168]. Here, to be mindful of this, we assessed the pulse-to-miR encapsulation and chose the least number of pulses required for miR-loading. However, in this study we only load one miR, if multiple miR loading was desired in the future, the concern of nucleic acid aggregation should be further investigated.

An important aspect of sEV-based therapies is sEV uptake or endocytosis for cargo trafficking. Several mechanisms of sEV uptake have been established including direct fusion, clathrin or caveolin-mediated endocytosis, lipid-raft mediated endocytosis and macropinocytosis [169]. Although the role of exact membrane components is underexplored, sEV membrane components such as PS have been implicated in sEV uptake processes [170]. Further, given the challenges of systemic clearance with synthetic sEV mimics, this further highlights the potential benefit of an sEV-like membrane in ELV composition. Here, we show that the uptake of ELVs is similar to that of sEVs, despite their modified cargo,

without active trafficking into the lysosome for degradation (Figure 4A and B) which indicates the importance of the vesicle membrane and warrants further study.

Upon internalization, the cargo composition of sEVs can drastically alter the cardioprotective effects of the sEV therapies [171]. Specifically, several miRs have been associated with angiogenesis, anti-fibrosis and ischemic recovery after MI, but the incorporated miRNA profile is dependent on external factors such as parent cell type (e.g., CPC or MSC), age and culture conditions, limiting our control over the cargo [9,60,172]. Further, despite their benefit, miRNA yield in sEVs is very limited, minimizing sEV potency [154]. For this study, miR-126 was specifically selected as it is pro-angiogenic, involved in endothelial cell survival and repair, anti-inflammatory, anti-fibrotic and anti-hypertrophic, making it a favorable miRNA for myocardial recovery after ischemia [173–176]. The encapsulation of miR-126 in TFH and electroporation-synthesized ELVs allows incorporation of miRNA of choice, not only enriching pro-reparative miRNA but also loading cardioprotective miRNA with low expression levels in the corresponding sEVs (Figure 3B).

Prior studies of CPC-sEVs have shown their pro-angiogenic potential and several inherent sEV-miRNA associated with angiogenic function [88]. Here, the results show that the functional effect of miR-126+ ELVs was also confirmed through endothelial tube formation (Figure 5B and C). Interestingly, ELVs increased tube formation parameters compared to sEVs despite being actively loaded with only one miRNA. This highlights the further scope of ELV-based therapies, particularly if higher doses or multiple miRs are loaded into the ELVs, allowing simultaneous targeting of several MI-relevant outcomes (e.g. fibrosis, inflammation, hypertrophy). Further, with recent advances in RNA

sequencing, several miR associated with improvements in myocardial outcomes have been established [9,60,88]. This knowledge allows for most targeted and customized miR combinations to be loaded into ELV for repair after MI. In addition, ELVs also provide a vehicle for experimentally validating this repository of cardioprotective miRNA.

This study provides the groundwork for combining the benefits of sEV membranes and modulating inherent cargo. TFH allows for tailored miRNA-loaded ELV synthesis with functional improvements compared to sEVs, and electroporation allows for more controllable ELV synthesis and cargo-loading tunability. However, given the need of organic solvents in TFH lipid film creation, there is a possibility that sEV membrane proteins are denatured in ELVs. As membrane proteins can enhance cell-specific targeting of vesicles and immune evasion, attempts to preserve or re-incorporate membrane proteins would be valuable for minimally invasive, cardiac-specific ELVs. Further, for multiple miR loading into electroporated ELVs, the effect of voltage pulsing on miR aggregation should be assessed in more detail. In addition, in-depth study of the exact roles of different CPC-sEV membrane lipids and proteins and the effect of inner and outer leaflet lipid presence in sEV trafficking and uptake by cardiac cells will allow better selection of sEVs for ELV synthesis. In summary, an improved understanding of sEV membrane components and selection of pro-reparative miRNA for MI treatment will allow further advancement of the ELVs engineered in this study.

CHAPTER 4. TO ASSESS WHETHER ELV DELIVERY TO A FAILING LV MYOCARDIUM IMPROVES CARDIAC FUNCTION AFTER MI

4.1 Introduction

Clinical trials assessing cardiac cell therapy for recovery after MI show increases in viable heart mass, improved contractility, and reduced scar mass[177]. Moreover, a trial investigating the combinatorial effect of CPCs and MSCs for heart failure, found improvements in patient quality of life and major adverse cardiac events. Although these trials involve direct cell therapy administration to patients, sEV based signaling likely plays a key role in the observed effects. In fact, studies have found that the improvements observed from stem or progenitor cell therapies might not be directly affected by the cell implantation but rather through the paracrine factors, specifically sEVs, that the cells release[77,178].

In animal models, sEVs are known to induce cardiac repair when administered after MI[9]. Prior studies in rodent models using MSC- and adipose derived stem cell-sEVs found improvements in cardiac function specifically through improvements in LV ejection fraction and fractional shortening[179,180]. In a porcine model of MI, cardiosphere-derived-sEVs decreased infarct size and promoted neovascularization[97]. Similarly, in a rat model of MI, CPC-sEVs reduced infarct size and improved ejection fraction[92]. Although sEV therapies in animal models are still in a more nascent stage, particularly those derived from

CPCs, these findings show that sEVs can be therapeutic and can have similar cardiac benefits as the direct delivery of the parent stem or progenitor cells.

However, a limitation with these current sEV studies is the extent of the improvements. The *in vivo* therapeutic benefit results in roughly ~3% increase in echocardiographic parameters[181]. In addition, the reparative capacity of the sEVs is cell dependent and varies based on CPC conditions such as microenvironmental oxygen levels and parent cell age[58,60]. Specifically, sEVs derived from younger CPCs and in hypoxic conditions have been more reparative. Further, it's shown that the miR cargo profile of sEV also differs with changes in parent cell conditions. All this suggests that despite the reparative capacity of CPC sEVs, there is high variability in outcomes. This is reflected across the animal studies wherein the therapeutic benefits and improvements are inconsistent across studies.

One avenue for this variability is the cargo present within the sEVs. Synthetic mimics on the sEV scale minimize the cargo variability but experience rapid wash out when administered *in vivo*. Therefore, there remains value is understanding the effect of ELVs derived from CPC-sEVs. Unlike completely synthetic mimics, ELVs being sEV-derived likely maintain a similar membrane to that of the CPC sEVs which could aid in their uptake when delivered *in vivo*. Further, they allow for cargo customizability, especially for large scale cardiac therapies, and thereby could bolster the reparative effects observed from sEVs *in vivo* and minimize the batch-to-batch variations.

In this study, we engineered miR-126+ ELVs with a modified sonication-electroporation approach (Chapter 3). We used a rat model of IR with temporary ligation of the left anterior descending artery (LAD) as our animal model of MI. We chose an acute model of MI, to

recapitulate the desired clinical case where patients ideally receive treatment within 3 hours of MI onset, and injected our ELV treatment immediately after IR. The animals were assessed for 28-days and we report global and regional echocardiographic responses as well as tissue level assessment of infarct size, fibrosis, and hypertrophy. Given the ELVs are loaded with miR-126, an endothelial specific marker, we investigate vessel histological improvements as well.

The objective of this work was to validate the therapeutic benefit of ELVs in an *in vivo* environment, and to also assess the response of loading selective miR-cargo into the ELVs when compared to direct delivery of CPC-sEVs. Our findings show that the global cardiac functional response with both sEVs and ELVs is variable, similar to prior animal studies. However, at the tissue level, ELV administration reduced infarct size, improved fibrosis, and improved hypertrophy. Interestingly, miR-126+ELVs increased several vessel-specific parameters at the tissue level, which is crucial for recovery after the onset of ischemia. This study underscores the value of maintaining an sEV-like membrane while allowing customizable cargo loading and confirms that the benefits seen with miR-126+ELVs *in vitro* can translate *in vivo* as well.

4.2 Materials and Methods

4.2.1 CPC sEV isolation

2D cultures of CPCs (~100×10^6 cells between passages 11-15 were grown to 90% confluency in Hams-F-12 media. Upon reaching confluency, the CPCs were transferred to

serum-free media (FBS and growth factor-free) and cultured for 24 hours after which the conditioned media was collected. sEVs were isolated from the condition media with differential ultracentrifugation (Optima XPN-100, Beckman Coulter). Briefly, the CPC conditioned media was depleted of cells at 1000 RPM for 5 minutes (Centrifuge 5810 R, Eppendorf,), depleted of cell debris at 15,000 RPM for 20 minutes (SW32Ti, Beckman Coulter) and then sEVs were pelleted at 31,000 RPM for 114 minutes (SW32Ti, Beckman Coulter) [160]. The sEVs were collected from the bottom 500-1000 µL fraction, resuspended in PBS as required and stored at -80°C until further use.

4.2.2 CPC ELV synthesis

For the animal studies, ELVs were synthesized from the sEVs using a modified electroporation method. For this, sEVs were depleted of inherent cargo and then cargo of choice was selectively loaded. First, inherent cargo was depleted from 3-4 $\times 10^9$ CPC sEVs with repeated sonication cycles. For this, samples were treated with 100 µg/mL RNase A (Thermo Fisher Scientific) and sonicated at #3 with probe-tip sonicator for 8-10 cycles (each cycle consisted of a 3 minute-duration of 15 seconds on/off sonication, with samples kept on ice during off-cycles to minimize sample heating). Samples were then incubated for 30 minutes at 37°C with constant rotation. Next, samples were treated with 40 units/20 µL ribonuclease inhibitor (RNAseOUT, Invitrogen, Carlsbad, CA) and 1 mM DTT (Invitrogen) and the sonication step was repeated for another 8-10 cycles. Samples were then incubated for 1 hour at 37°C with constant rotation and then stored at -20°C overnight. Samples were then electroporated with 100 pmol miR-126 (Gene Pulser Xcell, Bio-Rad, Hercules, CA) in 0.1 cm electrode gap cuvettes using 2-10 pulses (750 Volt square wave, with 5 ms pulses). Samples were then neutralized with cold serum-free Ham's-F-12

medium and incubated for 30 minutes at 37°C with rotation followed by overnight incubation at 4°C. Any unbound miR-126 and larger debris was removed through differential ultracentrifugation (Optima XPN-100). Larger debris was depleted after centrifugation at 1000 RPM for 5 minutes (Centrifuge 5810 R), smaller debris after ultracentrifugation at 15,000 RPM for 20 minutes (SW32Ti, Beckman Coulter) and finally the ELVs were pelleted after ultracentrifuging at 31,000 RPM for 114 minutes (SW32Ti, Beckman Coulter). ELVs were resuspended in PBS and stored at -80°C until further use.

4.2.3 Rat LV IR model

All studies were approved by the Emory Institutional Animal Care and Use Committee. Adult male Sprague-Dawley rats were obtained from Envigo RMS LLC. Rats aged 5-6 weeks old weighing 150-175 g were used for all studies. After 1 week for acclimatization, rats were subject to IR injury as described previously[182]. Briefly, the animals were subject to anesthesia (1-3% isofluorane) and the LAD artery was occluded for 30 minutes using an 8-0 prolene suture (Ethicon, Raritan, NJ). After occlusion, suture is removed to initiate reperfusion injury. Two studies were performed, first a dosage study to determine final ELV treatment dose, next the main study with the finalized dosages. Immediately after reperfusion, animals were subject to one of the treatment groups (refer next section) depending on if it was the dosage or main study. Sham rats underwent the same procedure except for ligation of the LAD. After completion of surgery, animals were housed at the Emory Animal Research Facility.

4.2.4 sEV or ELV treatment in-vivo

Administration of all treatments was in a randomized and blinded manner. Treatment groups included: sham, IR-only (saline treatment), sEV low, sEV high, ELV low, ELV high. For the dosage study, miR-126+ELVs are 2.5, 5.0 and 10.0 µg/kg were administered in 150 µL saline or saline only. For the main study, sEVs or miR-126+ELVs at 5.0 or 10 µg/kg were administered in 150 µL saline or saline only. Treatments were injected into 3 areas of the ischemic border zone with a 30-gauge insulin syringe (Ultra-fine needle, BD, Franklin Lakes, NJ).

4.2.5 Infarct size staining and quantification

Twenty-four hours after IR surgery, each animal's myocardium was accessed again through the initial surgical incision, and the LAD was re-ligated with a suture left in place during the initial IR surgery. The LV wall was then injected with 50-80 µL of Evans blue dye, adjusted for heart size, to perfuse the remote myocardium. The heart was then resected and washed in a Petri dish of PBS to remove excess Evans blue dye and blood. The heart was then wrapped in Saran wrap and stored at -20°C to -80°C to solidify the tissue. After solidification, the heart was cut into 1.5-2 mm slices along the short axis (SAX) with a cold blade atop a pre-frozen granite tile. Cut cross-sections were then incubated with freshly made 1% 1-2-3 triphenyl tetrazolium chloride (TTC) in 0.9% NaCl for 15 minutes at 37 °C, under constant rotation to expose the area at risk and area of necrosis[183]. The cross-sections were then fixed in 10% neutral-buffered formalin for up to 90 minutes and stored in PBS at 4°C until imaging. Samples were imaged using a Nikon DS600 camera and the area of necrosis (white region), area at risk (red region) and remote myocardium (deep blue region) were outlined and quantified using ImageJ software[161]. Area at risk was noted as a

percentage of the whole heart and area of necrosis was noted as a percentage of the area at risk.

4.2.6 Echocardiography and Strain analysis

Rats were anesthetized with inhaled 1-4% isoflurane and subject to echocardiography prior to surgery (baseline), at day 7, day 14 and day 28 post-surgery with a high frequency transducer. M-mode and B-mode SAX and parasternal long axis (PSLAX) views were taken using a Vevo 2100 digital high-frequency ultrasound system (FujiFilm Visualsonics, Loveland, CO) for global hemodynamic values and regional strain analyses respectively. An average of 3-6 consecutive cardiac cycles were taken for each measurement and this was taken 3 times per animal in a blinded manner. Data were analysed using VevoLAB software.

4.2.7 Histological tissue sectioning and staining

At day 28, after the completion of the study, animals were sacrificed, and the hearts resected. The hearts were fixed in 10% formalin overnight and then transferred to 30% sucrose buffer for 2-3 days until the sucrose penetrated through the tissue (and the hearts 'sank'). The hearts were then embedded in Optimal Cutting Temperature compound (Tissue-Tek, Fisher Scientific) and stored at -80°C. For histological analysis, embedded hearts were sectioned into 8 μm thick slices with the Leica CM1520 Cryostat and immunostained with isolectin-B4 (Vector Laboratories FL-1201) for capillary assessment, wheat germ agglutinin (WGA) (Vector Laboratories, RL10225) for hypertrophy assessment, and alpha-smooth muscle actin (SMA) (C6198 Millipore Sigma) or smooth muscle myosin heavy chain-11 (SM-MHC) (Ab50967, Abcam) for arteriole and vessel

assessment. The sections were also stained with picrosirius red connective tissue stain (Ab150681, Abcam) to assess myocardial fibrosis. All stained sections were imaged by the Cancer Tissue Pathology Core at 20X immunofluorescence or brightfield microscopy, as required.

4.2.8 Statistical Analysis

All statistical analysis was performed using GraphPad PRISM 8 software (GraphPad, San Diego, CA) with specific testing details outlined in figure captions.

4.3 Results

4.3.1 Intramyocardial delivery and uptake of vesicles

CPC-derived sEVs were isolated from CPC conditioned media and CPC-ELVs were engineered with miR-126+ cargo using the electroporation method described in Chapter 2. To assess the suitable concentration of ELVs required for in-vivo studies, a preliminary dose-response study was conducted (Figure 11A) by administering 3 doses of miR-126+ELV intramyocardially into the infarct site immediately after IR injury. The doses used were 2.5, 5.0 and 10.0 µg/kg of ELV in 150 µL of PBS. ELV treatment was injected into the infarct border zone in 3-5 sites, and sample delivery was detected as a cloudy region (Figure 11B). To confirm initial retention of sample, ELV pre-labelled with near-infrared fluorescent dye DiR (DiIC18(7);1,1′-dioctadecyl-3,3,3′,3′-tetramethylindotricarbocyanine iodide) were administered after IR and successful retention

of ELVs in the LV was assessed 24 hours after treatment with the IVIS Spectrum imaging system (Figure 11C).

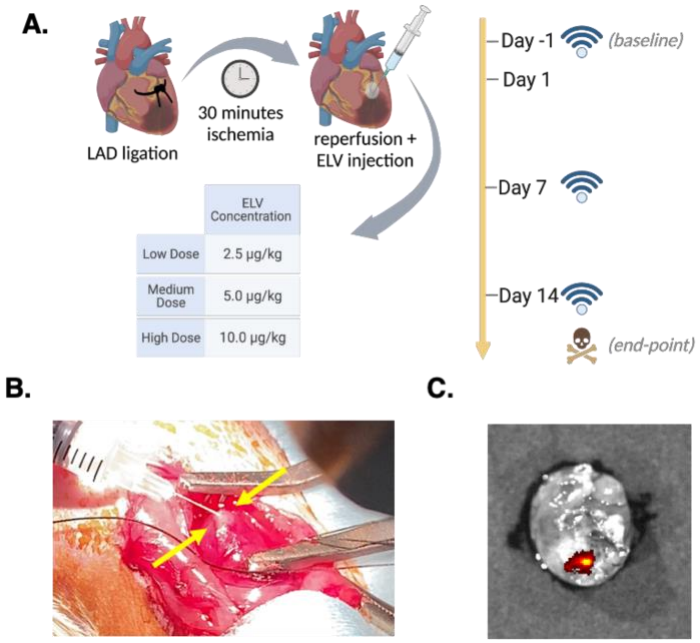

Figure 11. Injection of vesicles and retention of ELVs after 24 hours. (A) Workflow to determine suitable dosage of ELVs for main *in-vivo* study, low dose = 2.5 µg/kg, medium dose = 5.0 µg/kg and high dose = 10.0 µg/kg ELV. (B) Representative image of intramyocardially injected sEV/ELV into the rat LV immediately after removal of LAD ligation and LV reperfusion. Yellow arrows show one site of injection into the border zone, highlighted cloudy region corresponds to delivery of sEV/ELV sample (C) Representative image of *in vivo* live imaging of DiR+ELVs 24 hours after intramyocardial injection into border zone of rat LV myocardial wall.

4.3.2 Determination of suitable ELV dosage for LV myocardium

Cardiac function of animals was assessed over a 14-day period using echocardiography to determine if the ELV dosage affects global cardiac metrics. Trends showed that in both LV EF (Figure 12A) and FS (Figure 12B) there is dose-based variations with the ELV high group having consistently improved EF and FS at Day 7 and 14, compared to low or

medium groups. Further, as the sample administration after IR is targeted to the LV anterior wall (into the infarct border zone), segmental radial stain in the LV was also assessed (Figure 12C). Interestingly, the effect of treatment was more prominent in the anterior and apical segments compared to the posterior region, which corresponded to the injection sites. Given the ELV dose-based trends in cardiac improvement, we determined that higher doses of ELVs will be used for the main animal study. Further, to continue to explore the dose-based effects of treatment, two doses were selected, namely 5.0 µg/kg and 10.0 µg/kg of ELV.

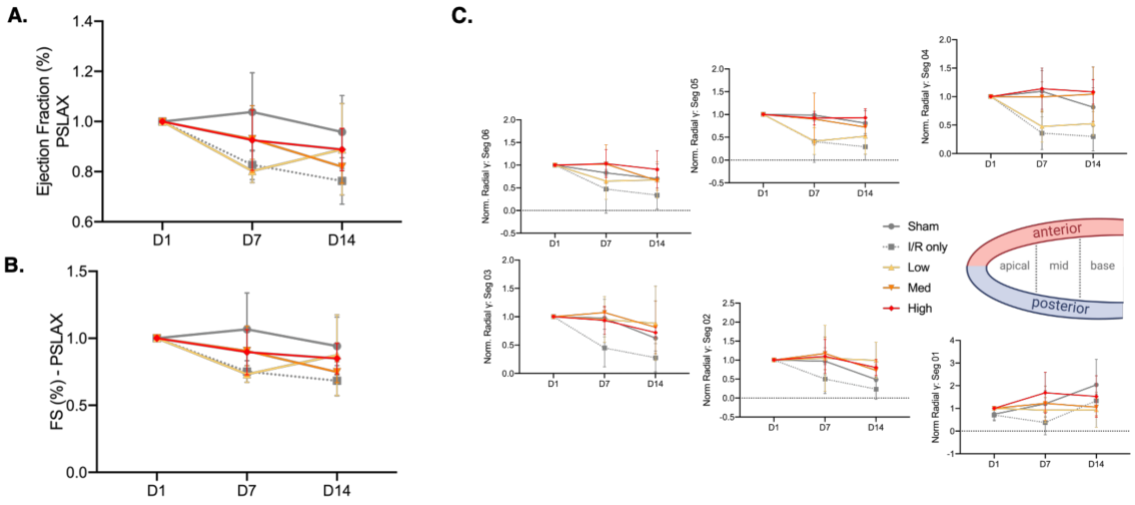

Figure 12. Dosed-based cardiac function across 14 days after ELV dosage treatment. (A) LV ejection fraction and (B) LV fractional shortening in PSLAX measured by echocardiography until Day 14 after ELV injection, normalized to D0. (C) Segmental radial strain in anterior (segments 4-6) and posterior (segments 1-3) LV wall, normalized to D0. Segments split into apical (3, 6), mid (2, 5) and base (1, 4) regions. Low = 2.5 µg/kg, medium = 5.0 µg/kg and high = 10.0 µg/kg of ELV in PBS.

4.3.3 ELVs significantly reduce infarct size in LV myocardium after 24 hours

For the main animal study, the same 30-minute IR model with immediately intramyocardial injection of treatment was used. Here, both CPC-sEV and ELV samples were administered at 5.0 or 10.0 µg/kg in PBS. To assess longer-term responses after treatment, the study was extended to 28 days, with some animals sacrificed at day 1 to assess infarct size (Figure 13).

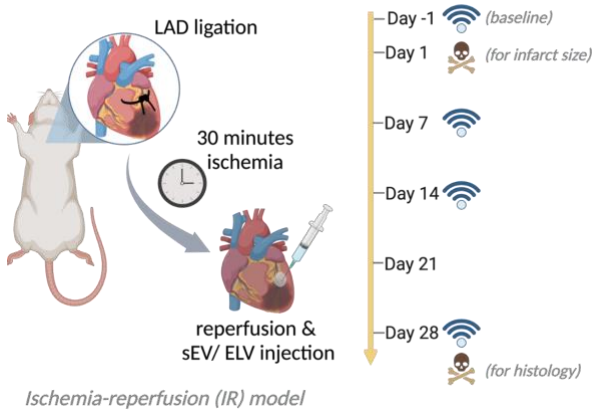

Figure 13. IR model and animal study workflow. Vesicle injection performed immediately after reperfusion to represent an acute model of MI. Echocardiography taken at baseline, Day 7, 14 and 28. Animals sacrificed 24 hours post IR for infarct size assessment and at Day 28 for histological analysis of myocardial tissue.

After 24 hours, infarct size was determined with TTC and Evans Blue dye staining. The Evans Blue stains the remote myocardium blue, the TTC stains the infarct area of risk red and the necrosed region of the infarct bleaches white. (Figure 14A). Sequential imaging of the whole myocardial tissue from apex to base was studied to account for slight variations in the exact infarct location. Upon quantification of area of necrosis (% area of necrosis/area at risk), both ELV low and high doses and the sEV high dose significantly reduced the infarct size compared to the IR control. Further, the ELV high group reduced the infarct size significantly more than the sEV low group, despite the short timepoint.

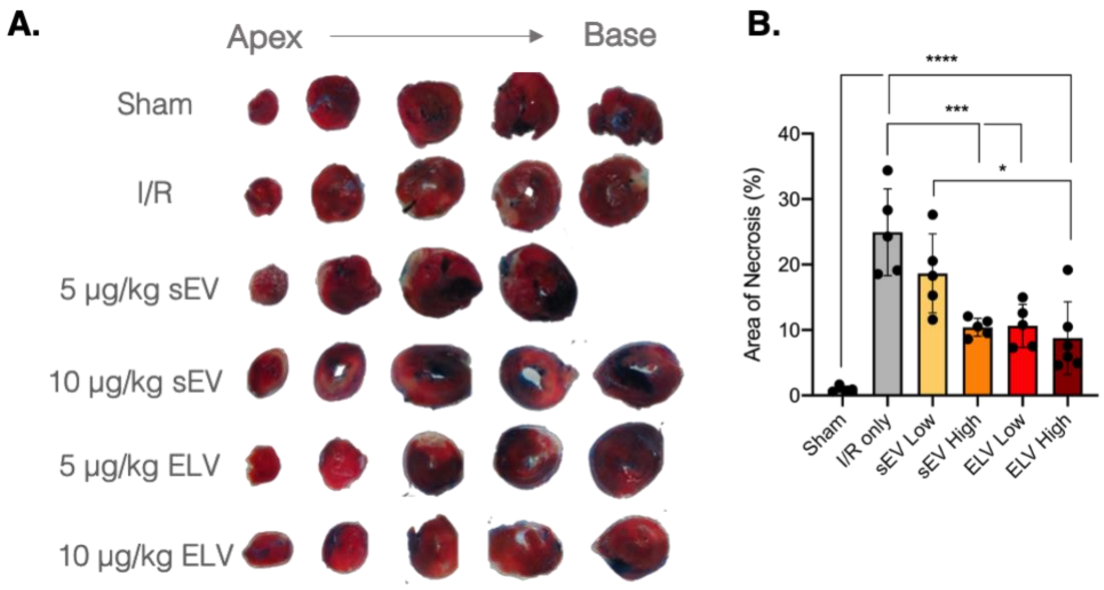

Figure 14. miR-126+ ELV administration reduces infarct size 24 hours after vesicle administration. (A) Representative images of myocardial tissue slices (thickness ~2 mm) from apex (left) to base (right) stained with 2,3,5-triphenyl tetrazolium chloride (TTC) and Evans Blue dye for infarcted and remote myocardium, respectively. (B) Quantification of percentage tissue necrosed within infarcted tissue. Low = 5 µg/kg and high = 10.0 µg/kg of ELV in PBS. Mean±SEM. Significance was tested with one-way ANOVA with Tukey post-hoc. *P<0.05, ***P<0.001, ****P<0.0001.

4.3.4 Treatment of vesicles improves myocardial function and improvements are more pronounced at Day 14

To determine the functional changes after treatment, LV EF (Figure 15A and B) and FS (Figure 15C and D) were assessed at Day 7, 14 and 28 and compared to baseline (D0) across the LV PSLAX and SAX. At Day 7, the sEV low and ELV low groups improved EF and FS compared to IR control in the PSLAX view, but these improvements reduced at 14- and 28-day timepoints. The sEV high and ELV high groups improved EF and FS compared to the IR control in the SAX view with the EF improvements sustaining till Day

14 with ELV high treatment. For all the groups, the functional improvements were no longer detected at Day 28.

At Day 14, the improvements in EF and FS across groups is not significant in the PSLAX view, with larger deviation in function within sEV groups than ELV high groups. However, within the SAX view at Day 14, both sEV groups and the ELV high group significantly improve LV EF compared to the IR control. In addition, the sEV low group and the ELV high group significantly improve LV FS in the SAX view as well. Given that ELVs primarily contain miR-126 unlike sEVs which contain multiple combinations of miRs, the similar global improvements observed between sEVs and ELVs are promising for ELV therapy.

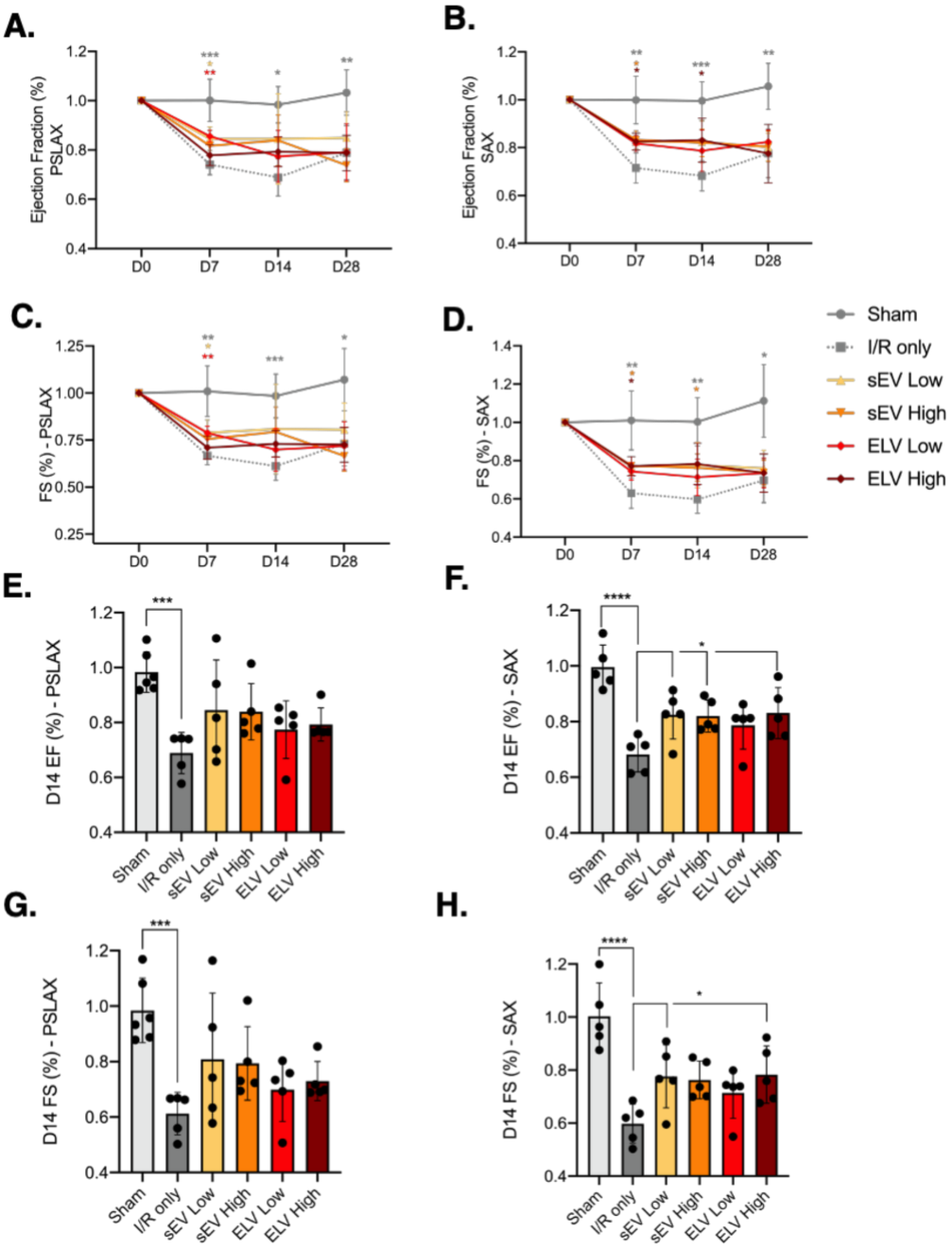

Figure 15. Changes in global myocardial function across 28 days after treatment with vesicles. (A, B) LV ejection fraction and (C, D) LV fractional shortening in PSLAX and SAX, measured at baseline, day 7, 14 and 28 after vesicle injection. (E-H) Differences in ejection fraction (E, F) and fractional shortening (G, H) as compared to IR group, at day 14. Mean±SEM. Significance was tested with two-way ANOVA with Dunnett's post hoc for A-D and with one-way ANOVA with Tukey post-hoc for E-H against the IR only control group. *P<0.05, **P<0.01, ***P<0.001, ****P<0.0001. Color of * corresponds to

experimental group: sham (grey *), sEV low (yellow *), sEV high (orange *), ELV low (red *), ELV high (dark red *). PSLAX = Parasternal long axis, SAX = short axis.

We also studied the segmental changes in cardiac function through radial strain analysis. Despite no statistically significant improvements, the effects of the treatment groups are more prominent on the apical wall than the posterior wall, with a marked improvement in ELV high-based response at Day 14 in segments 04-06. Similar to the ELV-dosage study response (Figure 12C), this corresponds to the treatment injection site which is into the infarct border zone of the free LV wall.

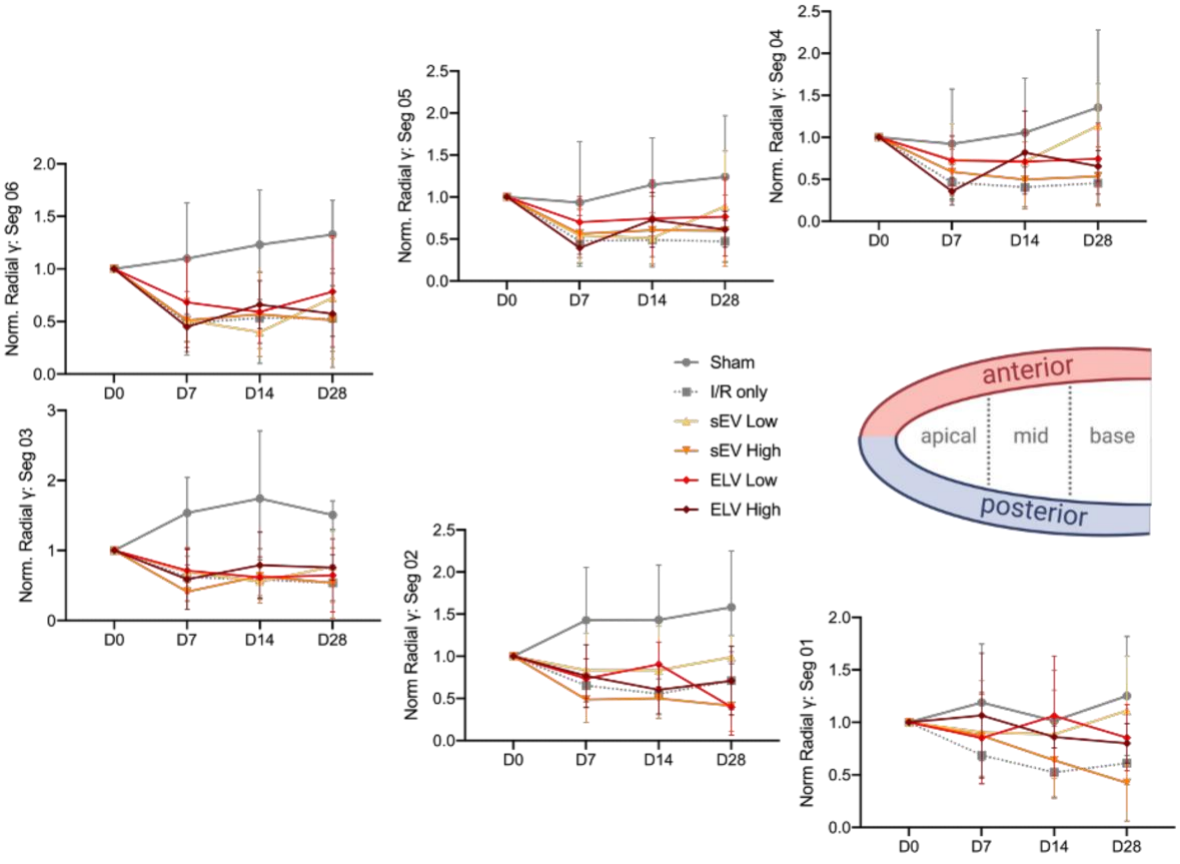

Figure 16. Changes in segmental cardiac function across 28 days after treatment with vesicles. Segmental radial strain in the anterior (segments 4-6) and posterior (segments 1-3) LV wall, normalized to baseline (D0). Segments split into apical (3, 6), mid (2, 5) and base (1, 4) regions.

4.3.5 ELV treatment significantly improves LV fibrosis and hypertrophy in the infarct border zone after 28 days

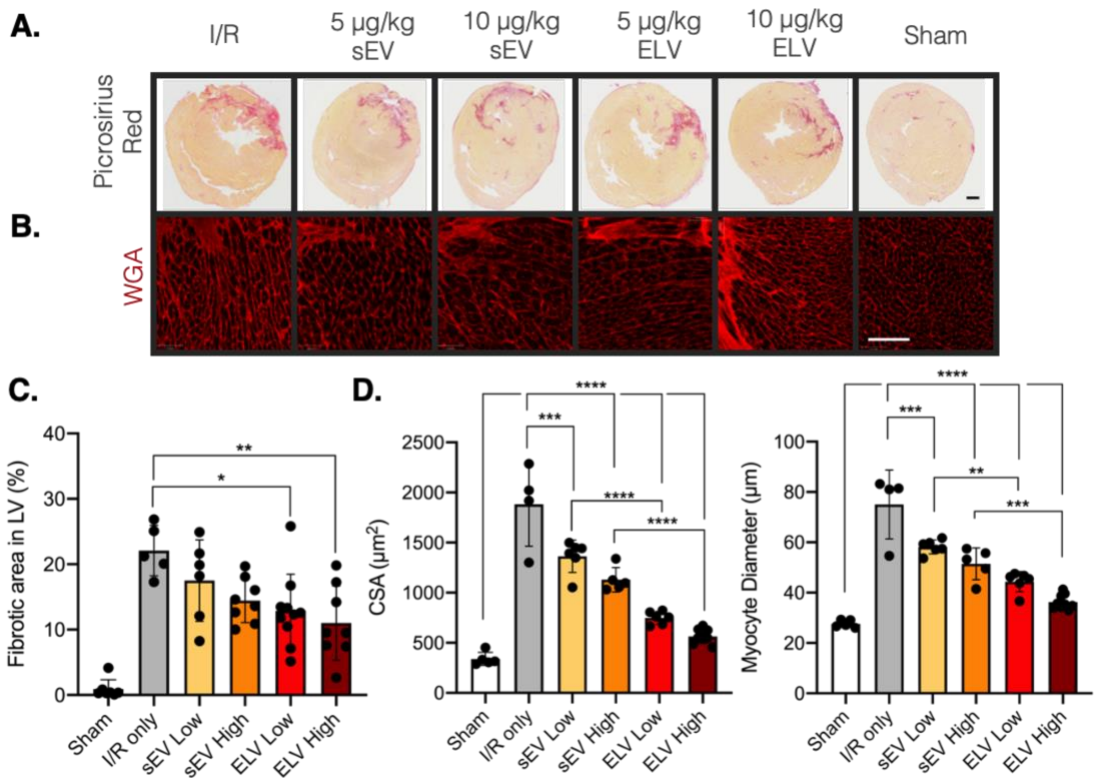

Figure 17. Administration of miR-126+ELVs reduces LV fibrosis and hypertrophy 28 days post treatment. (A) Representative images of Picrosirius red-stained myocardial sections and (B) WGA+ hypertrophic myocardium 28 days after vesicle treatment. (C) Quantification of fibrotic area in LV (pink) as percentage of total LV area. (D) Quantification of average myocyte cross-sectional area and myocyte diameter as measured from WGA+ images. Low = 5 µg/kg and high = 10.0 µg/kg of ELV in PBS. Mean±SEM. Significance was tested with one-way ANOVA with Tukey post-hoc. *P<0.05, **P<0.01, ***P<0.001, ****P<0.0001. Scale bar = 1.0 mm (A) and 100 µm (B).

After establishing that vesicle-based treatments have some effect on the global cardiac function, particularly in the SAX, we sought to understand the role of ELV treatment at the tissue-level. Animals were sacrificed at Day 28, sectioned and stained to look at histological parameters, as described in the methods section. Picrosirius-Red stain was used to mark connective tissue to assess LV fibrosis (Figure 17A) and WGA was used to bind

cell membrane glycoproteins and in turn assess LV hypertrophy (Figure 17B). Qualitatively, the representative images show a smaller fibrotic area per section and smaller myocyte size with vesicle treatment. Upon quantification, the fibrotic area in LV was significantly reduced by both ELV low and ELV high groups, unlike when sEVs were administered (Figure 17C). Further, the extent of improvement was more pronounced with the ELV high group ($p<0.01$) than ELV low group ($p<0.05$) suggesting a dose-based response. LV hypertrophy also reduced with vesicle treatment (Figure 17D), with both sEV groups and ELV groups significantly reducing myocyte cross-sectional area compared to the IR only group. Both sEV and ELV groups significantly reduced myocyte diameter compared to IR only as well. For hypertrophy, interestingly, the ELV low group significantly improved myocyte area and diameter compared to the sEV low group and similarly, the ELV high group significantly improved both hypertrophic parameters compared to the sEV high group. This shows a clear dose-based improvement with the ELV treatment compared to sEVs.

4.3.6 miR-126+ ELVs increase vessel density and size in LV after 28 days

Finally, we investigated the role of ELV cargo, miR-126, on the tissue-level cardiac response. Given miR-126 is an endothelial miR which has pro-angiogenic potential in-vitro, we chose to assess vessel-specific parameters in the LV after 28 days. Isolectin-B4 was used to detect capillaries and SMA and SM-MHC-11 to detect arterioles and larger vessels (Figure 18A). Qualitatively, differences in vessel density and in vessel size are noticeable between the experimental groups. For quantification, representative images

were taken on the endocardial and epicardial sides of the LV corresponding to either side of the infarcted region (as previously established by the WGA staining). The sEV high group and both ELV groups significantly increased LV capillary density compared to the control. Further, the ELV high group improved capillary density compared to the sEV low group. The ELV high group also increased the vessel size compared to infarct, and similar to the sham group. The ELV high group also significantly increased SMA-positive vessel size, and both ELV low and high groups increased SM-MHC-positive vessel size, which indicates that the miR-126 ELVs play a role in both the capillary and arteriole level. Combined, these results warrant the use of ELVs for cargo delivery and showcase that cargo tunability can have significant effects *in vivo*.

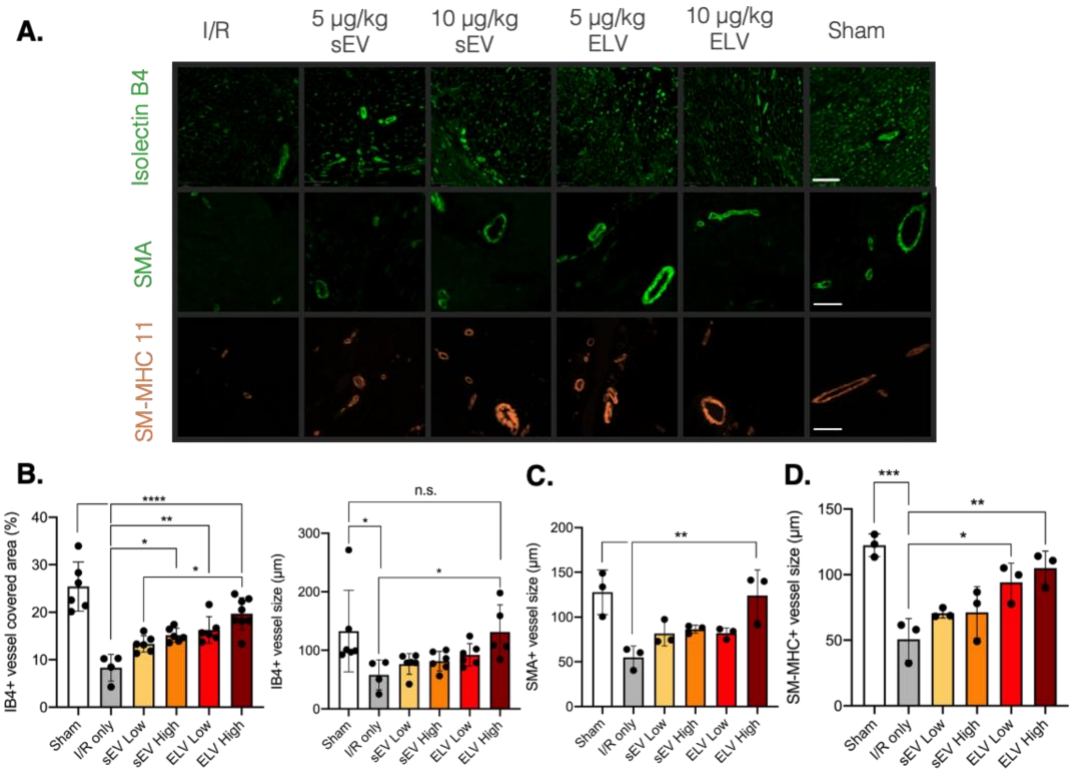

Figure 18. miR-126+ELVs increase vessel formation and vessel size 28 days after treatment. (A) Representative images of isolectin-B4+, SMA+ and MHC+ vessels in

ischemic myocardium 28 days after vesicle injection. (B) Quantification of isolectin-B4+ vessel area and vessel size in myocardium. (C,D) Quantification of SMA+ and MHC+ vessel size in myocardium. SMA = smooth muscle actin. SM-MHC = smooth muscle-myosin heavy chain. Significance was tested with one-way ANOVA with Tukey post-hoc. n.s. = not significant, *P<0.05, **P<0.01, ****P<0.0001. Scale bar = 100 μm.

4.4 Discussion

In vivo, sEVs are valuable therapeutics for cardiac repair and recovery after MI, with similar reparative effects to the delivery of stem or progenitor cells. However, despite their therapeutic benefits, the extent of improvement is often limited, with variability and inconsistencies in the observed repair and limited control over sEV cargo. Synthetic mimics mitigate some of the cargo-related variation, but they often suffer rapid wash out and loss when delivered *in vivo*. In this work, we show that the benefits observed with CPC-ELVs in Chapter 3 extend to an *in vivo* rat IR model when ELVs are administered intramyocardially. We observed global echocardiographic improvements in the SAX with the sEV and ELV high groups, though these are more variable across sEVs and ELVs. At the tissue level, we find significant reduction of infarct size after 24 hours, and a reduction in fibrosis and hypertrophy after 28 days. We also highlight the benefit of miR-126 with improvements in vessel parameters. Together, these data show the potential of ELVs as a vehicle for delivery of select miRs to the myocardium after MI and warrant further study into their therapeutic benefit.

In animal studies of MI, the IR model has been suggested to be a highly representative preclinical model for investigating cardiac therapies[184]. In patients, after suffering an acute MI, biotherapeutics or surgical interventions administered soon after the incident are

desirable to maximize the cardio-protection[185]. To recapitulate this rapid clinical response after an acute MI in the *in vivo* setting, there is value to administering the *in vivo* therapies right after the onset of IR. Moreover, a meta-analysis of 10 sEV-therapies for acute MI in small animal models shows that most sEV therapies are delivered between 0 to 60 minutes after the IR[181]. Based on these prior studies, to increase the clinical relevance of our work, and for ease of intramyocardial injection while the chest cavity is opened, we chose to deliver our CPC sEVs and ELVs immediately after IR.

However, it is well established that directly after IR, the native myocardium is undergoing significant remodeling and acute repair with chemokine and pro-inflammatory cytokine release, an influx of neutrophils, monocytes and macrophages and initial onset of fibrotic response and wound healing[186]. This complex interplay of injurious and reparative events at the intramyocardial level could affect the administration and cell-response to the sEV and ELV treatments, especially when they are delivered into the infarct border zone. In our study we found successful retention of ELV treatment after 24 hours and significant improvements at the tissue level, which suggest that despite the increase in cellular and paracrine activity in the infarcted zone, the ELVs did deliver therapeutic benefit. Having established that acute-delivery, similar to the clinical case, has its benefits, there would be value in assessing ELV delivery at later timepoints too. Echo-guided injections at Day 14 could be conducted, to separate the therapeutic benefits of the ELVs from the initial onslaught of cell and molecular response to the IR, so that we can develop a more complete understanding of the ELV's therapeutic role after MI.

In this study, we found that there were consistently significant improvements in histological parameters at Day 28, but on the global level significant improvements were

variable across time-points and tapered after Day 14. It should be noted that even within these improvements, no one group consistently improved global parameters over time. We suspect that the ELV treatments and miR-126 administration had tissue-level therapeutic benefit, but repeated or higher dosing could be required for that to translate to a global level. Moreover, the sample injection and the histological analysis was conducted in the infarct border zones, so perhaps despite cellular level repair in the immediate border, it is insufficient for a significant global improvement. In addition, the sEV and ELV dosing we used was 5.0 to 10 μg/kg, whereas several of the other small animal models for sEV therapies used doses from 0.2 to 2.0 μg/μL, an almost 1000-fold higher dosing[187,188]. Despite such high levels, their global functional improvements were around 3.7% with significant heterogeneity between groups, suggesting that with even higher doses, the ELV treatments, with selective cargo, could be more significant on the global scale as well.

In our ELV synthesis, we chose miR-126 as a proof-of-concept, as it is an endothelial specific marker and would clearly show successful cargo loading if administered to CPC-ELVs. Beyond this, miR-126 is known to be present in endothelial progenitor cell sEVs and CD34+ stem cell sEVs and is crucial for protecting endothelial cells against injury and for sEV proangiogenic nature *in vivo* after limb ischemia[189,190]. Similarly, miR-126 transfected MSCs also showed higher resistance to hypoxia and improved cardiac function when administered after IR[191]. Given that miR-126 is a major regulator of angiogenesis, we chose to continue using miR-126+ ELVs for our *in vivo* studies as well, with significant improvements detected in vessel density and size. However, to test the full scope of our ELVs, it would also be worthwhile to load other cardioprotective miRs (e.g., anti-fibrotic or anti-inflammatory miRs) and assess the cardiac responses both acute and longer term.

Vesicle administration *in vivo* can be through several methods including open-chest intramyocardial, echo-guided intramyocardial, intravenous, subcutaneous, or intraperitoneal delivery. As we were administering our treatments immediately after IR, we chose to inject intramyocardially into the LV wall. However, to address the invasives of this approach, an intravenous injection method should be explored. One concern with non-local delivery of the ELVs would be homing to the target site, as studies have shown that sEVs delivered intravenously, subcutaneously, or intraperitoneally are rapidly cleared from circulation into the liver, kidneys and spleen[111,192]. However, given ELVs are engineered, there is scope to embed homing peptides (e.g., cardiac homing peptide[91], myocardium-targeting peptide[193] or cardiomyocyte-specific peptide[194]) onto their surface to aid with delivery and uptake into the myocardium.

Another important aspect of vesicle delivery is the immunomodulation and its effects on ELV efficacy. As this study involved direct targeting into the LV wall, and assessment of ELVs' primary function was our focus, we didn't explore the role of the immune response (e.g., monocytes, cardiac tissue-resident macrophages etc.) on ELV potency. This would be important to study to further scale up the ELV therapy. In addition, assessing tissue-level responses through interleukins (e.g., IL-6, IL-8), TNF-α, ROS, and M1 and M2 macrophage polarization in the blood would help understand the role of the immune response on ELVs. This could also warrant tailoring the ELV cargo to include specific immunomodulatory miRs to aid with function and potency.

In summary, this work established that the ELV potency observed *in vitro* in Chapter 3, does translate to an *in vivo* model for MI, with significant tissue-level repair and marginal

global improvements. This work highlights the value of ELVs and the scope for using this vehicle beyond miR-126 for delivery of other cardioprotective miRs as well.

CHAPTER 5. TO STUDY THE EFFECTS OF PARENT CELL TYPE ON VESICLE UPTAKE AND FUNCTIONALITY

5.1 Introduction

CPC-derived ELVs have been potent vehicles for carrying custom cargo, with their delivery of miR-126 having preparative effects both *in vitro* and *in vivo* (Chapter 2 and 3). Moreover, despite also allowing cargo customizability, ELVs are not facing several of the uptake and retention challenges faced by synthetic mimics. This highlights the potential value of our ELVs being derived from sEVs and thereby maintaining a similar membrane to that of the sEV. However, the exact components of the sEV membrane that are important for uptake and targeting and the role of sEV origin on its membrane composition are less explored.

The sEV's amphiphilic bilayer membrane consists of phospholipids (e.g., PC, PE, SM, CHOL, CM), as well as transmembrane proteins (e.g., tetraspanins CD9, CD63, CD81)[113,195]. This complex membrane composition is often credited for efficient sEV uptake by cells with minimal clearance [85]. Further, the aqueous interior cavity of sEVs contains protein/nuclear cargo (e.g., mRNA, miR, proteins) which is often enriched from the parent cell, making sEVs potent therapeutics. For example, cardiac-derived sEVs elicit similar cardioprotective responses as the administration of the parent cells, with variations observed based on parent cell type[97].

sEV biogenesis in the parent cells begins in the cytosol with inward budding of the plasma membrane to form the early endosome, transition of the early endosome into the late

endosome, secondary inward budding of the late endosome to form sEVs within a multi-vesicular body, and finally fusion of the multivesicular body with the plasma membrane to release the sEVs into the extracellular space[139]. Once the sEVs reach the recipient cell, uptake of sEVs can occur through several mechanisms, which are broadly divided into phagocytosis (for particles >1 μm) and pinocytosis (for particles <1 μm)[196]. Pinocytosis is common for cells and consists of three major mechanisms: clathrin-mediated uptake, clathrin-independent uptake and macropinocytosis. Clathrin-independent uptake includes caveolae/lipid raft-, RhoA-, flotillin- Arf-6 mediated uptake, to name a few[197,198]. All these methods can be utilized by the recipient cell for sEV uptake, after which, sEVs can be trafficked into the cytoplasm or nucleus to initiate functional responses or fuse with the lysosome for degradation.

Although sEV biogenesis and the role of sEV cargo variations in sEV function are well understood, the determining factors relating sEV membrane composition to sEV function, specifically uptake, is still unclear. It has been established that there is asymmetry in the membrane lipids, and this can be enzymatically altered (via flippases, floppases etc.), but the purpose of this structure and ability to alter the lipid membrane is mostly unknown[199]. Similarly, it has been reported that variations in sEV surface proteins influence uptake by recipient cells, but this work is limited to cancer-cell derived sEVs and the specific roles of cardiac sEV proteins in uptake are understudied[169]. This notion of membrane importance for uptake is further supported when comparing sEVs to synthetic mimics, which despite similar size and shape, contain less intricate membranes and are often targeted and cleared by the mononuclear phagocyte system[200,201].

Given that sEVs are derived from their parent cells with inward budding from the cell membrane and then secondary inward budding to form sEVs, the bilayer membrane orientation of sEVs matches that of the parent cells. More importantly, this shows that the composition of the sEV membrane is directly derived (prior to alterations), from the parent cell. Therefore, to explore the differences in membrane composition on sEV uptake, sEVs derived from different parent cells should be studied.

One additional variable to this exploration is that sEV cargo varies based on several parameters (including the parent cell, cell age, cell environment etc.), therefore, potential differences in uptake and function could partially be masked by differences in cargo. Here, our ELVs engineered in Chapter 2 can help minimize this variability by allowing for specific cargo loading into ELVs derived from different parent cells.

In this chapter, we aim to explore the relationship between variations in the sEV lipid and protein profiles and elucidate if there is a correlation between these variations and the uptake mechanism employed by the recipient cells. We focus on four CVD-relevant cell types, namely, CPCs, MSCs, CECs and CFs to determine sEV membrane-uptake relationships in the cardiac context. We show that sEV uptake mechanism varies both based on the parent and recipient cell with variations in membrane lipid and protein composition by sEV origin. These uptake variations are related to both the donor and recipient cell type, with clathrin mediated uptake being most distinct. We then take this one step further to design ELVs from CPC and MSC-sEVs, both carrying the same miR-126 cargo. We then look at in-vitro functionality of MSC ELVs and their functional responses compared to CPCs. Given that CPC and MSC ELVs carry the same cargo, this helps us further elucidate the role of the membrane.

5.2 Materials and Methods

5.2.1 Isolation and culture of CPCs

Human CPCs were isolated from the right atrial appendage of neonatal pediatric patients undergoing surgical intervention for a congenital heart defect. Neonatal patients were classified as patients 2 weeks of birth at the time of surgery. The CD-117+ cells were separated from the atrial tissue through magnetic bead sorting for c-kit, as previously described[58]. CPCs were the cultured in Ham's-F-12 medium (Corning Cellgro®, Corning, NY, USA) with 10% FBS, 1% penicillin-streptomycin, 1% L-glutamine and 0.04% human hFGF-β.

5.2.2 Culture of MSCs, CFs and CECs

BM-MSCs were purchased from Gibco (StemPro™ BM Mesenchymal Stem Cells, Gibco, Waltham, MA) and rat CFs were isolated from adult male Sprague-Dawley rats as previously described[60]. Both MSCs and CFS were cultured in Dulbecco's Modified Eagle Medium and Ham's-F-12 medium with 10% FBS, 1% penicillin-streptomycin, 1% L-glutamine and 0.04% hFGF-β. Rat primary CECs (R2111, Cell Biologics Inc., Chicago, IL) were cultured in EGM-2 (Endothelial Cell Growth Medium-2 BulletKitTM, Lonza, Bend, OR) supplemented with 1% penicillin- streptomyocin and 2% FBS, 0.4% hFGF-β, 0.1% VEGF, 0.1% R3-IGF-1, 0.1% ascorbic acid, 0.1% human hEGF, 0.1% GA-1000, 0.1% heparin, and 0.04% hydrocortisone, as per manufacturer's protocol.

5.2.3 sEV isolation from CPCs, MSCs, CECs and CFs

CPCs, MSCs, CECs and CFs (~50 × 10^6 cells) between passages 8-16 were cultured in 2D until 90% confluency. Cells were then washed 3 times with PBS to remove any serum-media and quiesced in serum- and growth-factor-free media in normoxic (18% oxygen) or hypoxic (2% oxygen) conditions for 12 hours. The oxygen conditioning was performed to recapitulate the ischemic conditions experienced during CVD. Further, previous studies from our group have shown that hypoxic-CPC derived sEVs had more pronounced reparative capacity, suggesting a possible difference in membrane composition[9]. sEVs were collected from the conditioned media through differential ultracentrifugation (Optima XPN-100, Beckman Coulter, Indianapolis, IN, USA). Briefly, the conditioned media was depleted of cells at 1000 RPM for 10 minutes (Centrifuge 5810 R, Eppendorf, Hamburg, Germany), then depleted of cell debris at 31,000 RPM for 20 minutes (SW32Ti, Beckman Coulter). Finally, sEVs were pelleted at 31,000 RPM for 114 minutes (SW41Ti, Beckman Coulter). The bottom two layers (1 mL each) were collected and stored at -80°C for further use.

5.2.4 CPC and MSC ELV Synthesis

ELVs were synthesized from CPC and MSC-derived sEVs depleting inherent cargo and then selectively loading cargo of choice. First, inherent cargo was depleted from 3-4 × 10^9 CPC or MSC sEVs with repeated sonication cycles. For this, samples were treated with 100 µg/mL RNase A (Thermo Fisher Scientific) and sonicated at #3 with a probe-tip sonicator for 8-10 cycles (each cycle consisted of a 3 minute-duration of 15 seconds on/off sonication, with samples kept on ice during off-cycles to minimize sample heating). Samples were then incubated for 30 minutes at 37°C with constant rotation. Next, samples were treated with 40 units/20 µL ribonuclease inhibitor (RNAseOUT, Invitrogen,

Carlsbad, CA) and 1 mM DTT (Invitrogen) and the sonication step was repeated for another 8-10 cycles. Samples were then incubated for 1 hour at 37°C with constant rotation and then stored at -20°C overnight. Samples were then electroporated with 100 pmol miR-126 (Gene Pulser Xcell, Bio-Rad, Hercules, CA) in 0.1 cm electrode gap cuvettes using 2-10 pulses (750 Volt square wave, with 5 ms pulses). Samples were then neutralized with cold serum-free Ham's-F-12 medium or Dulbecco's Modified Eagle Medium and incubated for 30 minutes at 37°C with rotation followed by overnight incubation at 4°C. Any unbound miR-126 and larger debris was removed through differential ultracentrifugation (Optima XPN-100). Larger debris was depleted after centrifugation at 1000 RPM for 5 minutes (Centrifuge 5810 R), smaller debris after ultracentrifugation at 15,000 RPM for 20 minutes (SW32Ti, Beckman Coulter) and finally the ELVs were pelleted after ultracentrifuging at 31,000 RPM for 114 minutes (SW32Ti, Beckman Coulter). ELVs were resuspended in PBS and stored at -80°C until further use.

5.2.5 sEV and ELV characterization

The sEV and ELV size and concentration profiles were quantified through NTA (Nanosight NS-300 with NTA 3.4 software, Malvern Panalytical, Malvern, UK) with three 60 second videos per sample. Vesicle protein content was assessed with the bicinchoninic acid assay (Pierce^{TM} BCA Protein Assay Kit, Thermo Fisher Scientific, Waltham, MA) as per manufacturer's instructions. sEV structure was determined with cryo-electron microscopy (JEOL JEM-1400, Peabody, MA) with the UltraScan 1000 CCD to initially visualize the bilayer and henceforth with transmission electron microscopy (JEOL JEM-1400). Finally, vesicle polydispersity index was assessed through DLS (DynaPro Plate Reader III, Wyatt, Santa Barbara, CA).

5.2.6 sEV uptake inhibition

CECs and CFs were cultured until 80% confluency and then seeded at 0.3×10^6 cells/well into 6 well plates. After incubation for cell attachment, the CECs and CFs were quiesced overnight in endothelial bare medium (FBS and growth factor free) or Dulbecco's modified eagle's medium (FBS free), respectively, with 1% penicillin-streptomycin. CECs or CFs were then treated with one of four small molecule inhibitors of sEV uptake: Dynasore (Dynamin inhibitor), Pitstop-2 (clathrin inhibitor), Nystatin (caveolae/lipid raft mediated uptake inhibitor) or Amiloride (Na^+/H^+ pump mediated macropinocytosis inhibitor) for 1 hour at 37°C as per Table 1. Following inhibition, cells were treated with either normoxic or hypoxic calcein-stained sEVs from CPCs, MSCs, CECs or CFs at 20 µg/mL and incubated at 37°C for 2 hours. The sEVs were pre-stained with membrane dye, calcein (Thermo Fisher Scientific, Waltham, MA) and treated to CECs and CFs (without inhibitor treatment) incubated at 37°C and 4°C were the negative and positive controls, respectively. After the 2-hour incubation, uptake of sEVs by CECs and CFs was quantified through flow cytometry, Briefly, CECs or CFs were washed 3 times with sterile PBS to remove free or partially bound sEVs. Cells were then detached and each sample resuspended in 200 µL flow buffer (2% FBS in PBS). Uptake of sEVs was quantified for $\lambda_{Ex}/\lambda_{Em}$ = 495/515 nm corresponding to calcein+ sEVs.

To confirm successful inhibition with the small molecule inhibitors, inhibition of fluorescein isothiocyanate (FITC)-conjugated albumin (A9771, Sigma Aldrich) and tetramethylrhodamine (TRITC)-conjugated transferrin (009-0034, Rockland Immunochemical Inc., Baltimore, MD) was assessed as positive controls. For this, similar to above, CECs and CFs were treated with the small molecule inhibitors for 1 hour followed

by treatment of 20 µg/mL of albumin-FITC+ or transferrin-TRITC for 2 hours and uptake of the albumin or transferrin was assessed through flow cytometry for $\lambda_{Ex}/\lambda_{Em}$ = 495/515 nm and $\lambda_{Ex}/\lambda_{Em}$ = 550/570 nm, respectively.

Table 2. Dosage of small molecule inhibitors for sEV uptake

Small molecule inhibitor	Target uptake pathway	Dosage
Dynasore	Dynamin-mediated	5 µg/mL[202]
Pitstop-2	Clathrin-mediated	10 µM[203]
Nystatin	Caveolae/lipid raft-mediated	50 µg/mL[204]
Amiloride	Na^+/H^+ pump mediated macropinocytosis	20 µM[205]

5.2.7 Live-dead assay

To determine any cytotoxic effects of the small molecule inhibitors on CECs or CFs, cell viability after treatment was assessed. Here, cells were cultured until 80% confluency and seeded at 0.05×10^6 cells/well into 24 well plates. Cells were then treated with the four small molecule inhibitors of uptake (dynamin, clathrin, nystatin or amiloride) as per Table 1. and incubated for 3 hours at 37°C to recapitulate the sEV uptake inhibition study (5.2.6). Untreated CECs and CFs at 37°C and 4°C were positive and negative controls, respectively. After 3 hours, cells were detached and treated with Zombie Red™ viability dye (423109, Biolegend, San Diego, CA) as per manufacturer's instructions and incubated at room temperature for 15-30 minutes. Cells were then washed and resuspended in flow

buffer (2% FBS in PBS). Percentage of Zombie Red+ cells were quantified by flow cytometry for $\lambda_{Ex}/\lambda_{Em}$ = 561/624 nm.

5.2.8 'Omic data processing

Label-free quantification lipid and protein mass spectrometry experiments were performed.Peak intensities for protein and lipid data were considered. Features were annotated and proteins/lipids with medium or high confidence were considered. For duplicate lipid names, lipids with the lowest average coefficient of variation value among quality-control samples were considered. Lipid isomer peaks (identical annotations with different retention times, $\Delta > 0.3$ minutes) were summed. Data from all EVs and oxygen conditions (n=24) were combined for proteins and lipids. Features were filtered to first remove species with more than 12 missing values, and then to denoise data sets by filtering features by their interquartile range. The resulting datasets consisted of 532 proteins and 158 lipids. Next, missing values were replaced by ⅕ the minimum value in the corresponding sample and EV samples were normalized by their median. Data were log10 transformed and features were auto-scaled (mean-centered and divided by the standard deviation of each feature). Principal component analyses of normalized lipidomic and proteomic data were performed using R built-in prcomp function. Differential expression analyses of lipids and proteins in normoxic EVs from CPCs, MSCs, CECs, and CFs was performed using limma in R.

5.2.9 Partial Least Squares Regression Model

To connect lipid/protein 'omic data to EV uptake mechanism, a partial least squares (PLS) regression model was constructed using normoxic EV data. Experimental uptake data were scaled and centered with the mdatools package in R before use in regression models. The mdatools package was also used to construct PLS regression models using the SIMPLS algorithm. First, 3-component models were constructed using all features and leave-one-out cross validation. VIP scores were calculated for the model and lipids/proteins with an average score >1 across all uptake mechanisms were selected. Then, a 3-component final, reduced model was constructed from the 303 VIP lipids/proteins. Model performance of the cross-validated training set was assessed with root-mean-square error (RMSE) and R2 measurements.

5.2.10 Tube formation assay

CECs were cultured until 90% confluency. CECs were then quiesced in endothelial bare media (FBS and growth factor free) with 1% penicillin-streptomycin. Quiesced CECs were seeded at 10,000 cells/well onto µ-slide Angiogenesis slide (IBIDI) pre-coated with 10 µL/well Matrigel (Matrigel® Matrix, Corning) as per manufacturer's protocol. CECs were then treated overnight at 5.00×10^8 sEVs or miR-126+ ELVs per 1.00×10^6 cells (from CPCs or MSCs). CECs were then stained with calcein-AM (Thermo Fisher Scientific) and imaged using a fluorescent microscope (Olympus IX71) such that each image captured one complete well, representing one technical replicate of a sample group. ImageJ software was used to quantify different tube length parameters (Fiji, National Institutes of Health, Bethesda, MD) [161]. The Angiogenesis Analyzer plug-in for ImageJ, specifically created to

analyze the vascular organization of endothelial cells, was used to quantify images (three technical replicates per group)[162]. Output parameters of number of tubules, total tube length and total segment length were calculated, with lengths measured in pixels. Negative and positive controls consisted of quiesced CECs with no treatment, and EGM-grown CECs with no treatment, respectively.

5.2.11 Proliferation assay

CEC proliferation assay was performed using the Click-iT EdU Microplate Assay (C10214, ThermoFisher Scientific). CECs were plated onto a 96 well plate at 8,000 cells per well and incubated overnight for cell attachment. CECs were then treated with CPC or MSC sEVs or CPC or MSC miR-126+ELVs at 5.00×10^8 sEVs or miR-126+ ELVs per 1.00×10^6 cells as well as 10 μM of 5-ethynyl-2'-deoxyuridine (EdU) and incubated for 48 hours. The CECs were then fixed and the Click-iT EdU assay performed as per manufacturer's protocol. Briefly, the CECs were treated with Oregon Green 488 and then anti-Oregon Green antibody conjugated to horse-radish peroxidase was added and reacted with Amplex Ultra-Red to elicit fluorescence. The fluorescence of the sample was read on a plate reader (BioTek Synergy 2) for $\lambda_{Ex}/\lambda_{Em}$ = 568/585 nm. Cells incubated in serum-free media and full media were used as negative and positive controls.

5.2.12 Cytotoxicity assay

For qualitative assessment, CECs were cultured until 90% confluency and were then seeded at 50,000 cells/well into a 96 well plate and incubated overnight for attachment. CECs were then quiesced in endothelial bare media (FBS and growth factor free) overnight with 1% penicillin-streptomycin. CECs were then treated with 5.00×10^8 sEVs or miR-126+ ELVs per 1.00×10^6 cells and incubated for 48 hours. CECs were then stained with 0.003 mM calcein-AM (live dye, Invitrogen) and 0.004 mM ethidium-homodimer-1 (dead dye, Thermo Fisher Scientific) for 30 minutes in full media followed by 3 washes with PBS. CECs were then imaged using a fluorescent microscope (Olympus IX71) such that each well had 1 image corresponding to one technical replicate (with biological replicates used for data analysis). Cells without sEV/ELV treatment were used as controls.

For quantitative assessment, CECs were again seeded into 96 wells and treated in the same manner with incubation for 48 hours. After 48 hours, 3 wells of untreated cells were killed with 0.1% Triton-X, as a negative control, by incubating at 37°C for 15-30 minutes. After this, the cell lysate was collected from all samples and spun down at 1000 RPM for 5 minutes (Centrifuge 5810 R, Eppendorf) to deplete any detached cells. The conditioned media was then used to run the LDH (LDH Cytotoxicity Assay Kit, Cayman Chemical, Ann Arbor, MI), as per manufacturer's protocol. 0.1% Triton-X treated cells were used as negative control and cells without sEV/ELV treatment were used as positive controls.

5.2.13 Statistical Analysis

All statistical analysis was performed using GraphPad PRISM 8 software (GraphPad, San Diego, CA) with specific testing details outlined in figure captions.

5.3 Results

5.3.1 sEVs successfully isolated and characterized from all four parent cell types

CPCs, MSCs, CECs and RCFs were cultured in 2D until 90% confluency and then cells were incubated in serum-free media in normoxic (18% oxygen) or hypoxic (2% oxygen) condition for 12 hours. sEVs were then isolated from the conditioned media through differential ultracentrifugation as described in the methods section. The sEV shape was detected through transmission electron microscopy and the membrane lipid-bilayer (white arrows) with cryo-electron microscopy (Figure 19A). The total protein content of each of the sEVs was assessed with a bicinchoninic acid assay, and most sEV protein content was independent of oxygen conditioning with only RCF-sEVs having significantly higher protein per vesicle with normoxic incubation (Figure 19B). Further, sEV diameter was within the expected range for all samples (106±1.8 to 150.7±5.8 nm) and all sEVs displayed some of the important sEV-markers: CD63, CD81, HSP90 and HSPA8 (Figure 19C and D). Finally, all sEVs had similar size-concentration profiles and were isolated at approximately 2×10^8 to 5×10^8 particles/mL (Figure 19E).

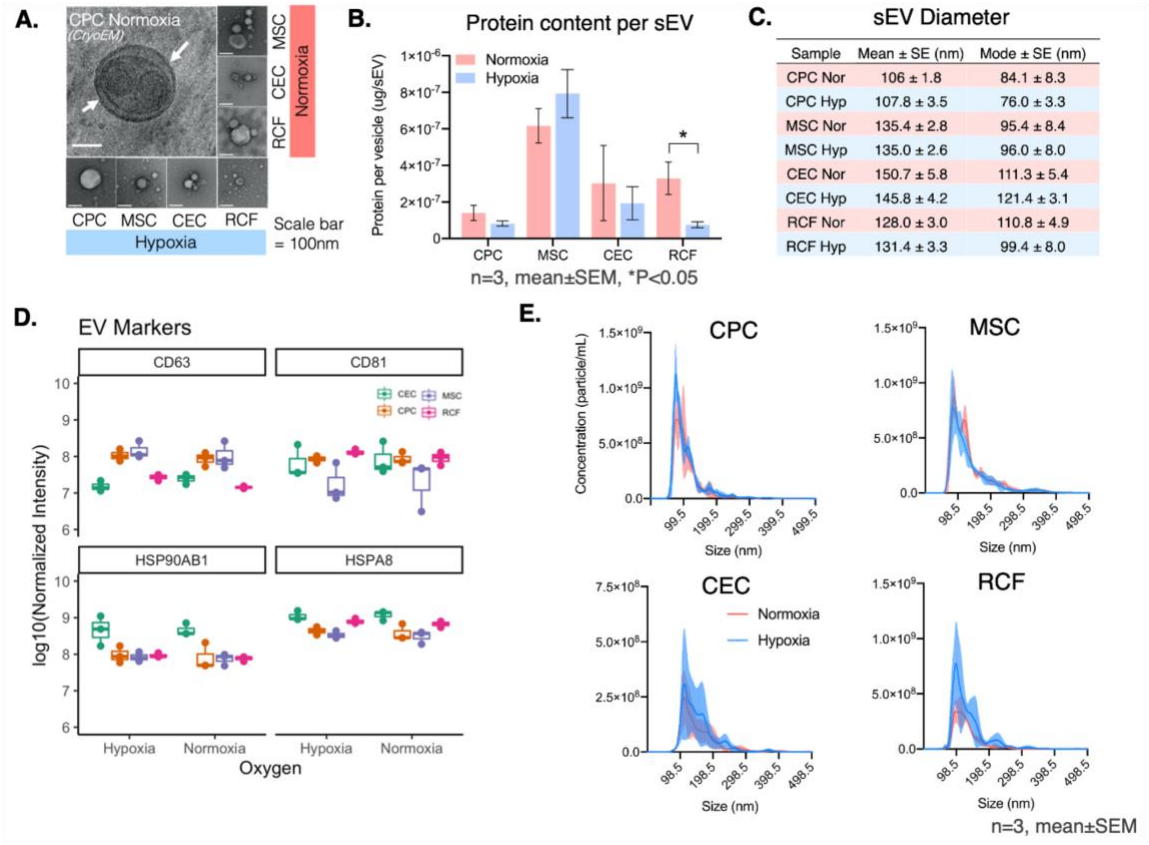

Figure 19. sEV isolation and characterization from CPCs, MSCs, CECs and RCFs. (A) Cryo- and transmission electron microscopy images of isolated sEVs from all four cell types. (B) Variation in protein content across 4 cell types based on oxygen conditioning. (C) Size profiles of sEVs from all four cell types. (D) Presence of transmembrane markers (CD63, CD81) and cytosolic markers (HSP90AB1, HSPA8), measured with mass spectrometry. For reference, minimum and maximum $\log_{10}$(normalized intensity) values are 2.94 and 10.7, respectively. (E) Concentration-size profile of isolated sEVs with NTA. Scale bar=100 nm. n=3, Mean±SEM, Significance was tested with two-way Student's paired *t* test. *P<0.05.

5.3.2 sEV uptake mechanism varies based on parent cell type and recipient cell type

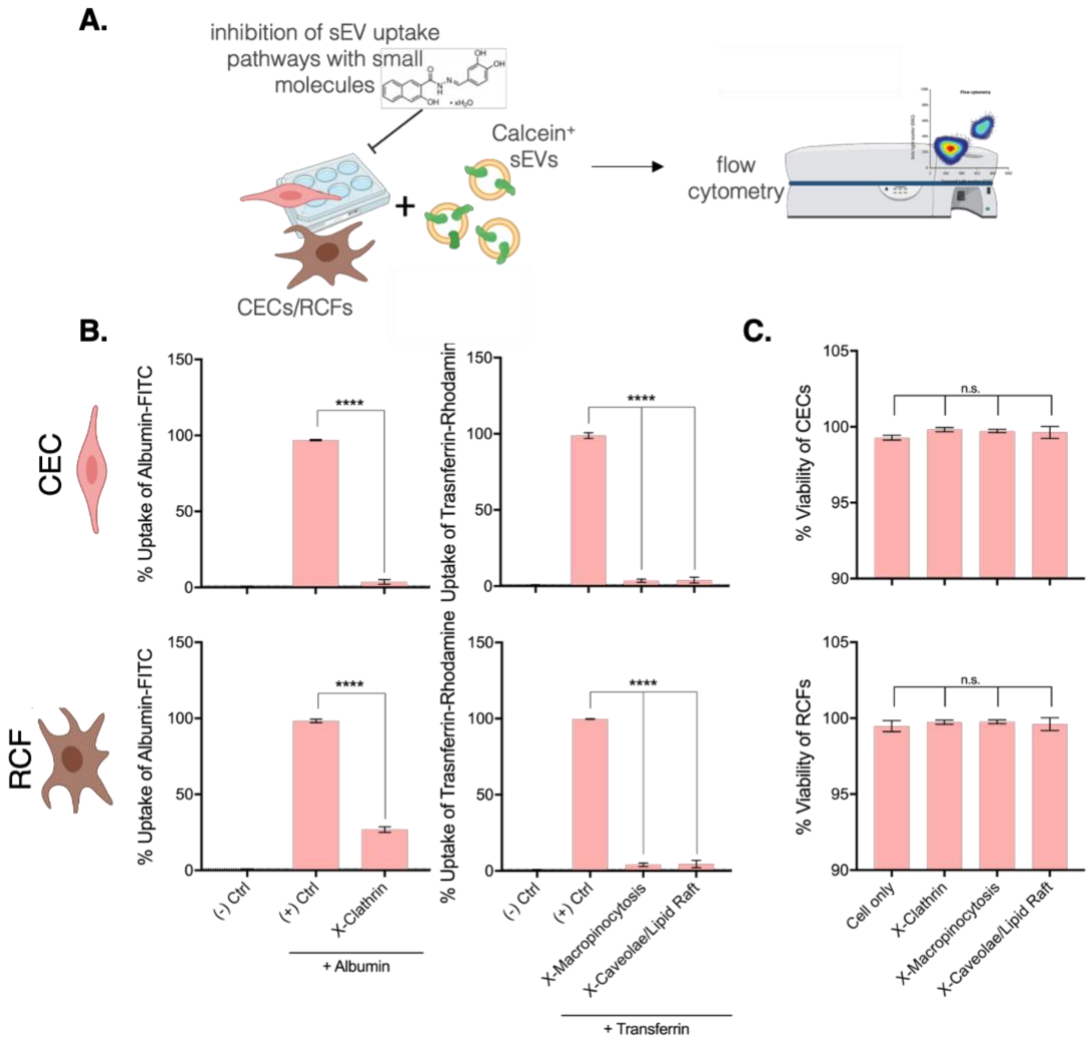

Figure 20. Small molecule inhibition to assess sEV uptake mechanisms. (A) Workflow of administration of small molecular inhibitors of uptake and downstream quantification of sEV uptake by CECs and RCFs using flow cytometry. (B) Extent of uptake inhibition by each small molecule inhibitor tested against albumin and transferrin (C) Effect of small molecular inhibitor on CEC and RCF cell viability. Mean±SEM. Significance was tested with one-way ANOVA with Tukey's post-hoc. n.s. = not significant. ****P<0.0001.

To assess the variations in uptake mechanism based on parent cell type, we delivered the sEVs to 2D cultures of CECs and RCFs. We chose these as they are abundant in cardiac repair and important cell types during remodelling and recovery after MI. Three uptake mechanisms, clathrin-mediated, macropinocytosis and caveolae/lipid-raft-mediated, were studied using small-molecule inhibitors to block each uptake pathway. Calcein+sEVs were

then administered and the uptake assessed through flow cytometry (Figure 20A). Concentrations of each inhibitor was determined based on prior literature review (Table 2), and successful inhibition was first confirmed using albumin and transferrin as positive controls (Figure 20B). All three small molecular inhibitors reduce sEV uptake significantly, to less than 10%. Finally, as small molecular inhibitors can be cytotoxic, the effect of our selected concentrations on CECs and RCFs were tested with a viability assay (Figure 20C). None of the selected small molecule inhibitor doses significantly affected CEC or RCF viability, so these concentrations were used here forth.

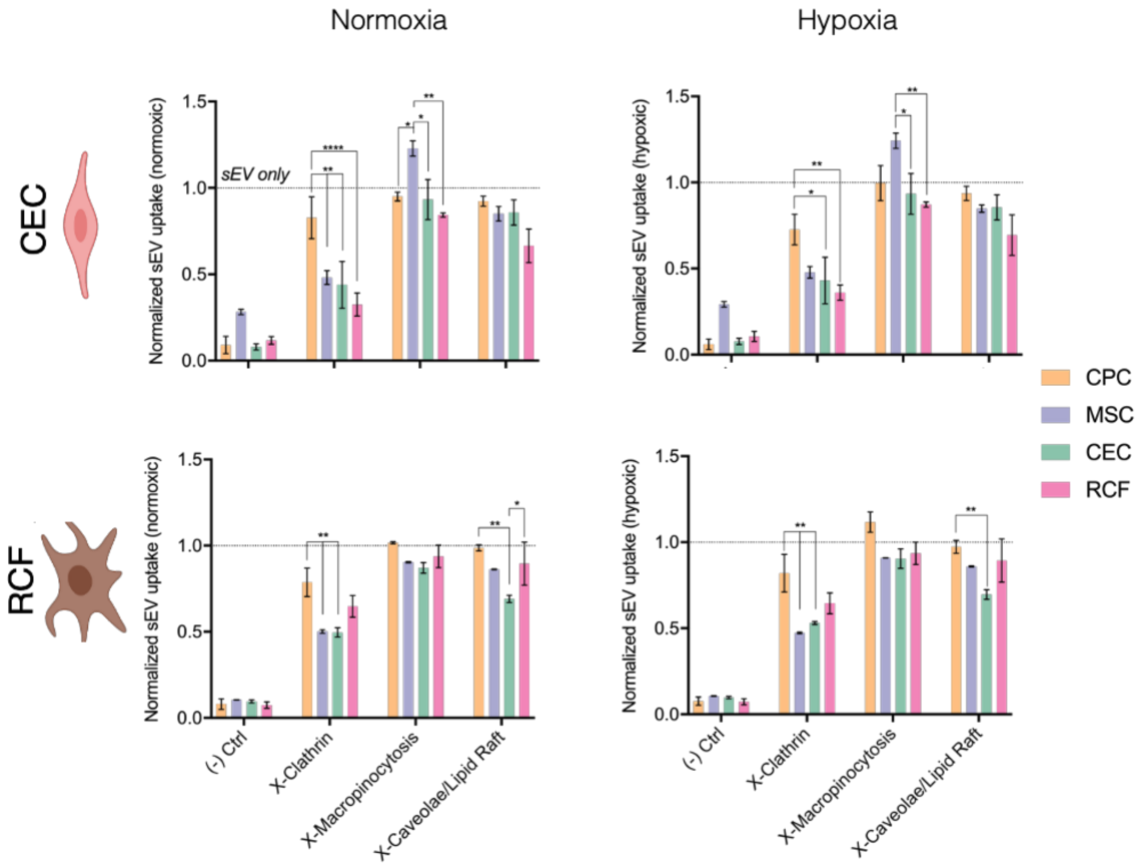

Figure 21. Mechanism of sEV uptake by recipient CECs and RCFs. Uptake mechanisms in recipient CEC/RCF cells inhibited by small molecule inhibitors clathrin (pitstop-2), dynamin (dynasore), macropinocytosis (amilioride), caveolae/lipid-raft (nystatin). Uptake of sEVs from the four cell types assessed through flow cytometry and

normalized to uninhibited controls. n=3. Mean±SEM. Two-way ANOVA with tukey's post hoc. n.s.=not significant. *P<0.05, **P<0.01, ****P<0.0001 Scale bar=100 nm.

After confirmation of the inhibition capacity and the cytotoxicity of the four small molecule inhibitors of uptake mechanisms, we explored the variations in uptake mechanism utilized by the different sEVs through flow cytometry, similar to (Figure 20A). Differences in uptake mechanisms were observed in both normoxic and hypoxic conditions which varied by both sEV-parent cell type (CPC, MSC, CEC, RCF) and the recipient cell type (CEC or RCF) (Figure 21). When administering sEVs to CECs, sEV origin played a role in the extent of clathrin and macropinocytosis based uptake, but not in caveolae/lipid raft mediated uptake. Here, MSC-sEV and CEC-sEV uptake were more dependent on these uptake mechanisms. However, when administering sEVs to RCFs, sEV origin was more important for clathrin and caveolae/lipid raft-mediated uptake, but not for macropinocytosis. Again, MSC- and CEC-sEV uptake was more pathway dependent. Similar patterns of uptake mediated were observed when sEVs where conditioning in hypoxia, without much difference observed between normoxic and hypoxic conditioning for sEV uptake. Further, MSC-sEV administration to CECs and CPC administration to RCFs show almost equal of higher uptake with macropinocytosis is inhibited. Readers should note that the sEV uptake (normalized to 1) does not represent the 'maximum' uptake but rather the 'combined effect' of uptake when these three uptake mechanisms are not inhibited. Therefore, it is feasible that inhibiting macropinocytosis could indirectly increase sEV uptake further than uninhibited sEV treatment.

5.3.3 Lipidomics profiling of sEVs shows differences based on parent cell type

Next, we explored the membrane of sEVs by conducting mass spectrometry analysis of the sEV lipids and proteins. The lipid features detected in all the sEVs varied by parent cell type with CEC and CPC sEVs having the most unique lipid features at 83 and 72, respectively (Figure 22A). Using principal component analysis to assess lipid clustering, we observed that samples cluster by parent cell type and oxygen conditioning does not constitute the primary two components of variance (Figure 22B). As oxygen doesn't induce much variance, we next focussed on normoxic sEV lipids and their abundance by cell type (Figure 22C). CPC sEVs are the most upregulated in lipid classes, especially in PC and SM) and MSC sEVs are the least upregulated in most lipid classes. Within the MSC lipid profile, the LPC and triglyceride (TG) lipid classes are slightly more abundant, whereas CEC are more abundant in SMs. Further, the RCF lipid profile is relatively distributed across all the major lipid classes, but not to the extent of CPCs. To elucidate some of the parent-cell based variability more clearly, we also show example LPC and PC lipid profiles (normalized intensity) wherein LPC is less prevalent in CECs and even within PCs, some are more abundant in CPCs, others in CECs, underscoring that sEV lipid profile does depend on sEV parent cell type (Figure 22D).

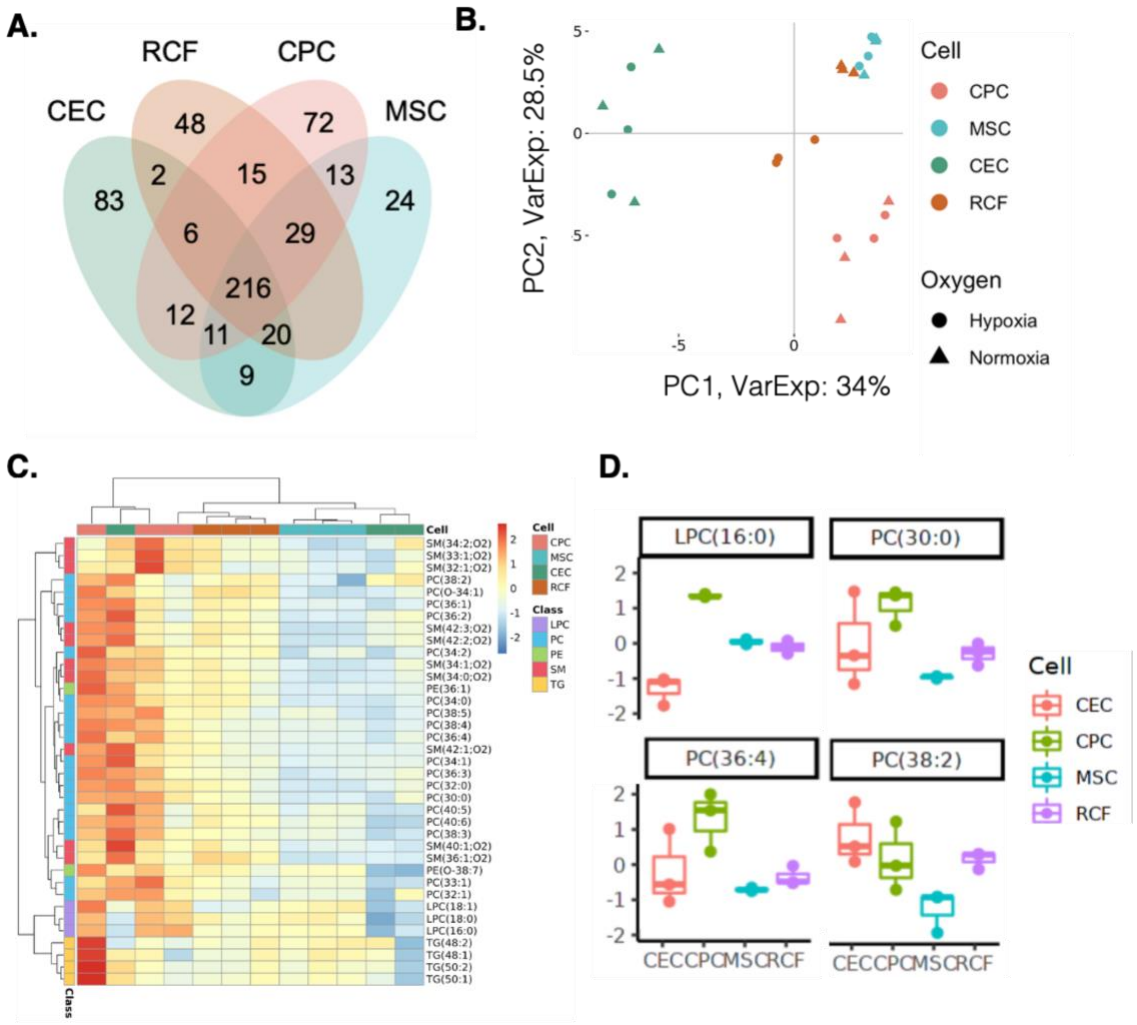

Figure 22. Variations in lipidomics profile of sEVs. (A)Venn diagram of lipids across all four cell types. (B) Principal component analysis of lipids clustered across component 1 (34% variance) and component 2 (28.5% variance), split by cell type and oxygen conditioning. (C) Heatmap of all lipid classes in normoxic samples and their abundance across the 4 cell types. (D) Representative lipids from (C) highlighting the variation of lipid abundance across the cell types. PC = phosphatidylcholine, LPC = Lysophosphatidylcholine.

5.3.4 Proteomics profiling of sEVs shows differences based on parent cell type

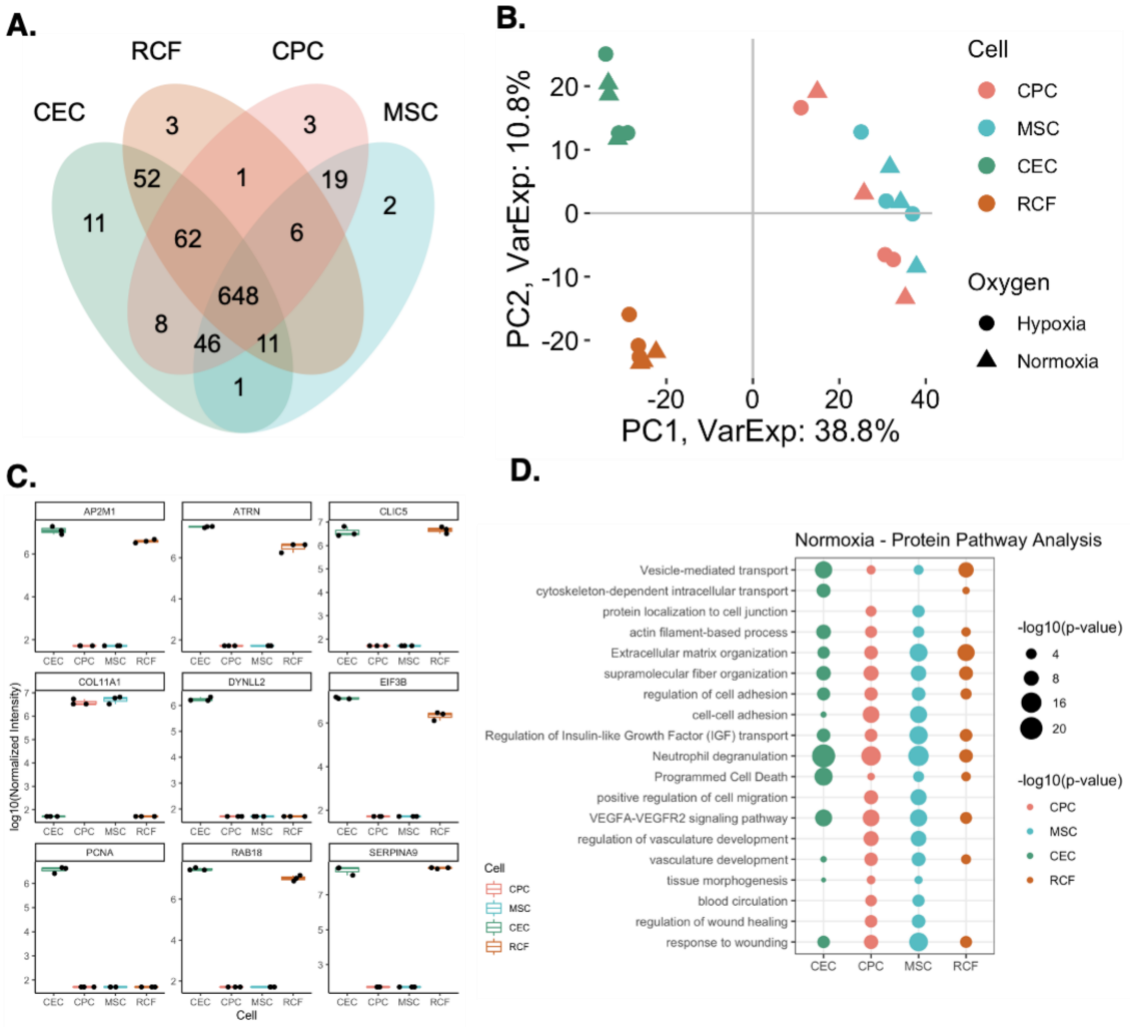

Figure 23. Variations in proteomics profiles of sEVs. (A) Venn diagram of proteins across all four sEV parent cell types. (B) Principal component analysis of proteins clustered across component 1 (38.8% variance) and component 2 (10.8% variance), split by cell type and oxygen conditioning. (C) Top differentially expressed normoxic proteins and their variations by parent cell type. (D) Downstream signaling pathways for normoxic proteins present in each sEV type.

We also explored the variations in sEV proteins across the different cell types. Similar to the lipid features, the proteins detected in the sEVs varied by parent cell type with CEC and RCF sEVs accounting for 52 distinct proteins and CPC and MSC sEVs accounting for 19 (Figure 23A). Using principal component analysis, the samples again cluster by parent cell type and independent of oxygen conditioning with CECs and RCFs more distinctly

clustered by cell type (Figure 23B). As oxygen does not account for the primary two sources of variance (component 1 = 38.8% and component 2 = 10.8%), we then focussed on the top differentially expressed normoxic sEVs and assessed their abundance by cell type (Figure 23C). As expected, the protein profiles varied based on parent cell with COL11A1 upregulated in CPC and MSC sEVs, other common sEV proteins such as RAB18 and SERPINA9 upregulated in CEC and RCF sEVs and DYNLL2 and PCNA specifically upregulated in CEC sEVs. Looking at the downstream protein pathways of these differentially expressed proteins, we observed that all four have proteins involved with vesicle mediated transport, and CEC and RCF sEVs are more pronounced in these (Figure 23D). All four sEV types are conserved in proteins for extracellular organization, VEGF pathways and wound healing, all important for cardiac recovery after MI. Further, CPC and MSC sEVs are more pronounced in vessel-specific protein pathways including vasculature development, blood circulation and tissue morphogenesis. In addition, of the 4 sEV types, RCF sEVs have the least distinct protein pathways activated.

5.3.5 sEV origin affects uptake mechanism and in turn recipient cell response.

A.

Recipient cell type	Uptake Mechanism	X Cumulative Variance		Y Cumulative Variance		R^2		RMSE	
		Full	Reduced	Full	Reduced	Full	Reduced	Full	Reduced
CEC	X-Clathrin	67.53	85.32	71.22	63.55	0.800	0.623	0.427	0.585
	X-Macropinocytosis					0.744	0.603	0.483	0.601
	X-Caveolae/ Lipid Raft					0.706	0.641	0.517	0.571
RCF	X-Clathrin					0.706	0.710	0.467	0.514
	X-Macropinocytosis					0.632	0.623	0.578	0.585
	X-Caveolae/ Lipid Raft					0.633	0.613	0.578	0.593

B.

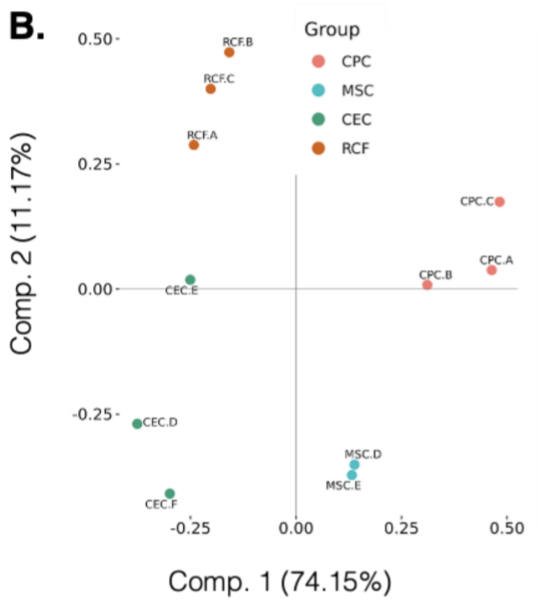

C.

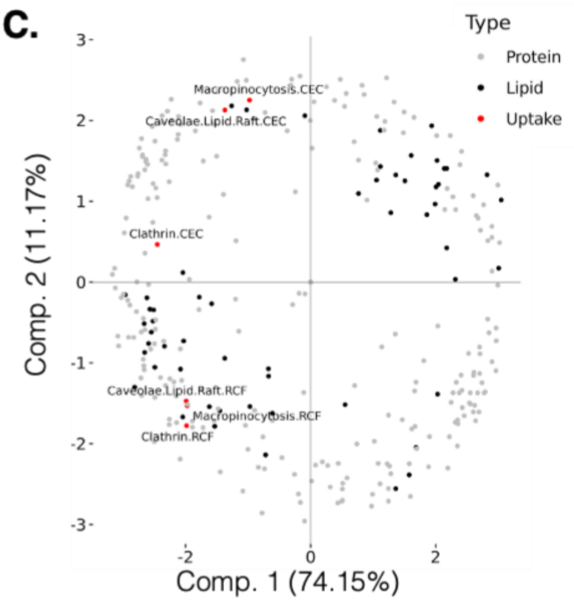

D.

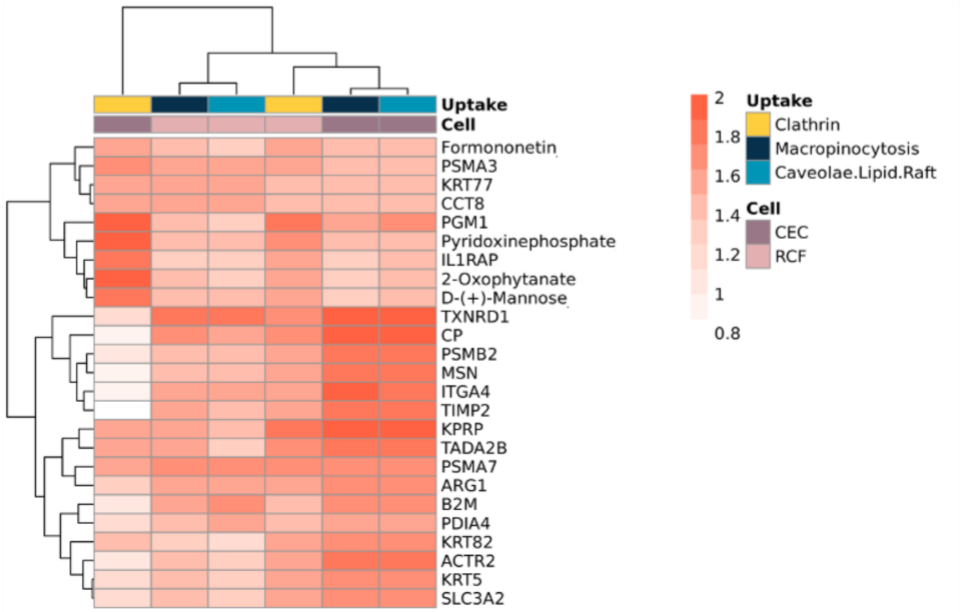

Figure 24. Relationship between sEV origin, uptake mechanism and recipient cell type. (A) Table of slope (R^2) and error (RMSE) for a PLS' regression analysis with full model (711 combined protein and lipid features) and a reduced model (top 303 protein and lipid VIPs). Only normoxic protein and lipid features used. (B) Scores plot of clustering from the 4 different sEV groups across component 1 (74.15% variance) and component 2 (11.17% variance). (C) Loadings plot of sEV proteins and lipids mapped with the CEC and RCF uptake mechanisms. (D) Heatmap of the top 25 VIPs groups by uptake mechanism and recipient cell type.

Having explored the variations in lipid and protein profiles and their differences based on sEV uptake and sEV parent cell type, we next sought to understand the relationship between the sEV membrane profiles and uptake mechanism. For this, a PLS regression model was developed with the full protein and lipid profiles and a reduced model with the top 303 VIP proteins and lipids. The reduced model with the top 303 VIPs comprised a similar extent of the variation of the full model with similar R^2 and RMSE values (Figure 24A). Also, the reduced model comprised a higher amount of variance in its top two components (85.32%) than the full model (67.53%). Therefore, the reduced model was used for all further analysis. With this supervised approach, the scores plot showed that the sEVs cluster distinctly by parent cell type even when accounting for uptake mechanism and recipient cell type (Figure 24B). Further, the loadings plot shows that the uptake mechanisms cluster by recipient cell type across component 2, with delivery to CECs in quadrant 4 and delivery to RCFs in quadrant 3 (Figure 24C). The lipids and proteins related to each of these recipient cell-based uptake mechanisms are also distinct. Finally, we explored the top 25 VIP proteins and lipids and found that for RCFs the top VIPs are similar despite the uptake mechanism, but for CECs the proteins and lipids associated with clathrin mediated uptake are more distinct.

5.3.6 Synthesis and characterization of MSC derived ELVs

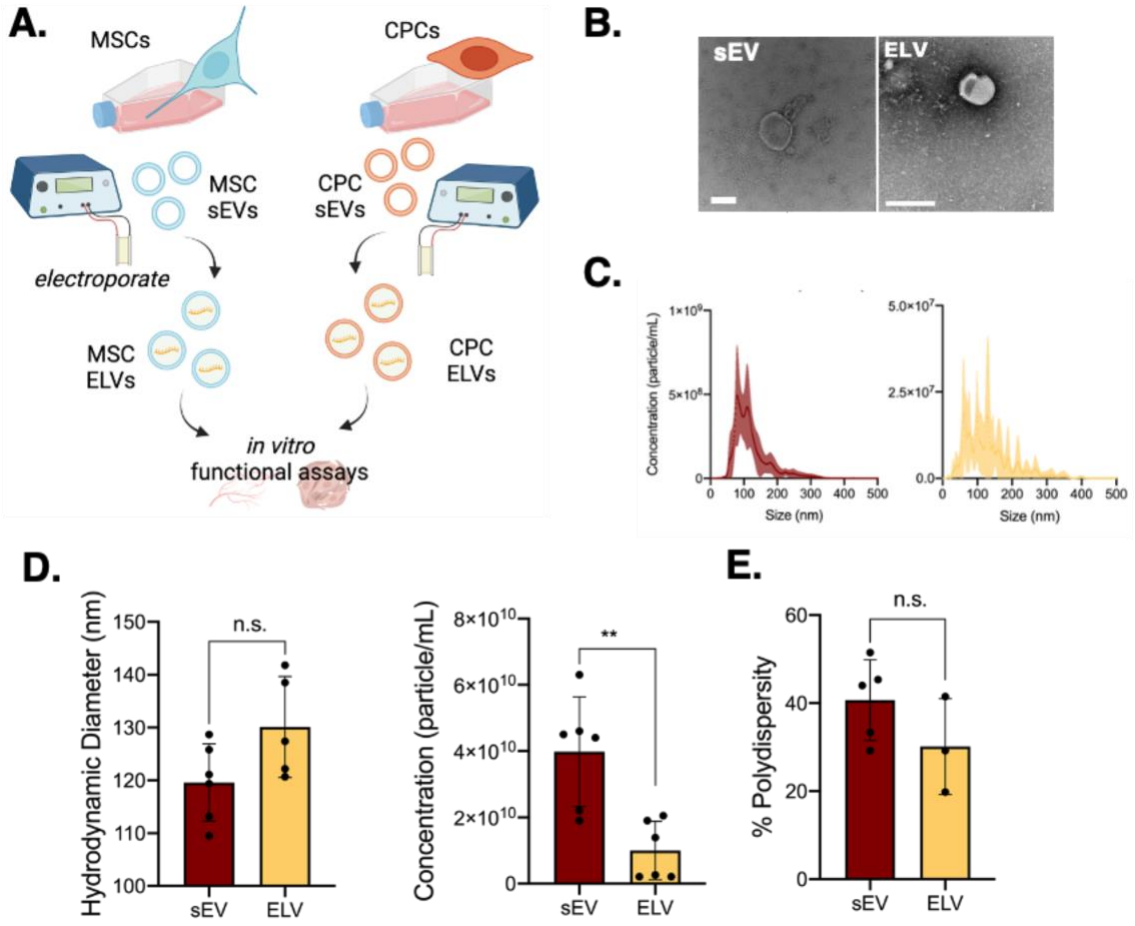

Figure 25. MSC sEV and ELV characterization. (A) Workflow of synthesis of MSC and CPC ELVs using electroporation and assessment of functional benefits of MSC and CPC ELVs compared to the MSC and CPC sEVs. (B) Representative transmission electron microscopy images of an MSC sEV and MSC ELV. (C) Size-concentration profiles of MSC sEVs and ELVs with NTA. (D) Comparison of ELV and sEV hydrodynamic diameter and concentration profiles. (E) Comparison of percentage polydispersity of ELVs and sEVs to determine population modality as measured with DLS. Scale bar = 100 nm. Mean±SEM. Significance was tested with two-way Student's paired *t* test. n.s. = not significant. **P<0.01. Scale bar = 100 nm.

Having established that the parent cell type plays are important role on sEV uptake mechanism and recipient cell type, we wanted to explore the effect different parent cell derived membranes have on ELV function. Specifically, we chose MSC derived ELVs as MSC-sEVs have been shown to be potent in cardiac therapies and our proteomics and lipidomics assessment showed differences in CPC and MSC-derived sEV profiles.

Therefore, we isolated sEVs from MSCs and CPCs, synthesized corresponding ELVs with miR-126 cargo using the electroporation method and then assessed functional differences between CPC and MSC sEVs and ELVs (Figure 25A). First, we synthesized and characterized the MSC ELVs and found that their shape was similar to that of sEV vesicles (Figure 25B). The concentration-size profiles of the MSC ELVs were also similar to that of MSC sEVs (Figure 25C). The hydrodynamic diameter of the vesicles was also similar although the concentration of ELVs was significantly lower than that of sEVs (Figure 25D). This was expected, as the same observation was made when synthesizing ELVs from CPC sEVs using electroporation, however, similar to that case, the batch-to-batch variation with ELVs was low and the concentration was still sufficient for downstream analyses. Finally, we quantified the percentage polydispersity between sEVs and ELVs and there are both similar suggesting a similar level of modality is maintained after ELV synthesis (Figure 25E).

5.3.7 Successful miR-126 loading into MSC ELVs

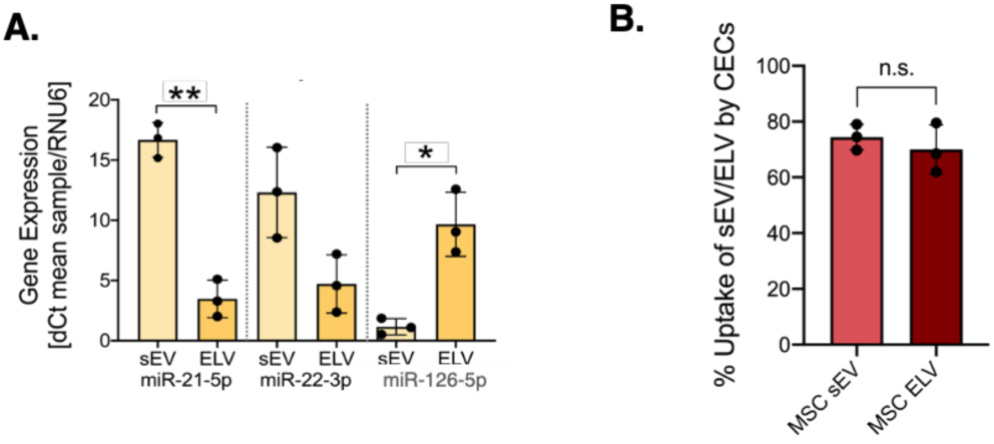

Figure 26. Successful cargo loading into MSC ELVs and uptake by CECs. (A) miR-126 was encapsulated into MSC-sEVs using sonication and electroporation as described in

Chapter 3. Inherent miR 21 and 22 are depleted and miR-126 loaded after the synthesis process is complete. (B) Quantification of uptake of calcein+MSC ELVs and sEVs by CECs through flow cytometry. Mean±SEM. Signficance was tested with two-way Student's paired *t* test. n.s. = not significant. *P<0.05, **P<0.01.

Having made the MSC ELVs, the next step was to confirm loading of miR-126 cargo into the ELVs (Figure 26A). Quantification of vesicles before and after miR loading showed that inherent MSC miR-21 and miR-22 were present in the sEVs, and depleted after ELV synthesis, whereas the endothelial-specific marker, miR-126, was lowly expressed in sEVs but significantly more abundant after electroporation for cargo loading. We also checked the uptake of MSC ELVs by 2D CEC cultures and found that there is no significant difference in uptake between the two groups (Figure 26B).

5.3.8 CPC and MSC-derived ELVs are not cytotoxic to CECs

Prior to testing the functional difference between CPC and MSC derived ELVs, we first confirmed that MSC-derived vesicles are similar to CPC-derived vesicles and are not cytotoxic when administered. We dosed equal concentrations (1×10^8 particles/mL) of CPC or MSC derived sEVs and ELVs to 2D cultures of CECs and assessed cytoxicity after 48 hours. When imaged, all groups showed mostly calcein-AM+ live cells (green) and only a few ethidium-homodimer+ dead cells (deep orange) (Figure 27A). Upon quantification of CEC viability with a LDH assay, all CECs were not significantly more cytotoxic than the cell-only group, with no significant differences in viability between groups either (Figure 27B & C).

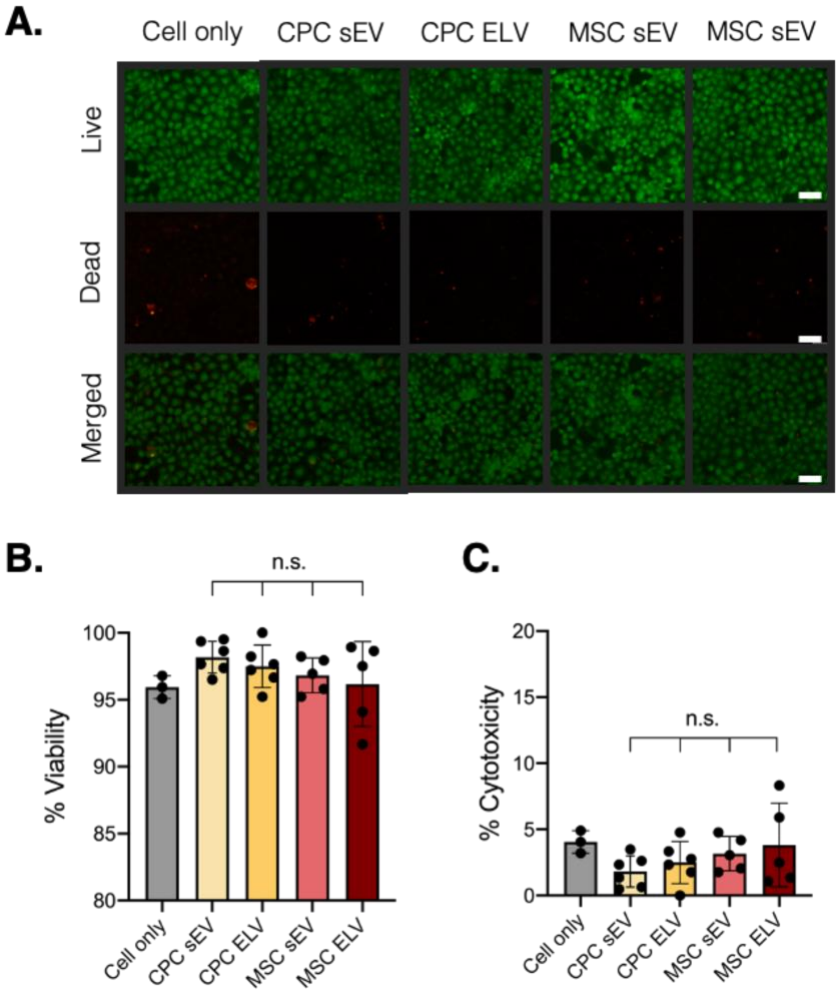

Figure 27. CPC and MSC ELVs are not cytotoxic when administered to 2D CEC cultures. (A) Live-dead analysis of 2D cultures of CECs with calcein-AM+ cells (live, green) and ethidium homodimer+ cells (dead, deep orange). (B) Quantification of cell viability through LDH after 48-hour CEC incubation with MSC and CPC ELVs. % Cytotoxicity represents 1-(% Viability). Scale bar = 50 µm.

5.3.9 miR-126+ MSC ELVs are pro-proliferative when administered to CECs

To assess the functional responses of MSC and CPC derived vesicles, we first investigated the effect of miR-126+ ELVs on CEC proliferation. miR-126 is known to target cell proliferation through the major PI3K-AKT pathway and the ERK pathways by inhibiting P13KR2 and SPREAD1, respectively, to the activate proliferation (Figure 28A). To study

this we dosed CPC and MSC vesicles (sEVs and ELVs) to 2D cultures of CECs along with EdU. After 48 hours incubation we performed the Click-iT EdU assay and quantified fluorescence to determine CEC proliferative capacity (Figure 28B). All groups induced proliferation of CECs but MSC ELVs significantly increased CEC proliferation compared to CPC sEVs alone (Figure 28C). Further, MSC ELVs significantly increased proliferation compared to MSC sEVs, but CPC ELVs did not induce significant improvement in proliferation (Figure 28D). This suggests that the MSC membrane could be playing a role is the proliferative capacity of the vesicles.

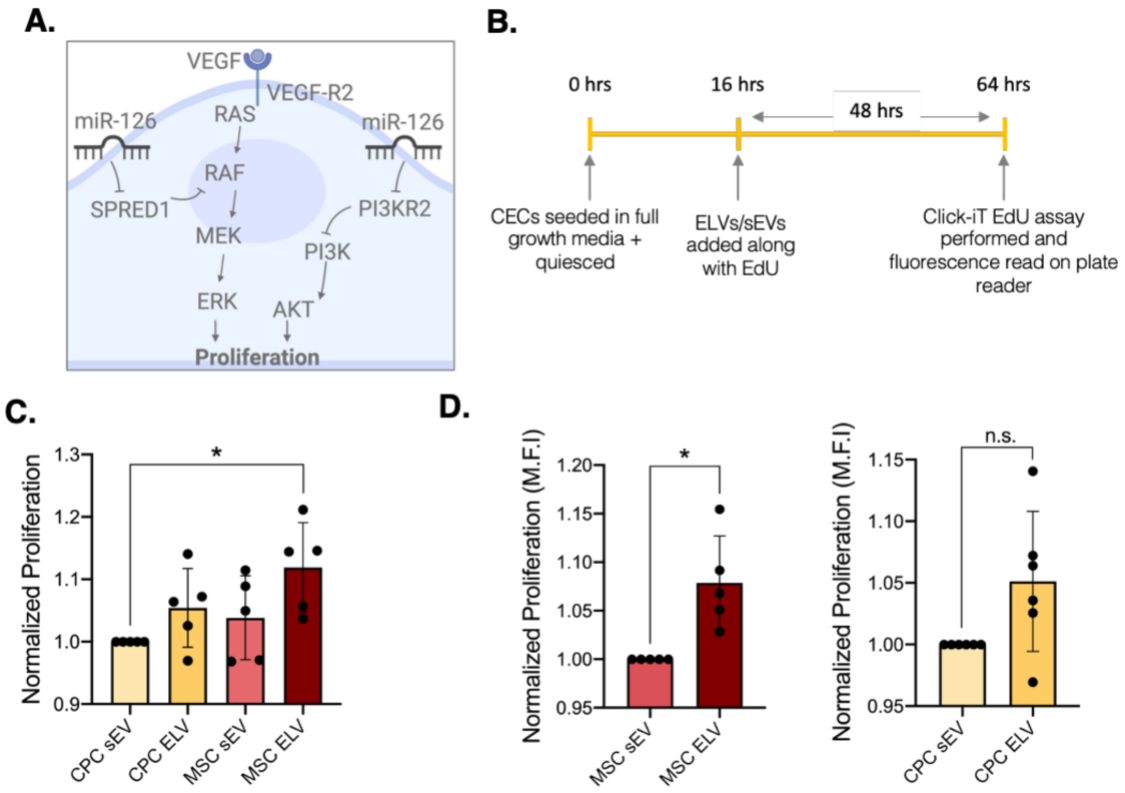

Figure 28. MSC ELVs improve CEC proliferative capacity. (A) Schematic of miR-126 mechanism of action for proliferation. VEGF: vascular endothelial growth factor; RAS: rat sarcoma virus; RAF: rapidly accelerated fibrosarcoma proto-oncogene; ERK: extracellular signal regulated kinase; AKT: protein kinase B; PI3K: Phosphoinositide 3-Kinase. (B) Timeline of CEC proliferation over 48-hours with Click-iT EdU assay. (C) Proliferation of CECs after treatment with CPC sEV/ELV or MSC sEV/ELV normalized to CPC sEV

group. (D) Inter-parent cell type differences in vesicle-induced CEC proliferation: within MSC-derived vesicles and within CPC-derived vesicles. Data normalized to corresponding sEV group. Mean±SEM. Significance was tested with two-way Student's paired *t* test. n.s. = not significant. *P<0.05.

5.3.10 miR-126+ MSC ELVs induce tube formation when administered to CECs more than miR-126+ CPC ELVs

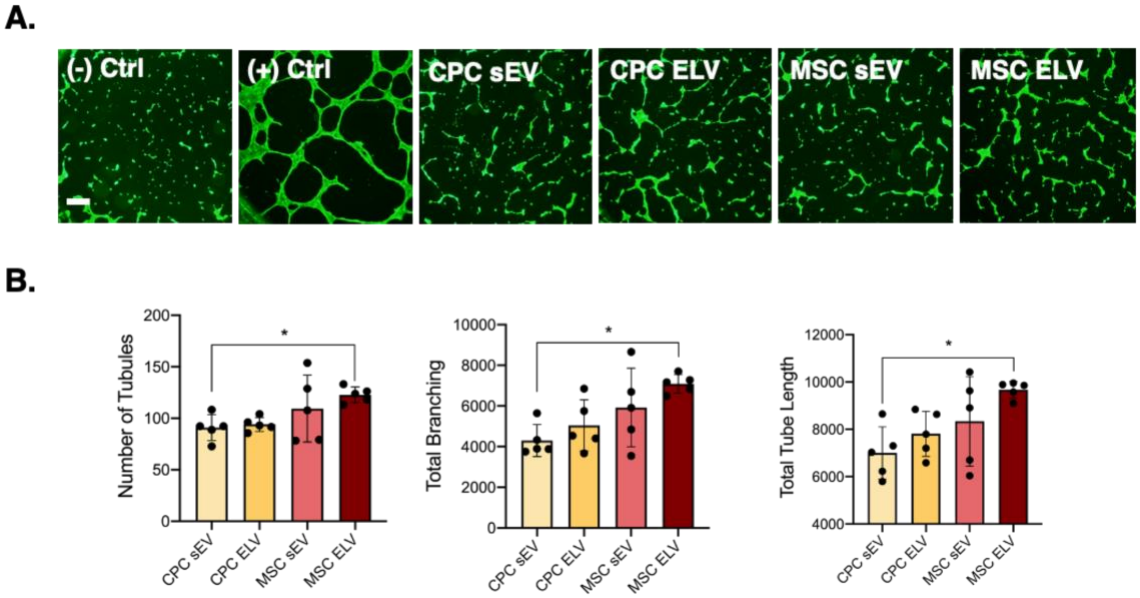

Figure 29. MSC ELVs induce pro-angiogenic response in CECs. (A) Calcein-AM+ CECs (green) treated with MSC or CPC-derived sEVs or ELVs incubated on Geltrex for tubes after overnight incubation. (B) Quantification of angiogenic parameters of number of tubes, total branching and total tube length show increase in parameters with MSC ELVs than CPC sEVs. Data normalized to negative control. Mean±SEM. Significance was tested with one-way ANOVA with Tukey post-hoc. *P<0.05. Scale bar = 200 µm.

Finally, we assessed the pro-angiogenic potential of MSC-vesicles and compared that to CPC vesicles which we established are pro-angiogenic in Chapter 3. When treated to CECs with overnight incubation on Geltrex, all groups induced the formation of tubes (Figure 29A). When quantified for tube formation parameters: number of tubules, total branching, and total tube length, MSC ELVs significantly increased tube formation compared to CPC

sEVs. Further, MSC ELVs functional response had less batch-to-batch variability that the corresponding MSC sEV groups (Figure 29B).

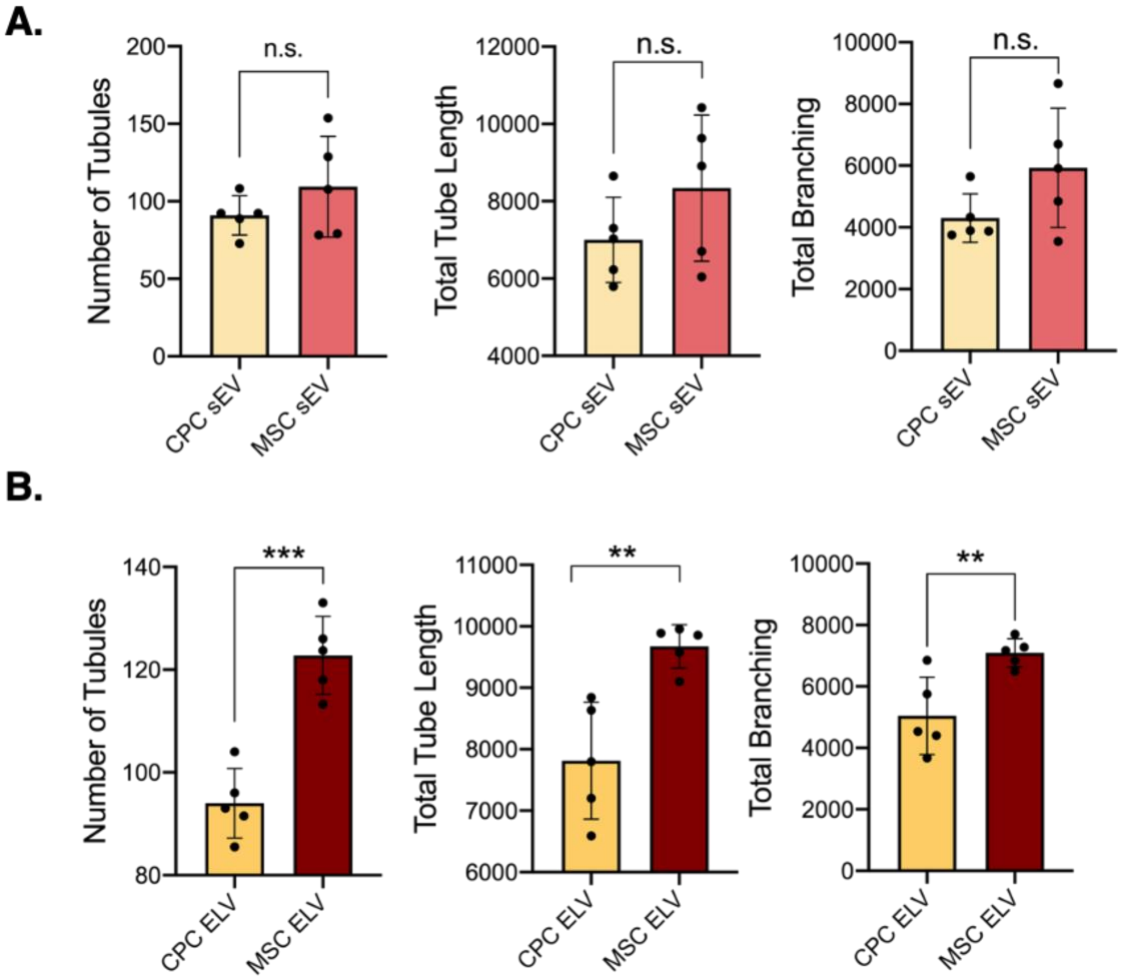

Figure 30. MSC ELVs are more pro-angiogenic than CPC ELVs. Quantification of number of tubules, total tube length and total branching. (A) Inter-parent cell type contribution to angiogenic potential between CPC and MSC derived sEVs. No significant difference induced by parent cell type. (B) Inter-parent cell type contribution to angiogenic potential between CPC and MSC derived ELVs. MSC ELVs are significantly more angiogenic than CPC ELVs. Mean±SEM. Significance was tested with two-way Student's paired *t* test. Data normalized to negative control. n.s. = not significant. **P<0.01, ***P<0.001.

Further, we sought to explore the role of the parent cell type of the functional response so we compared CPC sEVs to MSC sEVs (Figure 30A) and CPC ELVs to MSC ELVs (Figure

30B). There was no functional difference between the CPC and the MSC derived sEVs in inducing CEC tube formation. However, interestingly, when comparing CPC and MSC ELV groups, the MSC ELVs significantly improved all three measured tube formation parameters. Taken together, this suggests that the vesicle membrane does play a role in functional outcomes but also that the variable cargo within sEVs could be masking the effects which are then elucidated when controlling the internal cargo with our ELV design.

5.4 Discussion

sEVs consist of a complex lipid- and protein-based membrane, and this membrane composition varies based on the sEV's parent cell type. As sEVs are important mediators of cell-cell communication, and uptake of sEVs depends on interaction of the sEV membrane with the recipient cell, there is value to understanding the variations in sEV membranes and their effect on uptake. Moreover, as our ELVs are engineered from sEVs, this knowledge will help us determine which source-sEVs we should use for ELV synthesis, based on our desired cargo delivery mechanism. In this work, we explore the diverse lipid and protein profiles of sEVs derived from four cardiac-relevant cell types: CPCs, MSCs, CECs and RCFs. We establish that sEV parent cell type is one of the primary sources of variance in membrane composition, and that clathrin-mediated uptake varies the most across parent cell types with macropinocytosis varying when sEVs are treated to CEC recipient cells. We then connect the lipid-protein profiles to uptake mechanism and recipient cell type, finding that for a given recipient cell type, the membrane profile for a each uptake mechanism is distinct. In addition, we then synthesize MSC and CPC derived

ELVs and delivere miR-126 to CECs, with MSC ELVs significantly improving functional outcomes. Together, these data underscore the importance of understanding the membrane profile, its importance is sEV function and that the sEVs selected for ELV synthesis can impact ELV potency.

One source of variation in sEV function is oxygen conditioning. Prior work from our lab and others have shown that hypoxic conditioning of CPCs and MSCs can make their sEVs more reparative[9,60,96]. Although the role of the cargo (specifically miR) in the pro-reparative effects has been well explored, the potential role of the membrane wasn't studied. Here, we isolated sEVs from both CPCs and MSCs in normoxic and hypoxic conditions to assess if there were variations in the membrane profiles that could have affected uptake and in-turn function. No significant differences were observed in the lipid or protein profiles of the sEVs or in the uptake mechanisms utilized by the normoxic and hypoxic sEV counterparts. This reiterates that the cargo was the primary mediator of the observed differences and not the membrane or uptake efficiency. However, one aspect to note is that, for CPC sEVs, the hypoxic responses were conditional upon age, with hypoxic conditioning affecting sEV potency in CPCs derived from older patients[9]. Therefore, there is value in exploring age-dependency on the sEV membrane profile in the future as well.

To understand the role of different uptake mechanisms we used small-molecule inhibitors of each pathway. Upon quantification of the uptake efficiency, in some cases, inhibition of the macropinocytosis pathway seemed to further increase sEV uptake beyond the extent of sEV-only uptake (without any inhibitors). Although this appears counter-intuitive, it should be noted that the sEV-only uptake does not represent uptake of 100% of loaded sEVs but rather the *maximum* uptake without any inhibitors. Therefore, the greater-than-

one uptake when macropinocytosis is inhibited is still realistic. Despite this, the improvements in CPC- and MSC-sEV uptake by CECs and RCFs, respectively, upon inhibition of macropinocytosis is interesting. Prior studies assessing uptake in cancer cells found that inhibition of macropinocytosis reduced sEV uptake[196,206]. However, it's established that the capacity of clathrin-independent endocytosis methods, which includes macropinocytosis, can largely vary upon differences in experimental procedures (e.g., serum starvation), cell types, and cell physiological states (e.g., cell confluency)[207]. Further, we chose chemical small-molecule inhibitors for this study and validated their efficiency at inhibiting albumin and transferrin uptake. However, it should be noted that chemical inhibitors often have broad-targets and could partially affect other mechanisms of action of well. Taken together, this suggests that the increase in uptake of certain sEVs with macropinocytosis inhibition is realistic and may be inducing a compound effect that can be further explored.

Beyond understanding the role of sEV origin on uptake mechanism, we also explored the lipid and protein profiles of the different sEVs. Although few, other studies investigating sEV membrane lipids collected conditioned media over several days, whereas in our case, with the hypoxic conditioning, we isolated conditioned media after 12 hours[208,209]. This reduced the concentration of sEVs in our studies, and despite several methods to increase sEV concentration, remained on the lower end of the mass spectrometry requirements. Consequently, despite successfully obtaining 216 lipid features, after downstream processing, the unique lipid features were too few to establish robust pathway analysis. This did not affect the scope of our study as we focused on the combinatorial effects of the membrane lipids and proteins, but in the future, warrants further exploration of sEV lipids.

This would then allow selective ELV engineering not just based on important protein pathways of interest, but also based on desired lipid pathways of interest too.

Having established the variations in sEV membrane and uptake, we focused on synthesizing ELVs from CPC and MSC-sEVs to assess the role of the membrane on delivering a uniform miR-126 cargo. Interestingly, miR-126 encapsulated in the MSC ELVs increased proliferation and angiogenesis in CECs, and the MSC ELVs significantly increased angiogenesis more than the CPC ELVs, but this did not reflect between MSC and CPC sEVs. As the MSC and CPC ELVs carry the same cargo, this suggests the MSC ELV membrane favors uptake by CECs. This is supported by our uptake study in which MSC uptake was significantly affected by clathrin and macropinocytosis inhibition, but CPC uptake was more pathway independent (Figure 21). However, given that MSC and CPC sEVs have similar membranes to the MSC and CPC ELVs, the lack of improvement with MSC sEVs suggests some cargo level mitigation of the pro-angiogenic extent of MSCs. Thus, this study of uptake with MSC- and CPC-ELV synthesis can help us further elucidate the role of the membrane and cargo in vesicle function by reducing the variability observed by sEVs.

In summary, this work has furthered our understanding of the sEV membrane components and its relation to uptake. Its also expanded the scope of the ELVs synthesized and verified in Chapters 3 and 4 to help (1) parse apart the effects of the membrane vs. cargo in functional responses and (2) to allow us to carefully select the parent-cell from which to synthesize our ELVs based on our desired downstream function.

CHAPTER 6. CONCLUSION

Myocardial infarction (MI) is the leading cause of mortality and morbidity worldwide[148]. Current therapies for MI include pharmacochemical and mechanical interventions to prolong relief but do not mitigate repeated ischemic attacks. Cellular therapies for MI have shown promise, but a recent paradigm shift has attributed the benefits of cell therapies to paracrine signaling, specifical through small extracellular vesicle (sEV) release[210]. sEVs are 30-150nm vesicles which a complex lipid-protein bilayer membrane and encapsulate cardioprotective and pro-reparative cargo. However, their synthesis and cargo encapsulation efficiency are highly variable, based on parent cell conditions, thereby minimizing the development of robust, scalable therapies. Synthetic sEV-mimics allow for cargo control but suffer poor stability and shelf life, likely attributed to their simplistic bilayer membrane. In this dissertation, we successfully engineered sEV-like vehicles (ELVs) consisting of an sEV membrane but allowing cargo customizability. We validate the potency of miR-126 loaded ELVs *in vitro* for angiogenesis and *in vivo* in a rat model of IR. In addition, we further delve into the role of the sEV membrane on sEV uptake mechanism and parse through the role of membrane on function by comparing the potency of ELV derived from ckit+ progenitor cells and mesenchymal stem cells. Taken together, this work showcases the value of our engineered ELVs as vehicles for cardiac therapy, both for MI and beyond.

CHAPTER 7. FUTURE WORK AND DIRECTIONS

In this dissertation we have established the importance of an engineered vehicle for cargo delivery. In chapter 3, we synthesized the ELVs from CPC-sEVs, characterized them and confirmed their potency for delivering pro-angiogenic miR-126 to CECs. In chapter 4, we validated our CPC-ELVs *in vivo,* in a rat model of IR, and showed strong tissue-level improvements with ELV dosing. In chapter 5, we explored the sEV membrane biology further, to understand the role of sEV lipids and proteins on uptake mechanism and recipient cell delivery. Further, having established the value of ELVs, we studied the effect of ELV source cell on ELV functionality, and confirmed that the sEV membrane does play a role on ELV potency. However, despite the progress made with this work, there remains certain limitations to the work and scope for future work to be conducted based on these findings. Some of these future directions are outlined and discussed below.

In Chapter 3, we chose miR-126 as a proof-of-concept miR to load into our ELVs. Being an endothelial-specific marker, which is less abundant in CPC-sEVs, the detection of miR-126 in our ELVs was a simple confirmation of selective cargo loading. Moreover, miR-126 is a well-established proponent of angiogenesis and therefore was a suitable cargo for our in vivo animal studies as well, where angiogenesis and neovascularization in the infarct border zone are important aspects of cardiac repair after MI. However, our ELV's scope is far beyond miR-126. It would be highly useful to assess the functional effect of loading other miRs into ELVs too (e.g., anti-fibrotic miRs, anti-inflammatory miRs, pro-migratory miRs, to name a few). It would be interesting to explore the direct loading of single miRs with other functions but also to study miR-combinations, to see how loading multiple miRs

for a given functional benefit compound the observed response. For example, we could load different pro-angiogenesis miRs that target different cellular pathways to create an ELV that is 'mega-angiogenic'. Beyond this, we can also study the effect of combining different miRs which each target a *different* functional outcome. In this manner, we could explore creating 'acute MI' ELVs which contain miRs to target angiogenesis, fibrosis, hypertrophy, and inflammation all in just one ELV. To aid with such studies, we can utilize the expanding field of bioinformatics. Our lab and others have explored the sEV cargo, specifically the mRNA and miR profiles to determine the 'top hit' mRNA and miRs related to each functional outcome[88,211]. Using this information, we can curate the miR cargo in ELVs and assess outcomes.

In Chapter 4, we delivered our ELV samples intramyocardially into the LV wall immediately after IR to assess the benefits of ELVs in an acute MI model. However, to make the therapeutic more translational, less invasive methods should be investigated, such as intravenous injection through the rat tail vein. With this, we'll also have to explore ELV targeting to the myocardium, which was less challenging when injecting directly into the myocardium. As our ELVs are made from sEVs, unlike synthetic mimics, we should also study the effect of wash-out upon injection. Further, if required, to aid with homing to the myocardium, we can explore embedding targeting peptides into the ELV membrane during the ELV synthesis process[91,212,213]. Beyond this, we should also look at the *in vivo* immunomodulatory responses to ELV injection, an aspect that we didn't investigate in this dissertation. For example, we could look at cytokine and chemokine release, neutrophil and monocyte trafficking, and macrophage polarization.

Another aspect that should be further explored is the global responses to ELV treatment. As mentioned in Chapter 4, although significant improvements of ejection fraction and fractional shortening were present, there was inconsistency between the groups and observed effects tapered after day 14. One reasoning for this is that the dosages that we used are significantly lower than those used in other acute MI models, which also achieved only approximately 3.6% improvements in function on average. Therefore, even higher concentrations of ELVs and sEVs can be administered. It would also be worthwhile to perform repeated dosing (e.g., another echo-guided injection at day 14) as the half-life of miRs is quite short (span of days) and therefore there's a chance the benefits of the miRs would have depleted by day 14. Moreover, to minimize such repeated injections, ELV therapies administered through cardiac patches can be explored[214,215]. Encapsulation into patches could allow controlled and sequential delivery over time, thereby prolonging the pro-reparative effects of the ELVs. Finally, we could also investigate the role of ELVs in a chronic model of MI, by delivering the ELVs two weeks after the onset of IR. Though not suitable for the focus of this study on acute MI, this would help distinguish any ELV benefits that are masked by the initial influx of immunomodulatory response and immediate cardiac remodeling.

When synthetic mimics are administered, another aspect that can alter or abrogate their therapeutic benefit is the protein corona that forms around them upon exposure to plasma or serum. The protein corona binds to the bilayer and acts as the biological 'identity' for that vesicle[216]. These coronas can comprise of several proteins including serum albumin, apolipoproteins (ApoA1, ApoE), immunoglobulins (IgG, IgM), fibrinogen and complement factor C3[217]. As ELVs also consist of a vesicle membrane and will be exposed

to serum proteins *in vivo*, extensive investigation into the extent of corona formation, the exact protein-profile of ELV coronas and its effects on ELV function can be studied. This was beyond the scope of this current work because of limitations with ELV yield. When performing proteomic profiling of sEVs for chapter 5, we established that the sEV concentrations we were working with were on the lower end of that required for mass spectrometry. Given that our ELV yield is currently lower than our sEV yield, we couldn't obtain a complete ELV profile to assess the corona. However, in the future, as the ELV production is scaled up and more initial sEVs are used for synthesis, this field can be thoroughly explored. Further, if the protein corona is impeding the ELV function, methods for corona mitigation on ELVs can be investigated as well.

In Chapter 5, we looked at the role of the vesicle membrane on sEV uptake and ELV function. In this work, we created an initial model to connect the sEV membrane proteins and lipids to uptake mechanism based on recipient cell. The next step would be to validate this model we have developed with *in vitro* testing so that we can expand the model into a predictive tool. Using this, for a desired functional outcome we can assess which uptake mechanism is more utilized and in-turn which lipid-protein membrane our ELVs should be comprised of for optimal uptake. Another aspect to this study was the uptake mechanism analysis. Here, we explored the effects of individually inhibiting each uptake pathway and the resulting outcome. However, several of these pathways work in tangent in cells and therefore, we can expand this study to look at the combinatorial effects of activating and inhibiting different uptake mechanisms in concert. Further, for this study we selected three uptake mechanisms that represent the clathrin-dependent, clathrin independent and macropinocytosis-based uptake. However, there are several more mechanisms present for

sEV uptake, so those could be investigated to establish a more complete picture of the sEV membrane role on uptake.

Finally, when investigating the role of sEV membrane composition on ELV function, we established that miR-126+MSC ELVs significantly improved angiogenesis in CECs compared to miR-126+CPC ELVs. As both ELVs have a similar cargo this suggested that the MSC membrane plays a role. However, the corresponding MSC sEVs did not significantly improve angiogenesis compared to CPC sEVs despite their membrane being like that of their partner ELVs. This indicated that there may be components of the MSC sEV cargo that mitigates the pro-angiogenic potential of the vesicles. Angiogenesis is one functional outcome that we measured in this Chapter, but there's scope for this to apply to other functional outcomes too. By utilizing the ELV design, future work can parse apart cases where the membrane or cargo are masking some of the sEV benefits. Further, by performing transcriptomic sequencing of CPC and MSC cargo, we can use computational approaches to detect the specific mRNA/miRs that are impeding function and thereby silence them to increase sEV potency.

APPENDIX

Appendix A: mature microRNA 126 sequence

Hsa-miR-126-5p RNA sequence: CArUrUArUrUACrUrUrUrUGGrUACGCG

REFERENCES

1. Virani, S. S. *et al.* Heart Disease and Stroke Statistics—2020 Update: A Report From the American Heart Association. *Circulation* **141**, e139–e596 (2020).

2. Mayourian, J. *et al.* Exosomal microRNA-21-5p Mediates Mesenchymal Stem Cell Paracrine Effects on Human Cardiac Tissue Contractility. *Circ Res* **122**, 933–944 (2018).

3. Bolli, R. *et al.* Rationale and Design of the CONCERT-HF Trial (Combination of Mesenchymal and c-kit(+) Cardiac Stem Cells As Regenerative Therapy for Heart Failure). *Circ Res* **122**, 1703–1715 (2018).

4. Bao, L. *et al.* C-Kit Positive Cardiac Stem Cells and Bone Marrow-Derived Mesenchymal Stem Cells Synergistically Enhance Angiogenesis and Improve Cardiac Function After Myocardial Infarction in a Paracrine Manner. *J Card Fail* **23**, 403–415 (2017).

5. Lee, C. *et al.* Exosomes mediate the cytoprotective action of mesenchymal stromal cells on hypoxia-induced pulmonary hypertension. *Circulation* **126**, 2601–2611 (2012).

6. Sang-Ging Ong Won Hee Lee, Kazuki Kodo, Antje D. Ebert, Ya Ma, Wen-Ya Chen, Joseph C. Wu, B. C. H. Microfluidic Single Cell Analysis of Transplanted Human Induced Pluripotent Stem Cell-Derived Cardiomyocytes Following Acute Myocardial Infarction. *Circulation* **132**, 762–771 (2016).

7. Barile, L. *et al.* Cardioprotection by cardiac progenitor cell-secreted exosomes: role of pregnancy-associated plasma protein-A. *Cardiovasc Res* **114**, 992–1005 (2018).

8. Cosme, J., Guo, H., Hadipour-Lakmehsari, S., Emili, A. & Gramolini, A. O. Hypoxia-Induced Changes in the Fibroblast Secretome, Exosome, and Whole-Cell Proteome Using Cultured, Cardiac-Derived Cells Isolated from Neonatal Mice. *J Proteome Res* **16**, 2836–2847 (2017).

9. Agarwal, U. *et al.* Experimental, systems, and computational approaches to understanding the MicroRNA-mediated reparative potential of cardiac progenitor cell-derived exosomes from pediatric patients. *Circ Res* **120**, 701–712 (2017).

10. Bonios, M. *et al.* Myocardial substrate and route of administration determine acute cardiac retention and lung bio-distribution of cardiosphere-derived cells. *J Nucl Cardiol* **18**, 443–450 (2011).

11. Soltani, F., Parhiz, H., Mokhtarzadeh, A. & Ramezani, M. Synthetic and Biological Vesicular Nano-Carriers Designed for Gene Delivery. *Curr Pharm Des* **21**, 6214–6235 (2015).

12. Nkanga, C. I., Bapolisi, A. M., Okafor, N. I. & Krause, R. W. M. General Perception of Liposomes: Formation, Manufacturing and Applications. in *Liposomes - Advances and Perspectives* (IntechOpen, 2019). doi:10.5772/intechopen.84255.

13. Guyton, A. C. & Hall, J. E. Textbook of Medical Physiology. in *Elsevier Inc.* 249–253 (Elsevier, 2011).

14. DeWood, M. A. *et al.* Prevalence of Total Coronary Occlusion during the Early Hours of Transmural Myocardial Infarction. *New England Journal of Medicine* **303**, (1980).

15. Frangogiannis, N. G. Pathophysiology of myocardial infarction. *Compr Physiol* **5**, 1841–1875 (2015).

16. Heusch, G. & Gersh, B. J. The pathophysiology of acute myocardial infarction and strategies of protection beyond reperfusion: A continual challenge. *European Heart Journal* vol. 38 Preprint at https://doi.org/10.1093/eurheartj/ehw224 (2017).

17. Jennings, R. B. Historical perspective on the pathology of myocardial ischemia/reperfusion injury. *Circulation Research* vol. 113 Preprint at https://doi.org/10.1161/CIRCRESAHA.113.300987 (2013).

18. Reimer, K. A., Lowe, J. E., Rasmussen, M. M. & Jennings, R. B. The wavefront phenomenon of ischemic cell death. 1. Myocardial infarct size vs duration of coronary occlusion in dogs. *Circulation* **56**, (1977).

19. Ibáñez, B., Heusch, G., Ovize, M. & van de Werf, F. Evolving therapies for myocardial ischemia/reperfusion injury. *Journal of the American College of Cardiology* vol. 65 Preprint at https://doi.org/10.1016/j.jacc.2015.02.032 (2015).

20. Schömig, A. *et al.* Mechanical reperfusion in patients with acute myocardial infarction presenting more than 12 hours from symptom onset: A randomized controlled trial. *JAMA* **293**, (2005).

21. Kajstura, J. *et al.* Apoptotic and necrotic myocyte cell deaths are independent contributing variables of infarct size in rats. *Lab Invest* **74**, 86–107 (1996).

22. Bialik, S. *et al.* Myocyte apoptosis during acute myocardial infarction in the mouse localizes to hypoxic regions but occurs independently of p53. *J Clin Invest* **100**, 1363–1372 (1997).

23. Braunwald, E. & Kloner, R. A. Myocardial reperfusion: A double-edged sword? *Journal of Clinical Investigation* **76**, (1985).

24. Mann, D. L. Innate immunity and the failing heart: The cytokine hypothesis revisited. *Circulation Research* vol. 116 Preprint at https://doi.org/10.1161/CIRCRESAHA.116.302317 (2015).

25. Morimoto, H. *et al.* MCP-1 induces cardioprotection against ischaemia/reperfusion injury: Role of reactive oxygen species. *Cardiovasc Res* **78**, (2008).

26. Davidson, S. M. *et al.* Remote ischaemic preconditioning involves signalling through the SDF-1α/CXCR4 signalling axis. *Basic Res Cardiol* **108**, (2013).

27. Mann, D. L. Inflammatory mediators and the failing heart: Past, present, and the foreseeable future. *Circulation Research* vol. 91 Preprint at https://doi.org/10.1161/01.RES.0000043825.01705.1B (2002).

28. Nahrendorf, M., Pittet, M. J. & Swirski, F. K. Monocytes: Protagonists of infarct inflammation and repair after myocardial infarction. *Circulation* vol. 121 Preprint at https://doi.org/10.1161/CIRCULATIONAHA.109.916346 (2010).

29. Frangogiannis, N. G. Regulation of the inflammatory response in cardiac repair. *Circulation Research* vol. 110 Preprint at https://doi.org/10.1161/CIRCRESAHA.111.243162 (2012).

30. Li, Z. *et al.* Single-cell transcriptome analyses reveal novel targets modulating cardiac neovascularization by resident endothelial cells following myocardial infarction. *Eur Heart J* **40**, 2507–2520 (2019).

31. AE, S. *et al.* Mesenchymal stem cell therapy: A promising cell-based therapy for treatment of myocardial infarction. . (2018).

32. Frangogiannis, N. G. Cardiac fibrosis. *Cardiovasc Res* **117**, 1450–1488 (2021).

33. Gao, X. M., White, D. A., Dart, A. M. & Du, X. J. Post-infarct cardiac rupture: Recent insights on pathogenesis and therapeutic interventions. *Pharmacol Ther* **134**, 156–179 (2012).

34. Lu, L., Liu, M., Sun, R., Zheng, Y. & Zhang, P. Myocardial Infarction: Symptoms and Treatments. *Cell Biochem Biophys* **72**, 865–867 (2015).

35. Brandt, E. J. *et al.* Impact of left ventricular assist devices and heart transplants on acute myocardial infarction and heart failure mortality and readmission measures. *PLoS One* **15**, e0230734 (2020).

36. Grothusen, C. *et al.* Coronary artery bypass surgery within 48 hours after cardiac arrest due to acute myocardial infarction. *Eur J Cardiothorac Surg* **52**, 297–302 (2017).

37. Zhang, W. *et al.* Necrotic myocardial cells release Damage-Associated Molecular Patterns that provoke fibroblast activation in vitro and trigger myocardial inflammation and fibrosis in vivo. *J Am Heart Assoc* **4**, (2015).

38. Eschenhagen, T. *et al.* Cardiomyocyte regeneration: A consensus statement. *Circulation* **136**, (2017).

39. Pinto, A. R. *et al.* Revisiting cardiac cellular composition. *Circ Res* **118**, (2016).

40. Gray, G. A., Toor, I. S., Castellan, R. F. P., Crisan, M. & Meloni, M. Resident cells of the myocardium: more than spectators in cardiac injury, repair and regeneration. *Current Opinion in Physiology* vol. 1 Preprint at https://doi.org/10.1016/j.cophys.2017.08.001 (2018).

41. He, L. *et al.* Preexisting endothelial cells mediate cardiac neovascularization after injury. *Journal of Clinical Investigation* **127**, (2017).

42. Turner, N. A. Inflammatory and fibrotic responses of cardiac fibroblasts to myocardial damage associated molecular patterns (DAMPs). *Journal of Molecular and Cellular Cardiology* vol. 94 Preprint at https://doi.org/10.1016/j.yjmcc.2015.11.002 (2016).

43. Mylonas, K. J. *et al.* 11β-HSD1 suppresses cardiac fibroblast CXCL2, CXCL5 and neutrophil recruitment to the heart post MI. *Journal of Endocrinology* **233**, (2017).

44. Nakaya, M. *et al.* Cardiac myofibroblast engulfment of dead cells facilitates recovery after myocardial infarction. *Journal of Clinical Investigation* **127**, (2017).

45. Chen, B. & Frangogiannis, N. G. Immune cells in repair of the infarcted myocardium. *Microcirculation* vol. 24 Preprint at https://doi.org/10.1111/micc.12305 (2017).

46. Li, W. *et al.* Heart-resident CCR2+ macrophages promote neutrophil extravasation through TLR9/MyD88/CXCL5 signaling. *JCI Insight* **1**, (2016).

47. Lavine, K. J. *et al.* Distinct macrophage lineages contribute to disparate patterns of cardiac recovery and remodeling in the neonatal and adult heart. *Proc Natl Acad Sci U S A* **111**, (2014).

48. Rodriguez, A. M. & Yin, V. P. Emerging Roles for Immune Cells and MicroRNAs in Modulating the Response to Cardiac Injury. *J Cardiovasc Dev Dis* **6**, (2019).

49. Beltrami, A. P. *et al.* Adult cardiac stem cells are multipotent and support myocardial regeneration. *Cell* **114**, (2003).

50. Messina, E. *et al.* Isolation and expansion of adult cardiac stem cells from human and murine heart. *Circ Res* **95**, (2004).

51. French, K. M. & Davis, M. E. Isolation and expansion of C-Kit-positive cardiac progenitor cells by magnetic cell sorting. *Methods in Molecular Biology* **1181**, (2014).

52. Sultana, N. *et al.* Resident c-kit + cells in the heart are not cardiac stem cells. *Nat Commun* **6**, (2015).

53. van Berlo, J. H. *et al.* C-kit+ cells minimally contribute cardiomyocytes to the heart. *Nature* **509**, (2014).

54. Bittle, G. J. *et al.* Stem cell therapy for hypoplastic left heart syndrome mechanism, clinical application, and future directions. *Circulation Research* vol. 123 Preprint at https://doi.org/10.1161/CIRCRESAHA.117.311206 (2018).

55. Wehman, B. *et al.* Cardiac Progenitor Cells Enhance Neonatal Right Ventricular Function After Pulmonary Artery Banding. in *Annals of Thoracic Surgery* vol. 104 (2017).

56. Simpson, D. L. *et al.* A strong regenerative ability of cardiac stem cells derived from neonatal hearts. *Circulation* **126**, (2012).

57. Shoja-Taheri, F. *et al.* Using Statistical Modeling to Understand and Predict Pediatric Stem Cell Function Farnaz. *Circ Genom Precis Med* **12**, e002403 (2019).

58. Agarwal, U. *et al.* Age-Dependent Effect of Pediatric Cardiac Progenitor Cells After Juvenile Heart Failure. *Stem Cells Transl Med* **5**, 883–892 (2016).

59. Trac, D., Maxwell, J. T., Brown, M. E., Xu, C. & Davis, M. E. Aggregation of child cardiac progenitor cells into spheres activates notch signaling and improves treatment of right ventricular heart failure. *Circ Res* **124**, 526–538 (2019).

60. Gray, W. D. *et al.* Identification of therapeutic covariant microRNA clusters in hypoxia-treated cardiac progenitor cell exosomes using systems biology. *Circ Res* **116**, 255–263 (2015).

61. Friedenstein, A. J., Chailakhjan, R. K. & Lalykina, K. S. THE DEVELOPMENT OF FIBROBLAST COLONIES IN MONOLAYER CULTURES OF GUINEA-PIG BONE MARROW AND SPLEEN CELLS. *Cell Prolif* **3**, (1970).

62. Dominici, M. *et al.* Minimal criteria for defining multipotent mesenchymal stromal cells. The International Society for Cellular Therapy position statement. *Cytotherapy* **8**, (2006).

63. Schu, S. *et al.* Immunogenicity of allogeneic mesenchymal stem cells. *J Cell Mol Med* **16**, (2012).

64. Najar, M. *et al.* Mesenchymal stromal cells and immunomodulation: A gathering of regulatory immune cells. *Cytotherapy* vol. 18 Preprint at https://doi.org/10.1016/j.jcyt.2015.10.011 (2016).

65. Chiossone, L. *et al.* Mesenchymal Stromal Cells Induce Peculiar Alternatively Activated Macrophages Capable of Dampening Both Innate and Adaptive Immune Responses. *Stem Cells* **34**, (2016).

66. Miteva, K. *et al.* Mesenchymal stromal cells modulate monocytes trafficking in coxsackievirus B3-induced myocarditis. *Stem Cells Transl Med* **6**, (2017).

67. Guo, Y., Yu, Y., Hu, S., Chen, Y. & Shen, Z. The therapeutic potential of mesenchymal stem cells for cardiovascular diseases. *Cell Death and Disease* vol. 11 Preprint at https://doi.org/10.1038/s41419-020-2542-9 (2020).

68. Ye, J. & Yeghiazarians, Y. Cardiac stem cell therapy: review of the native cardiac progenitor cells and future direction. *J Cardiovasc Pharmacol* **63**, 85–94 (2014).

69. Streeter, B. W., Xue, J., Xia, Y. & Davis, M. E. Electrospun Nanofiber-Based Patches for the Delivery of Cardiac Progenitor Cells. *ACS Appl Mater Interfaces* **11**, 18242–18253 (2019).

70. Bejleri, D. *et al.* A Bioprinted Cardiac Patch Composed of Cardiac-Specific Extracellular Matrix and Progenitor Cells for Heart Repair. *Adv Healthc Mater* **7**, e1800672 (2018).

71. Yoon, J. *et al.* Differentiation, engraftment and functional effects of pre-treated mesenchymal stem cells in a rat myocardial infarct model. *Acta Cardiol* **60**, 277–284 (2005).

72. Kaushal, S. *et al.* Study design and rationale for ELPIS: A phase I/IIb randomized pilot study of allogeneic human mesenchymal stem cell injection in patients with hypoplastic left heart syndrome. *Am Heart J* **192**, 48–56 (2017).

73. University of Miami. Autologous Cardiac Stem Cell Injection in Patients With Hypoplastic Left Heart Syndrome: An Open Label Pilot Study. Preprint at (2018).

74. Fisher, S. A., Zhang, H., Doree, C., Mathur, A. & Martin-Rendon, E. Stem cell treatment for acute myocardial infarction. *Cochrane Database of Systematic Reviews* vol. 2015 Preprint at https://doi.org/10.1002/14651858.CD006536.pub4 (2015).

75. Wollert, K. C. & Drexler, H. Cell therapy for the treatment of coronary heart disease: A critical appraisal. *Nature Reviews Cardiology* vol. 7 Preprint at https://doi.org/10.1038/nrcardio.2010.1 (2010).

76. Ratajczak, M. Z. *et al.* Pivotal role of paracrine effects in stem cell therapies in regenerative medicine: Can we translate stem cell-secreted paracrine factors and microvesicles into better therapeutic strategies. *Leukemia* vol. 26 Preprint at https://doi.org/10.1038/leu.2011.389 (2012).

77. Ibrahim, A. G. E., Cheng, K. & Marbán, E. Exosomes as critical agents of cardiac regeneration triggered by cell therapy. *Stem Cell Reports* **2**, 606–619 (2014).

78. Johnstone, R. M., Adam, M., Hammond, J. R., Orr, L. & Turbide, C. Vesicle formation during reticulocyte maturation. Association of plasma membrane activities with released vesicles (exosomes). *J Biol Chem* **262**, 9412–9420 (1987).

79. Barile, L., Milano, G. & Vassalli, G. Beneficial effects of exosomes secreted by cardiac-derived progenitor cells and other cell types in myocardial ischemia. *Stem Cell Investig* 93–93 (2017) doi:10.21037/sci.2017.11.06.

80. Williams, J. B., Jauch, E. C., Lindsell, C. J. & Campos, B. Endothelial microparticle levels are similar in acute ischemic stroke and stroke mimics due to activation and not apoptosis/necrosis. *Acad Emerg Med* **14**, 685–690 (2007).

81. Camussi, G., Deregibus, M. C. & Tetta, C. Paracrine/endocrine mechanism of stem cells on kidney repair: role of microvesicle-mediated transfer of genetic information. *Curr Opin Nephrol Hypertens* **19**, 7–12 (2010).

82. Lamichhane, T. N., Raiker, R. S. & Jay, S. M. Exogenous DNA Loading into Extracellular Vesicles via Electroporation is Size-Dependent and Enables Limited Gene Delivery. *Mol Pharm* **12**, 3650–3657 (2015).

83. Saraste, A. & Pulkki, K. Morphologic and biochemical hallmarks of apoptosis. *Cardiovasc Res* **45**, 528–537 (2000).

84. Hristov, M., Erl, W., Linder, S. & Weber, P. C. Apoptotic bodies from endothelial cells enhance the number and initiate the differentiation of human endothelial progenitor cells in vitro. *Blood* **104**, 2761–2766 (2004).

85. Liu, C. *et al.* Microfluidic Sonication To Assemble Exosome Membrane-Coated Nanoparticles for Immune Evasion-Mediated Targeting. *Nano Lett* **19**, 7836–7844 (2019).

86. Doeppner TR, Herz J, Görgens A, Schlechter J, Ludwig AK, Radtke S, de Miroschedji K, Horn PA, Giebel B, H. DM. Extracellular Vesicles Improve Post-Stroke Neuroregeneration and Prevent Postischemic Immunosuppression. **4**, 1131–43 (2015).

87. Luan, X. *et al.* Engineering exosomes as refined biological nanoplatforms for drug delivery. *Acta Pharmacol Sin* **38**, 754–763 (2017).

88. Trac, D. *et al.* Predicting Functional Responses of Progenitor Cell Exosome Potential with Computational Modeling. *Stem Cells Transl Med* (2019) doi:10.1002/sctm.19-0059.

89. Saha, P. *et al.* Circulating exosomes derived from transplanted progenitor cells aid the functional recovery of ischemic myocardium. *Sci Transl Med* **11**, (2019).

90. Colao, I. L., Corteling, R., Bracewell, D. & Wall, I. Manufacturing Exosomes: A Promising Therapeutic Platform. *Trends Mol Med* **24**, (2018).

91. Vandergriff, A. *et al.* Targeting regenerative exosomes to myocardial infarction using cardiac homing peptide. *Theranostics* **8**, 1869–1878 (2018).

92. Ciullo, A. *et al.* Exosomal Expression of CXCR4 Targets Cardioprotective Vesicles to Myocardial Infarction and Improves Outcome after Systemic Administration. *Int J Mol Sci* **20**, (2019).

93. Qiao, L. *et al.* microRNA-21-5p dysregulation in exosomes derived from heart failure patients impairs regenerative potential. *J Clin Invest* **129**, 2237–2250 (2019).

94. Bang, C. *et al.* Cardiac fibroblast–derived microRNA passenger strand-enriched exosomes mediate cardiomyocyte hypertrophy. *J Clin Invest* **124**, 2136–2146 (2014).

95. Liu, J. *et al.* miR-93-5p-Containing Exosomes Treatment Attenuates Acute Myocardial Infarction-Induced Myocardial Damage. *Mol Ther Nucleic Acids* **11**, 103–115 (2018).

96. Zhu, L.-P. *et al.* Hypoxia-elicited mesenchymal stem cell-derived exosomes facilitates cardiac repair through miR-125b-mediated prevention of cell death in myocardial infarction. *Theranostics* **8**, 6163–6177 (2018).

97. Gallet, R. *et al.* Exosomes secreted by cardiosphere-derived cells reduce scarring, attenuate adverse remodelling, and improve function in acute and chronic porcine myocardial infarction. *Eur Heart J* **38**, 201–211 (2017).

98. Lai, R. C. *et al.* Exosome secreted by MSC reduces myocardial ischemia/reperfusion injury. *Stem Cell Res* **4**, 214–222 (2010).

99. Arslan, F. *et al.* Mesenchymal stem cell-derived exosomes increase ATP levels, decrease oxidative stress and activate PI3K/Akt pathway to enhance myocardial viability and prevent adverse remodeling after myocardial ischemia/reperfusion injury. *Stem Cell Res* **10**, 301–312 (2013).

100. Junjie Xiao & Sanda Cretoiu. *Exosomes in Cardiovascular Diseases*. (2017).

101. Barile, L. *et al.* Extracellular vesicles from human cardiac progenitor cells inhibit cardiomyocyte apoptosis and improve cardiac function after myocardial infarction. *Cardiovasc Res* **103**, 530–541 (2014).

102. Feng, Y., Huang, W., Wani, M., Yu, X. & Ashraf, M. Ischemic Preconditioning Potentiates the Protective Effect of Stem Cells through Secretion of Exosomes by Targeting Mecp2 via miR-22. *PLoS One* **9**, e88685 (2014).

103. Yu, B. *et al.* Exosomes secreted from GATA-4 overexpressing mesenchymal stem cells serve as a reservoir of anti-apoptotic microRNAs for cardioprotection. *Int J Cardiol* **182**, 349–360 (2015).

104. Vicencio, J. M. *et al.* Plasma Exosomes Protect the Myocardium From Ischemia-Reperfusion Injury. *J Am Coll Cardiol* **65**, 1525 LP – 1536 (2015).

105. Helwa, I. *et al.* A Comparative Study of Serum Exosome Isolation Using Differential Ultracentrifugation and Three Commercial Reagents. *PLoS One* **12**, e0170628–e0170628 (2017).

106. Khan, M. *et al.* Embryonic stem cell-derived exosomes promote endogenous repair mechanisms and enhance cardiac function following myocardial infarction. *Circ Res* **117**, 52–64 (2015).

107. Sahoo, S. *et al.* Exosomes from human CD34(+) stem cells mediate their proangiogenic paracrine activity. *Circ Res* **109**, 724–728 (2011).

108. Aatonen, M. T. *et al.* Isolation and characterization of platelet-derived extracellular vesicles. *J Extracell Vesicles* **3**, 10.3402/jev.v3.24692 (2014).

109. Johnsen, K. B. *et al.* Evaluation of electroporation-induced adverse effects on adipose-derived stem cell exosomes. *Cytotechnology* **68**, 2125–2138 (2016).

110. Chevillet, J. R. *et al.* Quantitative and stoichiometric analysis of the microRNA content of exosomes. *Proceedings of the National Academy of Sciences* **111**, 14888–14893 (2014).

111. Smyth, T. *et al.* Biodistribution and delivery efficiency of unmodified tumor-derived exosomes. *J Control Release* **199**, 145–155 (2015).

112. Tian, T. *et al.* Dynamics of exosome internalization and trafficking. *J Cell Physiol* **228**, 1487–1495 (2013).

113. Li, S.-P., Lin, Z.-X., Jiang, X.-Y. & Yu, X.-Y. Exosomal cargo-loading and synthetic exosome-mimics as potential therapeutic tools. *Acta Pharmacol Sin* **39**, 542–551 (2018).

114. Sokolov, A. V, Kostin, N. N., Ovchinnikova, L. A., Lomakin, Y. A. & Kudriaeva, A. A. Targeted Drug Delivery in Lipid-like Nanocages and Extracellular Vesicles. *Acta Naturae* **11**, 28–41 (2019).

115. Grimaldi, N. *et al.* Lipid-based nanovesicles for nanomedicine. *Chem Soc Rev* **45**, 6520–6545 (2016).

116. Bangham, A. D. Liposomes: the Babraham connection. *Chem Phys Lipids* **64**, 275–285 (1993).

117. Monteiro, N., Martins, A., Reis, R. L. & Neves, N. M. Liposomes in tissue engineering and regenerative medicine. *J R Soc Interface* **11**, 20140459 (2014).

118. Lin, C. M., Li, C. S., Sheng, Y. J., Wu, D. T. & Tsao, H. K. Size-dependent properties of small unilamellar vesicles formed by model lipids. *Langmuir* **28**, 689–700 (2012).

119. Bartelds, R. *et al.* Niosomes, an alternative for liposomal delivery. *PLoS One* **13**, e0194179–e0194179 (2018).

120. Rajera, R., Nagpal, K., Singh, S. K. & Mishra, D. N. Niosomes: a controlled and novel drug delivery system. *Biol Pharm Bull* **34**, 945–953 (2011).

121. Yang, L. *et al.* Mechanism of transdermal permeation promotion of lipophilic drugs by ethosomes. *Int J Nanomedicine* **12**, 3357–3364 (2017).

122. Cevc, G., Gebauer, D., Stieber, J., Schätzlein, A. & Blume, G. Ultraflexible vesicles, Transfersomes, have an extremely low pore penetration resistance and transport therapeutic amounts of insulin across the intact mammalian skin. *Biochim Biophys Acta* **1368**, 201–215 (1998).

123. Duangjit, S., Opanasopit, P., Rojanarata, T. & Ngawhirunpat, T. Characterization and In Vitro Skin Permeation of Meloxicam-Loaded Liposomes versus Transfersomes. *J Drug Deliv* **2011**, 418316 (2011).

124. Wissing, S. A., Kayser, O. & Müller, R. H. Solid lipid nanoparticles for parenteral drug delivery. *Adv Drug Deliv Rev* **56**, 1257–1272 (2004).

125. Campbell, R. B., Ying, B., Kuesters, G. M. & Hemphill, R. Fighting cancer: from the bench to bedside using second generation cationic liposomal therapeutics. *J Pharm Sci* **98**, 411–429 (2009).

126. Xie, Y. *et al.* Importance of cell-cell contact in the therapeutic benefits of cardiosphere-derived cells. *Stem Cells* **32**, 2397–2406 (2014).

127. Yamada, Y. *et al.* Postinfarct active cardiac-targeted delivery of erythropoietin by liposomes with sialyl Lewis X repairs infarcted myocardium in rabbits. *Am J Physiol Heart Circ Physiol* **304**, H1124-33 (2013).

128. Liu, X. *et al.* Pharmacokinetics of ligustrazine ethosome patch in rats and anti-myocardial ischemia and anti-ischemic reperfusion injury effect. *Int J Nanomedicine* **6**, 1391–1398 (2011).

129. Tang, J. *et al.* Therapeutic microparticles functionalized with biomimetic cardiac stem cell membranes and secretome. *Nat Commun* **8**, 13724 (2017).

130. Abu Lila, A. S. & Ishida, T. Liposomal Delivery Systems: Design Optimization and Current Applications. *Biol Pharm Bull* **40**, 1–10 (2017).

131. Guo, J., Ping, Q., Jiang, G., Huang, L. & Tong, Y. Chitosan-coated liposomes: characterization and interaction with leuprolide. *Int J Pharm* **260**, 167–173 (2003).

132. Immordino, M. L., Dosio, F. & Cattel, L. Stealth liposomes: review of the basic science, rationale, and clinical applications, existing and potential. *Int J Nanomedicine* **1**, 297–315 (2006).

133. Moghassemi, S., Hadjizadeh, A. & Omidfar, K. Formulation and Characterization of Bovine Serum Albumin-Loaded Niosome. *AAPS PharmSciTech* **18**, 27–33 (2017).

134. Touitou, E. *et al.* Intracellular delivery mediated by an ethosomal carrier. *Biomaterials* **22**, 3053–3059 (2001).

135. Wong, H. L., Bendayan, R., Rauth, A. M., Li, Y. & Wu, X. Y. Chemotherapy with anticancer drugs encapsulated in solid lipid nanoparticles. *Adv Drug Deliv Rev* **59**, 491–504 (2007).

136. Hu, C.-M. J. *et al.* Erythrocyte membrane-camouflaged polymeric nanoparticles as a biomimetic delivery platform. *Proc Natl Acad Sci U S A* **108**, 10980–10985 (2011).

137. Cao, H. *et al.* Liposomes Coated with Isolated Macrophage Membrane Can Target Lung Metastasis of Breast Cancer. *ACS Nano* **10**, 7738–7748 (2016).

138. Luo, L. *et al.* Fabrication of Synthetic Mesenchymal Stem Cells for the Treatment of Acute Myocardial Infarction in Mice. *Circ Res* **120**, 1768–1775 (2017).

139. Bheri, S., Hoffman, J. R., Park, H.-J. & Davis, M. E. Biomimetic nanovesicle design for cardiac tissue repair. *Nanomedicine* **15**, 1873–1896 (2020).

140. Pascucci, L. *et al.* Paclitaxel is incorporated by mesenchymal stromal cells and released in exosomes that inhibit in vitro tumor growth: A new approach for drug delivery. *Journal of Controlled Release* **192**, 262–270 (2014).

141. Kim, M. S. *et al.* Development of exosome-encapsulated paclitaxel to overcome MDR in cancer cells. *Nanomedicine* **12**, 655–664 (2016).

142. Wahlgren, J. *et al.* Plasma exosomes can deliver exogenous short interfering RNA to monocytes and lymphocytes. *Nucleic Acids Res* **40**, (2012).

143. Fuhrmann, G., Serio, A., Mazo, M., Nair, R. & Stevens, M. M. Active loading into extracellular vesicles significantly improves the cellular uptake and photodynamic effect of porphyrins. *Journal of Controlled Release* **205**, 35–44 (2015).

144. Haney, M. J. *et al.* Exosomes as drug delivery vehicles for Parkinson's disease therapy. *J Control Release* **207**, 18–30 (2015).

145. Jung, H. T. The origins of stability of spontaneous vesicles. *Proceedings of the National Academy of Sciences* **98**, 1353–1357 (2001).

146. Drulis-Kawa, Z. & Dorotkiewicz-Jach, A. Liposomes as delivery systems for antibiotics. *Int J Pharm* **387**, 187–198 (2010).

147. Ohno, S. I., Drummen, G. P. C. & Kuroda, M. Focus on extracellular vesicles: Development of extracellular vesicle-based therapeutic systems. *Int J Mol Sci* **17**, (2016).

148. Aparicio, H. J. *et al. Heart Disease and Stroke Statistics-2021 Update A Report from the American Heart Association*. *Circulation* (2021). doi:10.1161/CIR.0000000000000950.

149. Shafei, A. E. S. *et al.* Mesenchymal stem cell therapy: A promising cell-based therapy for treatment of myocardial infarction. *Journal of Gene Medicine* **19**, 1–10 (2017).

150. Puddighinu, G. *et al.* Molecular mechanisms of cardioprotective effects mediated by transplanted cardiac ckit(+) cells through the activation of an inflammatory hypoxia-dependent reparative response. *Oncotarget* **9**, 937–957 (2017).

151. Dergilev, K. *et al.* C-Kit Cardiac Progenitor Cell Based Cell Sheet Improves Vascularization and Attenuates Cardiac Remodeling following Myocardial Infarction in Rats. *Biomed Res Int* **2018**, 3536854 (2018).

152. Huang, P. *et al.* Combinatorial treatment of acute myocardial infarction using stem cells and their derived exosomes resulted in improved heart performance. *Stem Cell Res Ther* **10**, 300 (2019).

153. Dykes, I. M. Exosomes in Cardiovascular Medicine. *Cardiol Ther* **6**, 225–237 (2017).

154. Chevillet, J. R. *et al.* Quantitative and stoichiometric analysis of the microRNA content of exosomes. *Proc Natl Acad Sci U S A* **111**, 14888–14893 (2014).

155. Zhang, W. *et al.* Phospholipid-Free Small Unilamellar Vesicles for Drug Targeting to Cells in the Liver. *Small* **15**, e1901782 (2019).

156. Wang, X., Huang, H., Zhang, L., Bai, Y. & Chen, H. PCM and TAT co-modified liposome with improved myocardium delivery: in vitro and in vivo evaluations. *Drug Deliv* **24**, 339–345 (2017).

157. Song, T. *et al.* TPGS-Modified Long-Circulating Liposomes Loading Ziyuglycoside I for Enhanced Therapy of Myelosuppression. *Int J Nanomedicine* **16**, 6281–6295 (2021).

158. Tamaddon, L., Mohamadi, N. & Bavarsad, N. Preparation and Characterization of Mucoadhesive Loratadine Nanoliposomes for Intranasal Administration. *Turk J Pharm Sci* **18**, 492–497 (2021).

159. Abeesh, P., Vishnu, W. K. & Guruvayoorappan, C. Preparation and characterization of withaferin A loaded pegylated nanoliposomal formulation with high loading efficacy: In vitro and in vivo anti-tumour study. *Mater Sci Eng C Mater Biol Appl* **128**, 112335 (2021).

160. Cvjetkovic, A., Lötvall, J. & Lässer, C. The influence of rotor type and centrifugation time on the yield and purity of extracellular vesicles. *J Extracell Vesicles* **3**, (2014).

161. Rasband, W. S. ImageJ, U. S. National Institutes of Health, https://imagej.nih.gov/ij/. Preprint at https://imagej.nih.gov/ij/,.

162. Carpentier, G. *et al.* Angiogenesis Analyzer for ImageJ - A comparative morphometric analysis of 'Endothelial Tube Formation Assay' and 'Fibrin Bead Assay'. *Sci Rep* **10**, 11568 (2020).

163. Wang, W. *et al.* Exosomes derived miR-126 attenuates oxidative stress and apoptosis from ischemia and reperfusion injury by targeting ERRFI1. *Gene* **690**, 75–80 (2019).

164. Evers, M. J. W. *et al.* Functional siRNA Delivery by Extracellular Vesicle–Liposome Hybrid Nanoparticles. *Adv Healthc Mater* **n/a**, 2101202 (2021).

165. Xi, X. M., Chen-Meng, Xia, S. J. & Lu, R. Drug loading techniques for exosome-based drug delivery systems. *Pharmazie* vol. 76 Preprint at https://doi.org/10.1691/ph.2021.0128 (2021).

166. Kooijmans, S. A. A. *et al.* Electroporation-induced siRNA precipitation obscures the efficiency of siRNA loading into extracellular vesicles. *J Control Release* **172**, 229–238 (2013).

167. Potter, H. & Heller, R. Transfection by electroporation. *Curr Protoc Mol Biol* **2018**, (2018).

168. Fu, S., Wang, Y., Xia, X. & Zheng, J. C. Exosome engineering: Current progress in cargo loading and targeted delivery. *NanoImpact* vol. 20 Preprint at https://doi.org/10.1016/j.impact.2020.100261 (2020).

169. Corbeil, D. *et al.* Uptake and Fate of Extracellular Membrane Vesicles: Nucleoplasmic Reticulum-Associated Late Endosomes as a New Gate to Intercellular Communication. *Cells* **9**, 1931 (2020).

170. Matsumoto, A. *et al.* Role of Phosphatidylserine-Derived Negative Surface Charges in the Recognition and Uptake of Intravenously Injected B16BL6-Derived Exosomes by Macrophages. *J Pharm Sci* **106**, 168–175 (2017).

171. Parikh, M. & Pierce, G. N. A Brief Review on the Biology and Effects of Cellular and Circulating microRNAs on Cardiac Remodeling after Infarction. *Int J Mol Sci* **22**, 4995 (2021).

172. Moghaddam, A. S. *et al.* Cardioprotective microRNAs: Lessons from stem cell-derived exosomal microRNAs to treat cardiovascular disease. *Atherosclerosis* **285**, 1–9 (2019).

173. Pan, Q. *et al.* Exosomes Derived from Mesenchymal Stem Cells Ameliorate Hypoxia/Reoxygenation-Injured ECs via Transferring MicroRNA-126. *Stem Cells Int* **2019**, 2831756 (2019).

174. Li, H., Tian, X., Ruan, Y., Xing, J. & Meng, Z. Asiatic acid alleviates Ang-II induced cardiac hypertrophy and fibrosis via miR-126/PIK3R2 signaling. *Nutr Metab (Lond)* **18**, 71 (2021).

175. Yang, H.-H., Chen, Y., Gao, C.-Y., Cui, Z.-T. & Yao, J.-M. Protective Effects of MicroRNA-126 on Human Cardiac Microvascular Endothelial Cells Against Hypoxia/Reoxygenation-Induced Injury and Inflammatory Response by Activating PI3K/Akt/eNOS Signaling Pathway. *Cell Physiol Biochem* **42**, 506–518 (2017).

176. Harris, T. A., Yamakuchi, M., Ferlito, M., Mendell, J. T. & Lowenstein, C. J. MicroRNA-126 regulates endothelial expression of vascular cell adhesion molecule 1. *Proc Natl Acad Sci U S A* **105**, 1516–1521 (2008).

177. Makkar, R. R. *et al.* Intracoronary cardiosphere-derived cells for heart regeneration after myocardial infarction (CADUCEUS): a prospective, randomised phase 1 trial. *Lancet* **379**, 895–904 (2012).

178. Sahoo, S. & Losordo, D. W. Exosomes and cardiac repair after myocardial infarction. *Circ Res* **114**, 333–344 (2014).

179. Sun, L. *et al.* Long noncoding RNA UCA1 from hypoxia-conditioned hMSC-derived exosomes: a novel molecular target for cardioprotection through miR-873-5p/XIAP axis. *Cell Death Dis* **11**, (2020).

180. Huang, H. *et al.* Exosomes from SIRT1-Overexpressing ADSCs Restore Cardiac Function by Improving Angiogenic Function of EPCs. *Mol Ther Nucleic Acids* **21**, (2020).

181. Zheng, Y. *et al.* Stem cell-derived exosomes in the treatment of acute myocardial infarction in preclinical animal models: a meta-analysis of randomized controlled trials. *Stem Cell Res Ther.* **13**, 151-undefined (2022).

182. Seshadri, G. *et al.* The delivery of superoxide dismutase encapsulated in polyketal microparticles to rat myocardium and protection from myocardial ischemia-reperfusion injury. *Biomaterials* **31**, (2010).

183. Bohl, S. *et al.* Refined approach for quantification of in vivo ischemia-reperfusion injury in the mouse heart. *Am J Physiol Heart Circ Physiol* **297**, 2054–2058 (2009).

184. Bøtker, H. E. *et al.* Practical guidelines for rigor and reproducibility in preclinical and clinical studies on cardioprotection. *Basic Research in Cardiology* vol. 113 Preprint at https://doi.org/10.1007/s00395-018-0696-8 (2018).

185. Serebruany, V. L. & Atar, D. Assessment of bleeding events in clinical trials—Proposal of a new classification. *Am J Cardiol.* **99**, 288–290 (2007).

186. Peet, C., Ivetic, A., Bromage, D. I. & Shah, A. M. Cardiac monocytes and macrophages after myocardial infarction. *Cardiovascular Research* vol. 116 Preprint at https://doi.org/10.1093/CVR/CVZ336 (2020).

187. Xiao, C. *et al.* Transplanted mesenchymal stem cells reduce autophagic flux in infarcted hearts via the exosomal transfer of miR-125b. *Circ Res* **123**, (2018).

188. Wang, X. L. *et al.* Exosomes derived from human umbilical cord mesenchymal stem cells improve myocardial repair via upregulation of Smad7. *Int J Mol Med* **41**, (2018).

189. Mathiyalagan, P. *et al.* Angiogenic Mechanisms of Human CD34+ Stem Cell Exosomes in the Repair of Ischemic Hindlimb. *Circ Res* **120**, (2017).

190. Ma, C. *et al.* Moderate Exercise Enhances Endothelial Progenitor Cell Exosomes Release and Function. *Med Sci Sports Exerc* **50**, (2018).

191. Huang, F. *et al.* Mesenchymal stem cells modified with miR-126 release angiogenic factors and activate Notch ligand Delta-like-4, enhancing ischemic angiogenesis and cell survival. *Int J Mol Med* **31**, (2013).

192. Takahashi, Y. *et al.* Visualization and in vivo tracking of the exosomes of murine melanoma B16-BL6 cells in mice after intravenous injection. *J Biotechnol* **165**, 77–84 (2013).

193. Xu, W. *et al.* Engineered Exosomes With Ischemic Myocardium-Targeting Peptide for Targeted Therapy in Myocardial Infarction. *J Am Heart Assoc* **7**, e008737 (2018).

194. Mentkowski, K. I. & Lang, J. K. Exosomes Engineered to Express a Cardiomyocyte Binding Peptide Demonstrate Improved Cardiac Retention in Vivo. *Sci Rep* **9**, 10041 (2019).

195. Llorente, A. *et al.* Molecular lipidomics of exosomes released by PC-3 prostate cancer cells. *Biochim Biophys Acta* **1831**, 1302–1309 (2013).

196. Costa Verdera, H., Gitz-Francois, J. J., Schiffelers, R. M. & Vader, P. Cellular uptake of extracellular vesicles is mediated by clathrin-independent endocytosis and macropinocytosis. *Journal of Controlled Release* **266**, 100–108 (2017).

197. Mayor, S. & Pagano, R. E. Pathways of clathrin-independent endocytosis. *Nature Reviews Molecular Cell Biology* vol. 8 Preprint at https://doi.org/10.1038/nrm2216 (2007).

198. Doherty, G. J. & McMahon, H. T. Mechanisms of Endocytosis. *Annu Rev Biochem* **78**, 857–902 (2009).

199. Hankins, H. M., Baldridge, R. D., Xu, P. & Graham, T. R. Role of Flippases, Scramblases and Transfer Proteins in Phosphatidylserine Subcellular Distribution. *Traffic* vol. 16 Preprint at https://doi.org/10.1111/tra.12233 (2015).

200. Gustafson, H. H., Holt-Casper, D., Grainger, D. W. & Ghandehari, H. Nanoparticle Uptake: The Phagocyte Problem. *Nano Today* **10**, 487–510 (2015).

201. Zhang, Y.-N., Poon, W., Tavares, A. J., McGilvray, I. D. & Chan, W. C. W. Nanoparticle–liver interactions: Cellular uptake and hepatobiliary elimination. *Journal of Controlled Release* **240**, 332–348 (2016).

202. Massol, R. H., Boll, W., Griffin, A. M. & Kirchhausen, T. A burst of auxilin recruitment determines the onset of clathrin-coated vesicle uncoating. *Proc Natl Acad Sci U S A* **103**, (2006).

203. Riaz, M. A. *et al.* Identification of Lysinibacillus sphaericus Binary toxin binding proteins in a malarial mosquito cell line by proteomics: A novel approach towards improving mosquito control. *J Proteomics* **227**, (2020).

204. Oakley, F. O., Smith, R. L. & Engelhardt, J. F. Lipid rafts and caveolin-1 coordinate interleukin-1β (IL-1β)-dependent activation of NFκB by controlling endocytosis of Nox2 and IL-1β receptor 1 from the plasma membrane. *Journal of Biological Chemistry* **284**, (2009).

205. Liu, Y. *et al.* Transcytosis of Nanomedicine for Tumor Penetration. *Nano Lett* **19**, (2019).

206. Nakase, I., Kobayashi, N. B., Takatani-Nakase, T. & Yoshida, T. Active macropinocytosis induction by stimulation of epidermal growth factor receptor and oncogenic Ras expression potentiates cellular uptake efficacy of exosomes. *Sci Rep* **5**, (2015).

207. Ferreira, A. P. A. & Boucrot, E. Mechanisms of Carrier Formation during Clathrin-Independent Endocytosis. *Trends in Cell Biology* vol. 28 Preprint at https://doi.org/10.1016/j.tcb.2017.11.004 (2018).

208. Haraszti, R. A. *et al.* High-resolution proteomic and lipidomic analysis of exosomes and microvesicles from different cell sources. *J Extracell Vesicles* **5**, (2016).

209. Haraszti, R. A. *et al.* Serum deprivation of mesenchymal stem cells improves exosome activity and alters lipid and protein composition. *iScience* **16**, (2019).

210. R.G., R. *et al.* Intravenous infusion of cardiosphere-derived cells and their exosomes improve dystrophin-deficient cardiomyopathy in MDX mice. *Circulation* **136**, (2017).

211. Agarwal, U. *et al.* Experimental, Systems, and Computational Approaches to Understanding the MicroRNA-Mediated Reparative Potential of Cardiac Progenitor Cell-Derived Exosomes From Pediatric Patients. *Circ Res* **120**, 701–712 (2017).

212. Kanki, S. *et al.* Identification of targeting peptides for ischemic myocardium by in vivo phage display. *J Mol Cell Cardiol* **50**, 841–848 (2011).

213. Kim, H. *et al.* Cardiac-specific delivery by cardiac tissue-targeting peptide-expressing exosomes. *Biochem Biophys Res Commun* **499**, 803–808 (2018).

214. Zhu, D. *et al.* Minimally invasive delivery of therapeutic agents by hydrogel injection into the pericardial cavity for cardiac repair. *Nat Commun* **12**, (2021).

215. Cheng, G., Zhu, D., Huang, K. & Caranasos, TG. Minimally invasive delivery of a hydrogel-based exosome patch to prevent heart failure. *J Mol Cell Cardiol.* 113–121 (2022) doi:doi: 10.1016/j.yjmcc.2022.04.020.

216. Pattipeiluhu, R. *et al.* Unbiased Identification of the Liposome Protein Corona using Photoaffinity-based Chemoproteomics. *ACS Cent Sci* **6**, (2020).

217. Onishchenko, N., Tretiakova, D. & Vodovozova, E. Spotlight on the protein corona of liposomes. *Acta Biomaterialia* vol. 134 Preprint at https://doi.org/10.1016/j.actbio.2021.07.074 (2021).